ABSTRACT

TURBO SPACE-TIME CODED MODULATION: PRINCIPLES AND PERFORMANCE ANALYSIS

by
Dongzhe Cui

A breakthrough in coding was achieved with the invention of turbo codes. Turbo codes approach Shannon capacity by displaying the properties of long random codes, yet allowing efficient decoding. Coding alone, however, cannot fully address the problem of multipath fading channel. Recent advances in information theory have revolutionized the traditional view of multipath channel as an impairment. New results show that high gains in capacity can be achieved through the use of multiple antennas at the transmitter and the receiver. To take advantage of these new results in information theory, it is necessary to devise methods that allow communication systems to operate close to the predicted capacity. One such method recently invented is space-time coding, which provides both coding gain and diversity advantage.

In this dissertation, a new class of codes is proposed that extends the concept of turbo coding to include space-time encoders as constituent building blocks of turbo codes. The codes are referred to as *turbo space-time coded modulation* (turbo-STCM). The motivation behind the turbo-STCM concept is to *fuse* the important properties of turbo and space-time codes into a unified design framework. A turbo-STCM encoder is proposed, which consists of two space-time codes in recursive systematic form concatenated in parallel. An iterative symbol-by-symbol *maximum a posteriori* algorithm operating in the log domain is developed for decoding turbo-STCM. The decoder employs two *a posteriori* probability (APP) computing modules

concatenated in parallel; one module for each constituent code. The analysis of turbo-STCM is demonstrated through simulations and theoretical closed-form expressions. Simulation results are provided for 4-PSK and 8-PSK schemes over the Rayleigh block-fading channel. It is shown that the turbo-STCM scheme features full diversity and full coding rate. The significant gain can be obtained in performance over conventional space-time codes of similar complexity. The analytical union bound to the bit error probability is derived for turbo-STCM over the additive white Gaussian noise (AWGN) and the Rayleigh block-fading channels. The bound makes it possible to express the performance analysis of turbo-STCM in terms of the properties of the constituent space-time codes. The union bound is demonstrated for 4-PSK and 8-PSK turbo-STCM with two transmit antennas and one/two receive antennas. Information theoretic bounds such as Shannon capacity, cutoff rate, outage capacity and the Fano bound, are computed for multiantenna systems over the AWGN and fading channels. These bounds are subsequently used as benchmarks for demonstrating the performance of turbo-STCM.

TURBO SPACE-TIME CODED MODULATION: PRINCIPLES AND PERFORMANCE ANALYSIS

by
Dongzhe Cui

A Dissertation
Submitted to the Faculty of
New Jersey Institute of Technology
in Partial Fulfillment of the Requirements for the Degree of
Doctor of Philosophy in Electrical Engineering

Department of Electrical and Computer Engineering

May 2001

APPROVAL PAGE

TURBO SPACE-TIME CODED MODULATION: PRINCIPLES AND PERFORMANCE ANALYSIS

Dongzhe Cui

Dr. Alexander M. Haimovich, Dissertation Advisor — Date
Associate Professor of Electrical and Computer Engineering,
New Jersey Institute of Technology

Dr. Vahid Tarokh, Committee Member — Date
Associate Professor of Electrical Engineering and Computer Science,
Massachusetts Institute of Technology

Dr. Robert A. Soni, Committee Member — Date
Member of Technical Staff, Wireless Technology Laboratory,
Lucent Technologies

Dr. Hongya Ge, Committee Member — Date
Assistant Professor of Electrical and Computer Engineering,
New Jersey Institute of Technology

Dr. Zoi-heleni Michalopoulou, Committee Member — Date
Associate Professor of Mathematical Sciences,
New Jersey Institute of Technology

BIOGRAPHICAL SKETCH

Author: Dongzhe Cui

Degree: Doctor of Philosophy

Date: May 2001

Graduate Education:

- Doctor of Philosophy in Electrical Engineering,
  New Jersey Institute of Technology, Newark, New Jersey, U.S.A., 2001
- Master of Science in Electrical Engineering,
  No. 23 Institute of China AeroSpace Corporation, Beijing, P.R.China, 1995
- Bachelor of Science in Electrical Engineering,
  Northwestern Polytechnic University, Xi'an, P.R.China, 1992

Major: Electrical Engineering

Selected Publications and Presentations:

D. Cui and A.M. Haimovich, "Error Performance Analysis of Turbo Space-Time Trellis Coded Modulation over Fading Channels," *IEEE International Conference on Communications conference (ICC '01)*, June. 11-15, 2001, Helsinki, Finland.

D. Cui and A.M. Haimovich, "Design and Performance Analysis of Turbo Space-Time Coded Modulation", *IEEE Global Telecommunications conference, (Globecom '00)*, Vol. 3, Nov. 27-Dec. 1, 2000, San Francisco, CA.

D. Cui and A.M. Haimovich, "Performance Evaluation of Parallel Concatenated Turbo-Code with Antenna Diversity", *35th Annual Conference on Information Sciences and Systems (CISS '01)*, The Johns Hopkins University, Baltimore, Maryland, Mar. 21-23, 2001.

D. Cui and A.M. Haimovich, "Performance Analysis of Multilevel Turbo-Code with Antenna Diversity," *13th Annual International Conference on Wireless Communications (Wireless 2001)*, July 9-11, 2001, Calgary, Alberta, Canada.

D. Cui and A.M. Haimovich, "Error Performance Analysis of Multilevel Turbo-Code with Antenna Diversity," submitted to *IEEE Semiannual Vehicular Technology (VTC-2001/Fall) Conference*, Oct. 7-11, 2001, Atlantic City, New Jersey.

D. Cui and A.M. Haimovich," A New Bandwidth Efficient Antenna Diversity Scheme Using Turbo Code", *34th Annual Conference on Information Sciences and Systems (CISS '00)*, Vol. 1, TA-6.24-29, Princeton, New Jersey, Mar. 15-17, 2000.

D. Cui and A.M. Haimovich, "Performance of Parallel Concatenated Space-Time Codes," accepted by *IEEE Communications Letters*, 2001.

D. Cui and A.M. Haimovich, "Parallel Concatenated Turbo Multiple Antenna Coded Modulation: Principles and Performance Analysis," submitted to *IEEE Journal Selected Area on Communication*, 2001.

To my beloved family, as it is their hard work and conditionless care and love that made this work possible. Thank my dear wife *Li Zhao* who helped and encouraged me to finish my Ph.D. successfully.

ACKNOWLEDGMENT

First of all, I would like to express my sincere gratitude to my advisor and mentor, Dr. Alexander M. Haimovich, whose relentless enthusiasm for research in the field of telecommunications has instilled my perseverance to finish my Ph.D. I would also like to thank Dr. Vahid Tarokh, Robert A. Soni, Hongya Ge and Zoi-heleni Michalopoulou who served in my thesis committee and provided me with valuable feedback on various aspects of my thesis.

I would also like to acknowledge the financial support of NJIT Department of Electrical and Computer Engineering, Air Force Office of Scientific Research (AFOSR) Grant and the New Jersey Center for Wireless Telecommunications during the course of my graduate studies.

Last, but not the least, I would also like to give special thanks to Dr. Yeheskel Bar-Ness and the other faculty associated with the Center for Communications and Signal Processing Research (CCSPR) for their ongoing efforts in providing the center's students with the environment and infrastructure.

TABLE OF CONTENTS

Chapter **Page**

1 INTRODUCTION 1

1.1 Temporal Processing: Improving Data Transmission Reliability 2

1.1.1 Turbo Codes 2

1.1.2 Turbo Coded Modulation 5

1.2 Space-Time Array Processing 7

1.2.1 BLAST 9

1.2.2 Space-Time Codes 10

1.3 Related Work on Turbo Space-Time Codes 12

1.4 Overview of Thesis 17

2 INFORMATION THEORY CONSIDERATION OF SPACE-TIME CODING 19

2.1 Coded Modulation System over the AWGN Channel 19

2.2 Outage Capacity of Multiantenna Systems over the Fading Channel . 23

2.3 Frame Error Limit of Multiantenna System 25

2.4 Fano Lower Bound of Multiantenna System 28

2.5 Chapter Summary 30

3 TURBO SPACE-TIME CODED MODULATION 32

3.1 Turbo-STCM System Description 32

3.1.1 Recursive Systematic Space-Time Constituent Codes 32

3.1.2 Turbo-STCM Encoder 35

3.1.3 System Model 38

3.1.4 Full Diversity of Turbo-STCM Component Codes 40

3.1.5 Interleaver Design 42

3.2 Iterative Maximum A Posteriori Decoder 42

3.2.1 APP Algorithm 43

3.2.2 Log-APP Algorithm 48

TABLE OF CONTENTS
(Continued)

Chapter **Page**

3.3 Numerical Results 53

3.4 Chapter Summary 59

4 ERROR PERFORMANCE ANALYSIS OF TURBO-STCM 65

4.1 Definitions and Notations 66

4.2 Input-Output Weight Enumerator 68

4.3 Derivation of the Union Bound 73

4.4 Examples of Performance Analysis over the AWGN Channel 81

4.5 Union Bound for the Fading Channel 82

4.6 Numerical Results for the Fading Channel 86

4.7 Chapter Summary 88

5 CONCLUSIONS AND FURTHER WORK 94

REFERENCES 97

LIST OF FIGURES

Figure		Page
1.1	Turbo encoder.	3
1.2	Turbo decoder	5
1.3	An example of turbo-TCM encoder.	6
1.4	The block diagram of a BLAST system.	9
1.5	An example of space-time coding system. (a) the block diagram, (b) code trellis.	10
1.6	A serially concatenated turbo code with a space-time block code [42]	13
1.7	(a) Serial concatenated space-time code, (b) Self-concatenated space-time code [43].	14
1.8	BPSK full spatial diversity turbo space-time code [44].	14
1.9	Turbo code with bit interleaving [48, 53].	14
1.10	A space-time code is concatenated by rate 1 recursive code [45].	15
1.11	Space-time turbo code for two transmit antennas [47].	15
1.12	Turbo-STCM with component space-time codes [49, 50, 51, 52].	16
2.1	Block diagram of a multiantenna system over AWGN channel	20
2.2	Channel signal set over the AWGN channel.	21
2.3	Capacity and cut-off rate of multiantenna system.	23
2.4	Capacity of two transmit and multiple receive antenna system.	25
2.5	FER plot for multiantenna system.	26
2.6	Comparison of outage and Shannon capacity.	27
2.7	Fano lower bound of block-fading channel with multiple transmit and receive antennas.	30
3.1	Recursive systematic space-time encoder for 4 state 4-PSK, two transmit antennas, 2 bits/s/Hz: (a) code implementation, (b) code trellis.	33
3.2	Recursive systematic space-time encoder for 8 state 4-PSK, two transmit antennas, 2 bits/s/Hz: (a) code implementation, (b) code trellis.	33

Figure **Page**

3.3 Recursive systematic space-time encoder for 16 state 8-PSK, two transmit antennas, 3 bits/s/Hz: (a) code implementation, (b) code trellis. 34

3.4 Non-recursive systematic space-time encoder for 4 state 4-PSK, two transmit antennas, 2 bits/s/Hz: (a) code implementation, (b) code trellis. 35

3.5 Turbo-STCM encoder for two transmit antennas, 2 bits/s/Hz. 36

3.6 Schematic diagram of turbo-STCM transmission system. 38

3.7 Turbo-STCM decoder, the interleavers/deinterleavers are not shown. . . . 44

3.8 Notations for trellis transitions. 45

3.9 FER of 4 state 4-PSK turbo-STCM (2T1R) over the fading channel, with fixed interleaver (FIL) and averaged over interleavers (UIL). 54

3.10 FER of 4 state 4-PSK turbo-STCM (2T2R) over the fading channel, with fixed interleaver (FIL) and averaged over interleavers (UIL). 56

3.11 BER of 8 state 4-PSK turbo-STCM (2T2R) over the fading channel, averaged over interleavers (UIL) of size (symbols): (a) $K = 130$, (b) $K = 1300$, (c) $K = 5200$. 61

3.12 Iterations of 8 state 4-PSK turbo-STCM (2T2R) decoder, average over interleavers (UIL) of size $K = 1300$ symbols. 62

3.13 FER of 8 state 4-PSK turbo-STCM (2T1R) over the fading channel, with fixed interleaver (FIL) and averaged over interleavers (UIL) of size $K = 1300$ symbols. 62

3.14 FER comparison of turbo-STCM with other methods. 63

3.15 FER of 8 state 4-PSK turbo-STCM (2T2R) over the fading channel, with fixed interleaver (FIL) and averaged over interleavers (UIL) of size $K = 1300$ symbols. 63

3.16 FER of 16 state 8-PSK turbo-STCM (2T1R) over the fading channel, with fixed interleaver (FIL) and averaged over interleavers (UIL) of size $K = 1300$ symbols. 64

3.17 FER of 16 state 8-PSK turbo-STCM (2T2R) over the fading channel, with fixed interleaver (FIL) and averaged over interleavers (UIL) of size $K = 1300$ symbols. 64

4.1 Turbo-STCM encoder for two transmit antennas. 67

4.2 Union bound for 8 state 4-PSK turbo-STCM (2T1R) over the AWGN channel with interleavers of size (symbols): (a) $K = 130$, (b) $K = 1300$, (c) $K = 5200$. 89

4.3 Union bound for 8 state 4-PSK turbo-STCM (2T1R) over the block-fading channel with interleaver of size (symbols): (a) $K = 130$, (b) $K = 1300$ and (c) $K = 5200$. 90

4.4 Union bound for 8 state 4-PSK turbo-STCM (2T2R) over the block-fading channel with interleaver of size (symbols): (a) $K = 130$, (b) $K = 1300$ and (c) $K = 5200$. 91

4.5 Union bound for 16 state 8-PSK turbo-STCM (2T1R) over the block-fading channel with interleaver of size (symbols): (a) $K = 130$, (b) $K = 1300$ and (c) $K = 5200$. 92

4.6 Union bound for 16 state 8-PSK turbo-STCM (2T2R) over the block-fading channel with interleaver of size (symbols): (a) $K = 130$, (b) $K = 1300$ and (c) $K = 5200$. 93

CHAPTER 1

INTRODUCTION

The rapid growth of wireless voice subscribers, the internet and the quickly increasing use of portable devices suggest that wireless internet multimedia access will rise rapidly over the next few years. The world expects an explosion in wireless information services. Current second generation (2G) digital cellular systems GSM, IS-95 and IS-136 provide good quality voice anytime, anywhere. However, 2G systems provide low speed, and hence low quality, data transmission services. The desire to support higher-rate data services, in addition to wireless voice telephony, is the primary factor in the development of third or future generation systems. The 3G standards are converging on wideband code division multiple access (WCDMA) technology that will provide universal coverage for 144 kbits/s and 384 kbits/s data services as well as limited coverage for 2 Mbits/s data.

Barriers to the development of wireless communication services include *low bit rates*, *high power consumption*, and *high cost per bit.* The 3G wireless communication does begin to address the issues of bit rate and reduce the cost per transmitted bit. Signal processing methods can be applied to further lower error rate, lower power requirement and lower cost per bit. Signal processing also holds the key to meeting the future wireless data rate requirements without expanding current bandwidth efficiency. The following categories of signal processing are distinguished:

- Temporal processing: includes coded modulation, which merges channel coding and modulation together.

- Space-time array processing: employs multiple antennas at both transmitter and receiver.

This introduction begins with an overview of temporal processing, introduces turbo codes and turbo coded modulation. Then several space-time processing techniques

are briefly reviewed for leading to turbo space-time coding. We also defined the spatial and temporal diversity, present a short literature of the current state of the art of turbo space-time codes. Finally, there is the introduction of our turbo space-time coding scheme.

1.1 Temporal Processing: Improving Data Transmission Reliability

In 1948 C.E. Shannon [1] developed fundamental limits on the efficiency of telecommunication over noisy channels. The coding theorem asserts that there are special codes with code rates close to channel capacity and probability of error arbitrarily close to zero. Almost fifty years later, new channel coding schemes [2] for the additive white Gaussian noise (AWGN) channel have been discovered that come close to the fundamental limits predicted by Shannon.

Ever since Shannon's original paper [1], coding theorists have attempted to construct structured codes that achieve capacity with limited delay and low decoding complexity. Forney's [3, pp. 578] concatenated codes were the first step in finding a class of codes whose error probability decreases exponentially at a rate less than capacity, while decoding complexity increase only algebraically. He also showed that the soft-output operation is the optimum decoding method for cascaded codes and that inner decoder is required to estimate the a posteriori probabilities of the outer code symbols given the received channel sequence. Turbo codes [2] are the latest culmination of this effort of constructing powerful codes from simple codes.

1.1.1 Turbo Codes

Turbo codes were first presented in [2] and were formalized in [4]. The original turbo code is a parallel concatenation of two component codes. In Fig. 1.1, the constituent codes are from a subclass of convolutional codes known as recursive systematic convolutional (RSC) codes [5, pp. 33]. Two identical rate 1/2 RSC codes

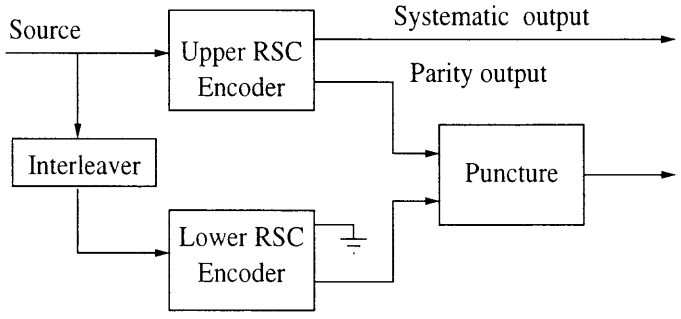

Figure 1.1 Turbo encoder.

work on the input data in parallel. The input data is permuted by an interleaver before being fed into the lower encoder. Because the encoders are *systematic* (one of the outputs is the input itself) and receive the same input (although in a different order), the systematic output of the lower encoder is completely redundant and does not need to be transmitted. Because of interleaver, the two RSC encoders do not receive their inputs in the same order. Thus if one encoder receives an input that causes a low weight output, then it is improbable for the other encoder to produce a low weight output. Thus, the effort of the interleaver is to decrease the probability of occurrence of multiple low weight codewords. Interleaver causes turbo codes random-like properties which facilitate significant good performance to approach Shannon capacity. The overall code rate of the parallel concatenated code is 1/3, although higher code rates can be obtained by *puncturing* (selectively removing outputs from the transmission stream) the parity output.

Due to the interleaver, turbo decoding involves the joint estimation of two Markov processes, one for each constituent code. While in theory it is possible to model a turbo code as a single Markov process, such a representation is extremely complex and does not lend itself to a practical *Viterbi decoding algorithm* [6]. Although the Viterbi algorithm accepts soft-inputs of prior information, it does

not produce soft-outputs of a posteriori probabilities and is therefore unsuitable for turbo decoding [1].

There are alternative trellis-based solutions for estimating the state sequence of a Markov process. Bahl, Cocke, Jelinek and Raviv [8] provided a solution for estimating the *a posteriori probabilities* (APP) of the states and trellis transitions for a Markov source. This algorithm came to be known as the BCJR algorithm. A practical iterative decoding algorithm was presented in [2] and its suboptimal BCJR algorithm in log-domain approaches good performance at low complexity. The idea behind the BCJR decoding strategy is to break the overall decoding problem into decoding each of the constituent codes with locally optimal solutions and share the information in an iterative way. Each decoder associated with each of the constituent codes is modified such that it produces a soft-output in the form of *a posteriori probabilities* of the data bits. The two decoders are cascaded as shown in Fig. 1.2. The lower decoder receives the soft-output of the upper decoder. At the end of the first iteration, the soft-output of the lower decoder is fed back to the upper decoder and used as a priori information during the next iteration. Decoding continues in an *recycling* iterative way until the desired performance is attained. Iterative decoding obeys a rule of diminishing returns which means the incremental gain of each additional iteration is less than that of the previous iteration. It is the decoding method that gives turbo codes their name because the feedback action of the decoder resembles a turbo-charged engine.

The original turbo code [2] used BPSK modulation, $(5, 7)$ constraint $K = 5$ RSC Ungerboeck encoders [9] and a 65536 long bits interleaver. The parity bits were punctured such that the overall code was a $(n = 131072, k = 65532)$ linear code. Simulation results showed that at bit error rate of 10^{-5}, the corresponding

[1] In [7], Hagenauer *et al.* proposed a modification to the Viterbi algorithm which produces the a posteriori probabilities of the trellis state transitions. This algorithm is known as the soft-output Viterbi algorithm (SOVA).

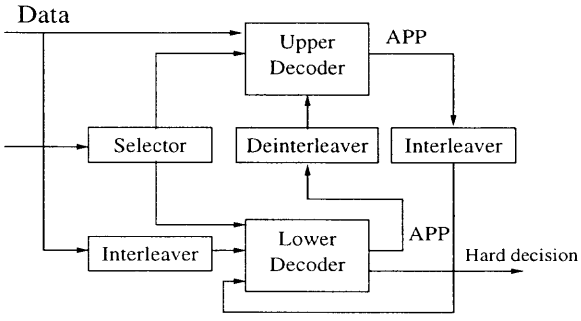

Figure 1.2 Turbo decoder

$E_b/N_0 = 0.7$ decibels (dB) after 18 iterations of decoding. Thus, the authors [4] claimed that turbo codes could come in with 0.7 dB of the Shannon limit [1].

Other researchers soon began to study other concatenation configurations, such as increasing the number of encoders and varying the types of component codes. For example, instead of two RSC codes in parallel, it is possible to concatenate three or more block or convolutional codes in serial [10], or parallel to obtain *multiple turbo codes* [11]. Overall it was found that the performance of turbo codes is much better than that of block codes.

1.1.2 Turbo Coded Modulation

The original components of turbo codes were binary error-correcting codes. In general, they are the low rate codes which require a considerable bandwidth expansion for high rate data transmission. In order to improve the transmission spectral efficiency, it is necessary to combine turbo codes with a bandwidth-efficient modulation. For instance, trellis coded modulation (TCM) [12, 13] would be a good candidate for such a scheme. Since turbo codes achieve good bit-error rate (BER) (10^{-5}) at very low SNR, it is natural to see if there are ways of applying the turbo coding principle to coded modulation systems to make use of their power without

sacrificing bandwidth. Different approaches to turbo coded modulation have been investigated in [14, 15, 16].

In [14], the encoded bits of the original turbo code as in Fig. 1.1 are mapped to a certain constellation such as 4-PSK, 8-PSK or 16-QAM. After puncturing some of the parity bits, a desired spectral efficiency can be obtained. In [16], there are two component convolutional codes whose inputs are the entire information source and the interleaved version of inputs. Therefore, both of the parity sequences are produced by the entire information block. Half of the information bits are punctured at the output of upper code, and another half are punctured at the output of lower code. Sub-interleavers have to be applied in order to prevent the puncturing of an information bit at both encoder outputs. Finally the systematic and parity bits are mapped to an appropriate constellation.

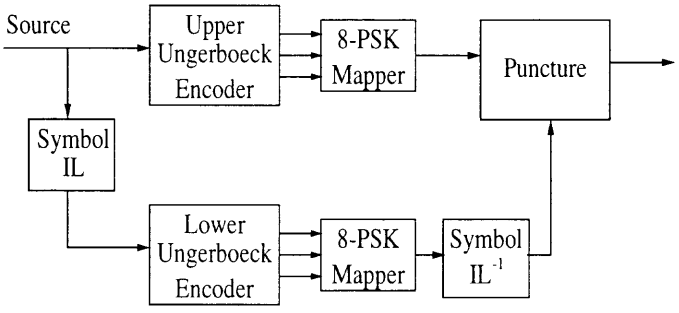

Figure 1.3 An example of turbo-TCM encoder.

Perhaps the most natural extension of binary turbo codes is presented in [15] as shown in Fig. 1.3. It employs two Ungerboeck-type codes [12, 13] in combination with TCM in recursive systematic form as component codes. The scheme is referred to as turbo trellis coded modulation (turbo-TCM). A simple example of turbo-TCM is shown in Fig. 1.3 for 8-PSK modulation, 2 bits/s/Hz and code rate 2/3. The basic principle of turbo coding is applied to TCM by retaining the important properties and advantages of both of their structures. TCM codes can be seen as recursive systematic convolutional codes followed by one signal mapper. Turbo-TCM employ

Ungerboeck codes as building blocks in a turbo coding scheme in a similar way as binary codes were used in the original turbo codes [4]. The interleaver (labeled as "IL") between two constituent encoders operates on symbol (groups of bits). The decoding algorithm is a generalized version of MAP decoding algorithm of the original binary turbo codes [4].

1.2 Space-Time Array Processing

Space-time array processing is the minimization of fading and multiple access interference through multiple antennas, advanced signal processing techniques, transceiver structures and error control coding. The increasing demand for wireless applications focuses interest on wireless system performance over the fading channel. Coding, essentially temporal processing, alone does not fully address the impairment of multipath fading. That means the capacity is limited in a small range for the given single-input single-output (SISO) channel. The use of multiple-element antenna arrays at the transmit and receive sides of a wireless links in combination with signal processing and coding is a promising means to improve the performance of a wireless communication system in a fading environment [17, 18]. The reason behind space-time processing (which include space-time coding as a special case) is the optimization of the spectral efficiency. In order to analyze space-time processing systems, a basic model of the communication system is required to identify inputs, outputs and the channel. For a general space-time processing system where multiple antennas are employed at transmitter and receiver [18], such a signal model is known as a multiple-input multiple-output (MIMO) model due to the fact that the desired signal has multiple inputs into the channel (the transmit antennas) as well as multiple outputs (the receiver antennas).

Clearly a MIMO system can be viewed as multiple SISO sub-channels The MIMO system's channel capacity is then the sum of the individual capacities of these

SISO sub-channels. In theory [19], the capacity over the MIMO fading channel can grow *linearly* with the number of transmit or receive antennas. Better performance can be achieved by exploiting the inherent spatial and temporal diversity associated with respective multipath wireless mobile channel. Space-time processing offers the potential for significant improvements in overall system capacity of wireless communication systems [20]. Although a single user is considered in this dissertation, a number of alternative channel configurations for single user scenarios are used in practice. For example, SIMO channel of downlink is the single user with single antenna input at mobile and multiple antenna outputs at the base station. MISO channel of uplink is the single user with multiple antenna inputs at the mobile unit and single antenna output at base station.

In a non-fading environment, multiple antennas can be used to increase transmit and receive effective antenna gain [17]. With higher sophistication, antenna patterns can be controlled to focus the energy in specified directions (beamforming) to minimize the interference to and from other antennas. In a fading environment, antenna arrays may be employed either at the transmitter or at the receiver. Diversity at the receiver (SIMO channel) is a well-studied subject backed up by a large body of literatures [21, 22, 23, 24, 25, 26]. If the transmitter also has an antenna array with sufficiently separated elements, this "nice" transmit and receive diversity mechanism effectively produces a rich plurality of sub-channels sharing the same RF bandwidth. Such a channel poses more degrees of freedom [27] than an unscattered SIMO channel.

Recently two major strategies have been proposed to deal with the unavoidable mutual interference among the multiple SISO sub-channels of one MIMO channel: Bell Laboratories Layered Space Time Wireless Architecture (BLAST) and space-time codes (STC). The central idea behind BLAST and STC is the exploitation,

rather than the mitigation, of the multipath channels in order to achieve high spectral efficiencies (bits/s/Hz).

1.2.1 BLAST

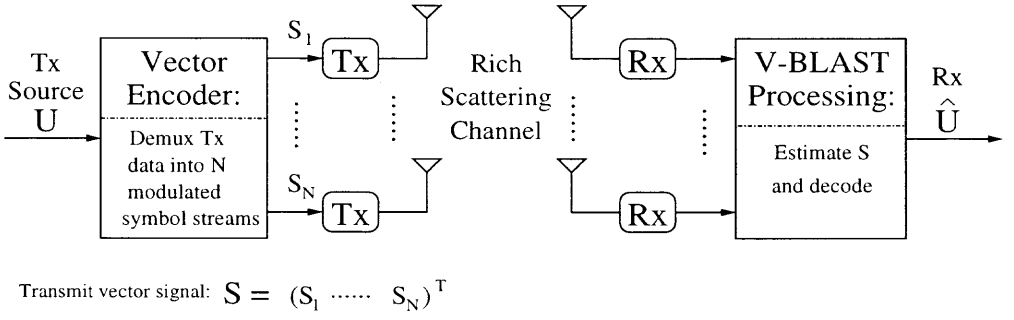

Figure 1.4 The block diagram of a BLAST system.

BLAST [28, 29, 30] is a bandwidth efficient approach to wireless communication which takes advantage of the spatial dimension by transmitting and detecting several independent co-channel data streams using multiple antennas. An example of BLAST is shown in Fig. 1.4. BLAST splits a single user's data stream into multiple substreams and applies multiple transmit antennas to simultaneously launch the parallel substream. All the substreams are transmitted in the same frequency band, so the spectrum is used very efficiently. The desired user data has multiple data copies into the channel (the transmit antennas) as well as multiple outputs (the receive antennas). At the receiver, multiple antennas pick up the multiple transmitted substreams and their scattered copies. Each receive antenna "sees" all of the transmitted substreams superimposed together. Using sophisticated signal processing, these sub-channel differences allow the data substreams to be separated and detected. BLAST system is much like a multi-user spread spectrum system where multiple transmit antennas play the role of the number of users, and the number of receiving antennas play the role of spread coding gain. Using nonlinear multi-user detection to separate the incoming signals at the receiver. In that way,

the wireless unavoidable multipath provide us a very useful spatial parallelism that greatly improve data transmission rates. Thus, the more multipath channel, the better data transmission, just the opposite of conventional systems.

1.2.2 Space-Time Codes

Space-time code (STC) is obtained when coding redundancy over time is introduced across transmit antennas. STC adds the spatial dimension to the time dimension and assumes unknown channel knowledge at the transmitter. Practical low-complexity STC geared to a few transmit and receive antennas were developed at AT&T Research Labs by V. Tarokh *et al.* [31, 32, 33, 34, 35]. With two antennas at both transmitter and receiver, the spectral efficiency of narrowband TDMA 2G channels can be increased by a factor of six [36, Fig.12, pp. 2589].

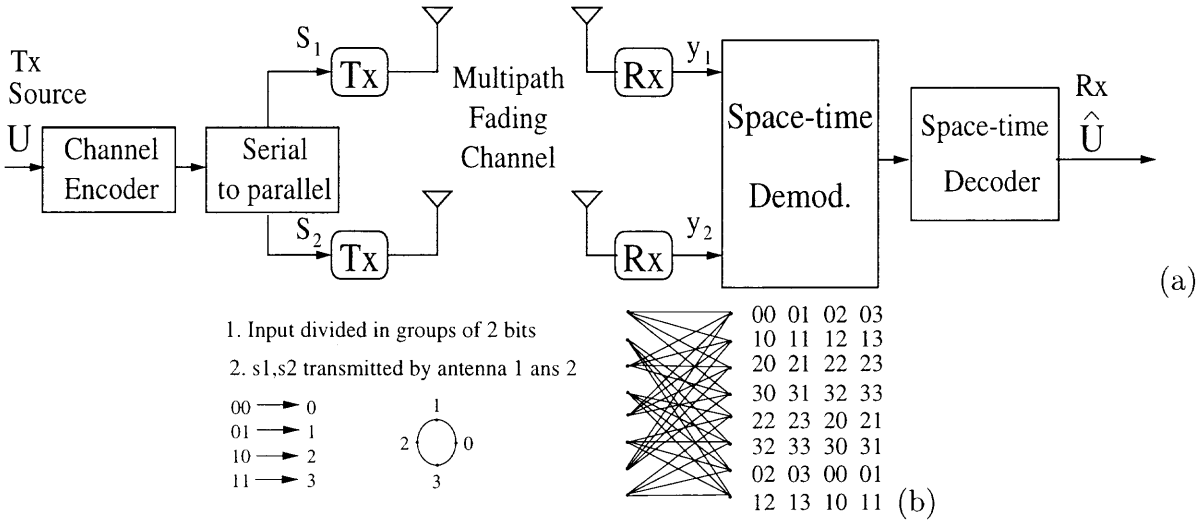

Figure 1.5 An example of space-time coding system. (a) the block diagram, (b) code trellis.

A simple example of a space-time coding system is shown in Fig. 1.5 for 4-PSK 2 bits/s/Hz space-time code. It illustrates a block diagram of space-time code with two antennas at both transmitter and receiver and an 8 state trellis diagram. Information source bits from a discrete alphabet U are encoded to signals $[s1, s2]$. After a serial to parallel converter, the encoded data is divided into $N = 2$ substreams. Each

substream is modulated and transmitted through different antennas. The decoder consists of a conventional Viterbi algorithm [6], which compute the trellis transition path metrics and then makes a decision based on the minimum accumulated metric.

Why we choose STC rather than BLAST?

Correlation of signals across the transmit antennas is the fundamental difference between STC and BLAST. Decoding complexity of space-time coding is similar to trellis codes for AWGN channel if the fading paths from the transmitter to the receiver are known to the receiver. In [37], Bevan *et al.* setup a simulation experiment to compare the performance of BLAST and space-time codes. Each data frame carried 400 information bits. The performance was quantified in terms of signal-to-noise ratio per bit E_b/N_0 at each receive antenna versus the frame error rate of FER $= 10^{-2}$. The space-time code was 32 state 4-PSK as in [31, Fig. 6]. It was shown that the space-time code has an advantage of 2-3 dB over the BLAST system. Thus, space-time codes offer the best tradeoff of performance against complexity.

Full spatial diversity

Full spatial diversity for a given number of transmit and receive antennas is the maximum achievable diversity advantage. N antennas at the transmitter provide N independent paths from transmitter to receiver. By spreading information data across the N paths, and by appropriate signal processing at the receiver, this MISO channel is much better than the SISO channel case.

According to the space-time code design of [31], each possible transmitted signal difference in a linear coded modulation generates a "signal" matrix. The rank of this complex-value "transmit signal" matrix determines the spatial diversity. Increasing this rank, that is, increasing the amount of diversity will also reduce the error probability which is represented by the asymptotic slope of the performance curve on a log-log scale. For example, a two transmit antenna -two receive antenna configuration has 4 dB/dB slope. If the codeword length in time is larger than the

number of transmit antennas N, the minimum possible rank of that "signal" matrix is N. It is shown [31, 38] that full spatial diversity can be obtained if and only if the rank of every "signal" matrix corresponding to the possible codeword pair is equal to N.

Work by Tarokh *et al.* [31], and almost at the same time independently by Guey *et al.* [38] on the problem of signal design for transmit diversity systems, derived the fundamental performance parameters for space-time codes over the block-fading channel [39]. According to the design criterion of space-time codes [31], two concepts are presented: (1) diversity advantage is denoted to describe the exponential decrease of decoding error rate versus signal-to-noise ratio (asymptotic slope of the performance curve on a log-log scale), (2) coding gain does not affect the asymptotic slope but results in a shift of the performance curve. In [31], Tarokh *et al.* present a number of interesting space-time trellis codes for two transmit antenna systems that provide full spatial diversity and good coding advantage. Subsequent work by Baro [40] has yielded new space-time trellis codes with somewhat improved coding advantage.

1.3 Related Work on Turbo Space-Time Codes

Turbo coding/decoding is a way to approach the Shannon limit of channel capacity, while space-time coding is a way to increase the bandwidth efficiency (capacity) by exploiting the multipath MIMO fading channels. Therefore, a specific combination of turbo space-time codes that incorporates the two concepts may provide even a practical way to both increase and approach the possible MIMO channel capacity [20].

Full coding rate

Full coding rate is achieved for turbo space-time codes when the number of overall output bits (all antennas) equals the output bits per constituent space-time code at one time slot. Codes that achieve full coding rate have a limit on transmission rate for each type of constellation [31, 41]. For example, a two transmit antenna configuration is considered with 2 bits/s/Hz 4-PSK transmitted signal per antenna. The input data bits at one time is 2 bits and the output coded bits of a constituent STC are 4 bits, which are partitioned and mapped to two 4-PSK symbols for two transmit antennas respectively. If two constituent STC encoders are considered, the overall output bits of turbo space-time code are 8 bits. In order to achieve full coding rate, the puncturing structure is necessary to be used for decreasing overall coded bits to 4 bits for all two transmit antennas.

Recently, several research groups have proposed different versions of turbo coding structures for multiantenna systems [42, 43, 44, 45, 46, 47, 48, 49, 50, 51, 52].

In [42], as shown in Fig. 1.6, the outer encoder consists of a standard binary turbo code or turbo-TCM. The inner encoder is a space-time block code [33, 34].

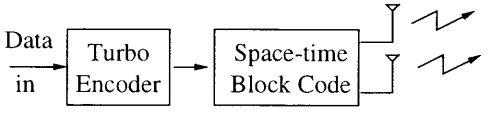

Figure 1.6 A serially concatenated turbo code with a space-time block code [42]

In [43], serial and parallel concatenated structures are suggested. Component encoders are recursive. The serial concatenated architecture uses a convolutional code as an outer encoder and a recursive space-time trellis code as inner encoder as shown in Fig. 1.7 (a). The parallel concatenated architecture is shown in Fig. 1.7 (b). It utilizes a self-concatenated recursive space-time code [10]. The turbo codes in [42, 43] guarantee full spatial diversity but the code rate can *not* achieve the full rate due to the lack of *puncturing.*

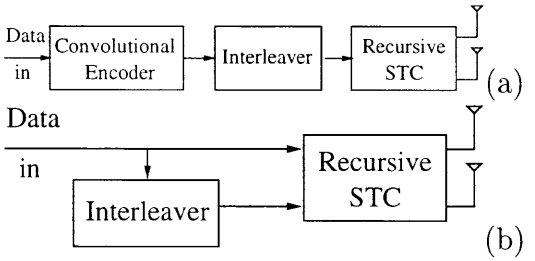

Figure 1.7 (a) Serial concatenated space-time code, (b) Self-concatenated space-time code [43].

In [44], a turbo coding scheme with two parallel concatenated recursive convolutional codes is used in conjunction with multiple transmit antenna system with BPSK modulation. The encoder structure is shown in Fig. 1.8. The code achieves 3 coded bits (one per antenna) for each input bit. The overall coding rate is 1/3. This rate can be improved to 1/2 by adding *puncturing* and reducing the number of transmit antennas to two.

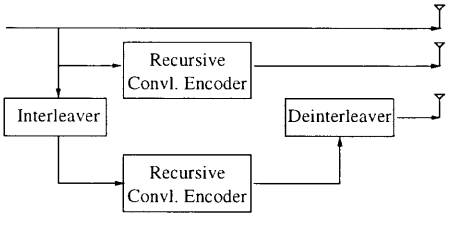

Figure 1.8 BPSK full spatial diversity turbo space-time code [44].

In [48, 53], the outputs of the turbo codes are serial-to-parallel bit-interleaved, mapped to 4-PSK symbols and transmitted using multiple antennas as shown in Fig. 1.9. Full coding rate is achieved but the code is not guaranteed to achieve full spatial diversity.

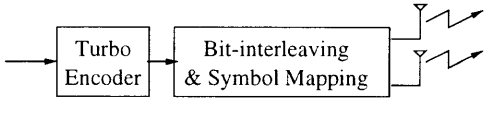

Figure 1.9 Turbo code with bit interleaving [48, 53].

In [45], serial concatenated turbo space-time code is presented for 4-PSK modulation as shown in Fig. 1.10. The outer encoder is a standard space-time code and a rate 1 recursive inner code is the inner code. This structure can achieve maximum possible rate, but it may result in codes without full spatial diversity since the interleavers are parallelly different for different transmit antennas.

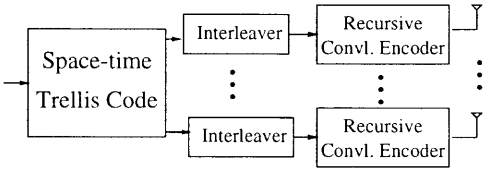

Figure 1.10 A space-time code is concatenated by rate 1 recursive code [45].

A 4-PSK full rate and full spatial diversity turbo space-time code has been introduced in [47] as shown in Fig. 1.11. This turbo code scrambles the multiple information bits input for different RSC encoders and can achieve full rate and full spatial diversity in a parallel concatenated structure. Although the authors claim "*robust performance*" over the fading channel, they recognize that the scheme may have convergence problems when both component STC outputs experience a deep fading at the same time.

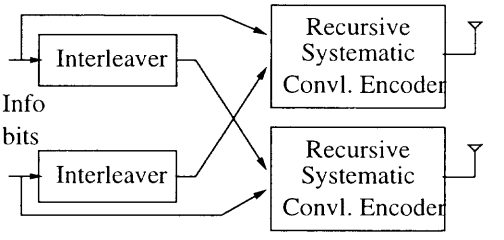

Figure 1.11 Space-time turbo code for two transmit antennas [47].

In this dissertation, a new turbo space-time code is suggested, referred to as "turbo-STCM". The work presented in this dissertation has been partially disseminated in our publications [49, 50, 51, 54, 52]. Our turbo-STCM scheme expands the turbo-TCM idea as shown in Fig. 1.3 [55] to multiantenna systems. The architecture

of the turbo-STCM is shown in Fig. 1.12. Recursive systematic space-time codes serve as component codes in the turbo-STCM. With this architecture, turbo codes and space-time codes are not concatenated but are rather *fused.*

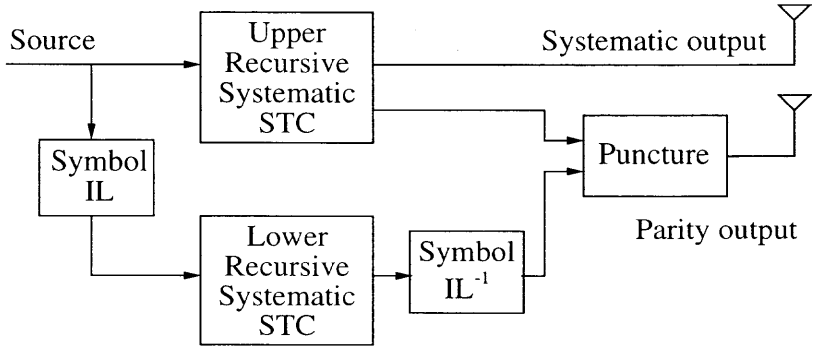

Figure 1.12 Turbo-STCM with component space-time codes [49, 50, 51, 52].

Turbo-STCM features full diversity and full coding rate. It combines the time domain turbo coding architecture in the temporal domain with spatial processing. Space-time constituent codes are connected parallelly rather than a concatenation of binary turbo codes and antenna diversity. An iterative symbol-by-symbol *maximum a posteriori* algorithm is developed for decoding turbo-STCM, which is different than other parallel schemes. In Chapter 3, the simulation results show its performance improvement than conventional STC or turbo-TCM [55] although keeping the similar decoding complexity of turbo-TCM. In terms of tradeoff between diversity advantage, transmit coding rate and decoding complexity, turbo-STCM has similar performance result with other modified turbo coding methods for multiple antenna systems [42, 43, 44, 45, 46, 47, 48]. Turbo-STCM can be viewed as an extension of the original turbo code in Fig. 1.1 [2] from the bit to the symbol level. In our view, turbo-STCM is a true generalization of the turbo coding scheme to include STC as component codes, rather than an ad-hoc concatenation of turbo and space-time codes.

1.4 Overview of Thesis

The first goal of this study is to propose a new coded modulation scheme that utilizes concatenated space-time codes with multilevel modulation and multiple transmit and receive antennas. Turbo-STCM is a bandwidth efficient coded modulation designed to operate over the fading channels. Our scheme is similar in complexity to other turbo space-time schemes proposed recently (for example, Narayanan [43], Fitz [47]), but it can be viewed as a more natural extension of classical turbo codes to multilevel signals and space-time processing. Unlike [42, 43, 44, 45, 48], our scheme ensures full spatial diversity and full coding rate. It is distinguished from other methods ([42, 43, 44, 45, 48]) by its parallel architecture and it features a different configuration and decoding algorithm from [47]. Turbo-STCM is presented as an improvement over conventional space-time codes.

A second goal of this thesis is to develop a theoretical performance analysis for turbo-STCM. In [56, 57], the union bound technique is developed for the error probability of turbo codes for multiantenna systems. The "uniform random interleaver" proposed in [56] overcomes analytical difficulties posed by the fixed interleaver structure. First, a union bound is found for the performance of turbo-STCM with suboptimal decoding over the AWGN channel with multiple transmit antennas [50]. This can be seen as an interim step that the bound is found first conditioned on the channel. Subsequently, the union bound analysis is extended over the block-fading channel [51, 52]. The bound makes it possible to express the performance analysis of turbo-STCM in terms of the constituent space-time code modules.

Outline

This Ph.D. dissertation is organized as follows. In Chapter 2, the space-time coding performance is studied from an information theoretic point of view, derive the frame error limit of multiantenna systems and develop the Fano lower bound of bit error probability with given transmission rate. In Chapter 3, we introduce the main

concept and schematic diagram of the proposed turbo-STCM system. An iterative symbol-by-symbol *maximum a posteriori* algorithm operating in the log domain is developed for decoding turbo-STCM. Some examples are given of 2 bits/s/Hz 4-PSK and 3 bits/s/Hz 8-PSK turbo-STCM. Numerical results illustrate that turbo-STCM schemes provide full spatial diversity and full rate. Two other aspects of turbo-STCM are also investigated: (1) recursive and non-recursive space-time constituent codes, (2) interleaver design. It is shown that this scheme provides performance improvement over conventional space-time codes of similar complexity. In Chapter 4, the union bound is derived for the performance of turbo-STCM schemes over the AWGN channel as a interim step. Using simple recursive systematic space-time component encoders, performance is studied by analysis for a 4-PSK and 8-PSK turbo-STCM with two transmit and one receive antenna over AWGN channel. After that, performance bounds are developed over the block-fading channels with two transmit and one/two receive antennas. Finally, in Chapter 5, we present the conclusions and suggest future research for turbo space-time coding.

CHAPTER 2

INFORMATION THEORY CONSIDERATION OF SPACE-TIME CODING

The next frontier in the development of wireless communications is the conversion from the current voice-based services to future high data rate applications such as the wireless internet. For example, sending video rather than speech requires the data rate to increase by two or three orders. Increasing link or channel bandwidth is a simple but costly and almost impossible approach. New powerful digital processing techniques will be the key to the success of this conversion. A more economical solution is to exploit spatial diversity and channel coding through multiple antennas at the transmitter and receiver. Traditionally, spatial processing has been designed separately from channel coding, e.g., equalizer and combining at receiver. An integrated design might have advantages over the conventional piecemeal approach. A step in this direction is the integration of spatial and temporal processing into what is now commonly referred to as space-time processing [23, 24, 26]. With space-time processing, it was recognized that a joint approach offers more benefits than temporal and spatial processing applied separately [18].

In this chapter, several theoretic concepts are computed to bound the performance of space-time systems. We begin with capacity and cut-off rate of multiple antenna systems over the AWGN channel. Then the outage capacity is considered for the fading channel [20]. Finally the Fano lower bound is derived over the Rayleigh fading channel for the relation between bit error probability and signal-to-noise ratio per information bits.

2.1 Coded Modulation System over the AWGN Channel

In an AWGN channel, antennas can be combined to increase effective transmit and receive antenna gain. Let us examine the channel capacity for a two transmit

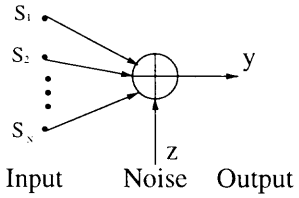

Figure 2.1 Block diagram of a multiantenna system over AWGN channel

antenna-single receive antenna (MISO) system as shown in Fig. 2.1. Assume that the source inputs μ bits are encoded by the error control code to generate codewords of nN bits, where N is the number of transmit antennas. We partition the nN bits output into N groups, which are mapped to the transmit signals s. The received signal y is the sum of the multiple inputs and noise,

$$y = \sum_{j=1}^{N} s_j + z \tag{2.1}$$

where s_j is the complex signal transmitted from antenna j. The total transmitted power is constrained to $P = E[\sum_{j=1}^{N} |s_j|^2]$ regardless of the number of transmit antennas N. The AWGN z is complex-valued with zero mean and variance $N_0/2$ per dimension.

We consider several channel capacity cases depending on the characteristic of the signal s_j.

Shannon capacity

In the most general case, the transmitted signals meet the requirement of the channel coding theorem [1]. Since the 2 transmit-1 receive antenna system is used in the band-limited channel with the new equivalent channel signal set and $N = 2$ sub-channels, the Shannon capacity limit [58, pp. 384] for 2-dimensional modulation should still be applied regardless of the antenna number and coding,

$$C_{shannon} = \log_2(1 + \frac{P}{N_0 W}) = \log_2(1 + \frac{\mu E_b}{N_0}) \tag{2.2}$$

where μ is the information bits per symbol, $E_s = \mu E_b$ and P, W, N_0 are the received signal power, channel bandwidth and noise power spectrum respectively.

Channel capacity of coded multiantenna system

Fig. 2.2 illustrates that the transmit diversity can be expressed by an equivalent channel signal set for the received signal y. s_j is the 4-PSK signals across $N = 2$ transmit antennas. Although the total transmit power P that is radiated is unchanged as N increases, it appears that one ultimately achieves the equivalent of $N = 2$ sub-channels. The received signal y can be viewed in the new channel signal set with 16 points in the constellation. Total signal power of transmit signal is assumed to be normalized and the signal-to-noise ratio at the receiver SNR$= 1/N_0$.

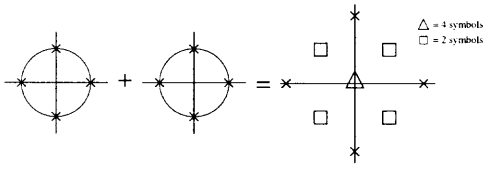

Figure 2.2 Channel signal set over the AWGN channel.

The capacity formula (Ungerboeck [9, (5)]) is applied from one transmit-one receive antenna (1T1R) to two transmit-one receive antenna (2T1R). As shown in Fig. 2.2, the received signal set has $\Omega = 16$ elements. The channel output signals $(y_1, \cdots, y_\Omega)$ are sums of pairs of transmitted 4-PSK signals. Note that they are ambiguous in the output signal constellation in the sense that multiple pairs of 4-PSK signals yield the same output. Let us further assume that the input signals are equiprobable, $P(s_j) = 1/4, j = 1, \cdots, 4$. Then it is shown that the channel capacity is given by,

$$C = \log_2(\Omega) - \frac{1}{\Omega}\sum_{k=1}^{\Omega} \mathbf{E}_z\{\log_2 \sum_{i=1}^{\Omega} \exp[-\frac{\|y_k + z - y_i\|^2 - \|z\|^2}{N_0}]\}, \qquad (2.3)$$

where $\mathbf{E}_z$ is the expectation over the normally distributed noise variable z. The channel capacity C is evaluated by Monte Carlo simulation of (2.3). Later there are the plot of the capacities $C_{shannon}$ and C as a function of signal-to-noise ratio per information bit for the signal sets depicted in Fig. 2.2.

Cut-off rate of coded modulation system

The reliable transmission close to Shannon capacity is possible only for very large temporal redundancy and very large encoding/decoding complexities. Often, the cut-off rate R_0 [3, pp. 522] is a function of transmission rate R and error probability $P(e) \leq 2^{-n(R_0-R)}$, $R \leq R_0$, where n is the data block length. Cut-off rate is used as a measure for a practical bound to the transmission rate. It is widely assumed that capacity becomes very expensive beyond the cut-off rate. However, the recent discovery of turbo codes [2] that admit a practical decoding algorithm and hence have performance close to capacity has somewhat diminished the importance of R_0 as a performance parameter.

Let us follow the above example of coded modulation system with 2 transmit antennas, when the signals $s_j, j = 1, 2$ are transmitted from the j transmit antenna over the AWGN channel with the equal probabilities q, the received signal y is located in the constellation of Fig. 2.2. From [59, pp. 29], the cut-off rate for a multiantenna system over the AWGN channel can be expressed,

$$R_0 = \log_2(\Omega) - \log_2 \frac{1}{\Omega} \sum_{k=1}^{\Omega} \sum_{i=1}^{\Omega} \exp[-\frac{\|y_k - y_i\|^2}{4N_0}] \tag{2.4}$$

Fig. 2.3 shows the Shannon capacity (2.2), channel capacity (2.3) and the cutoff rate (2.4) versus signal-to-noise ratio per information bit E_b/N_0 (dB) for 4-PSK, the two transmit-one receive antenna configuration (labeled as 2T1R). When the capacity C and cutoff rate R_0 equal to 2 bits/s/Hz, the corresponding signal-to-noise ratio per information bit E_b/N_0 are 2.1 dB and 4.4 dB, respectively. Those results will be used for comparison to turbo-STCM over the AWGN channel in a later

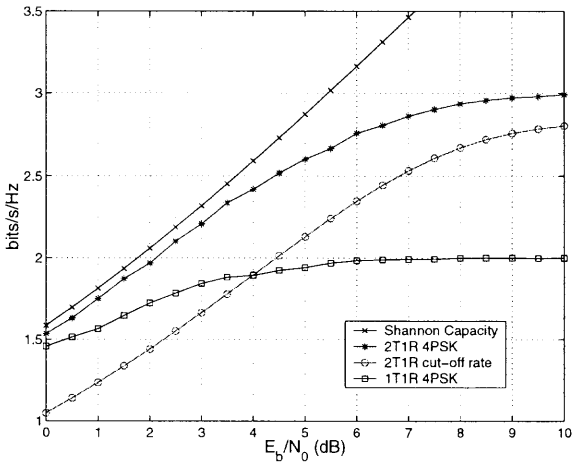

Figure 2.3 Capacity and cut-off rate of multiantenna system.

chapter. The capacity of 4-PSK, the two transmit-one receive antenna configuration (1T1R) (Ungerboeck [9, (5)]) is also shown for comparison. At bandwidth efficiency 2 bits/s/Hz over the AWGN channel, the two transmit antenna-one receive antenna (2T1R) configuration has an almost 5 dB advantage than 1T1R case. That shows us that expanding signal in spatial domain instead of temporal domain is also an effective way to increase channel capacity. The curves show the transmission rate bound before considering different coded modulation designs with *finite complexity.*

2.2 Outage Capacity of Multiantenna Systems over the Fading Channel

In [17, 18], multiple antenna arrays are shown to improve the performance of a wireless communication system in a fading environment. Antenna arrays may be employed either at the transmitter or the receiver. Traditionally, transmit diversity was viewed as more difficult to exploit than receiver diversity because the transmitter is assumed to know less about the channel than the receiver.

Multiple transmit and receive antennas allow a signal space having higher dimensionality without a commensurate increase in bandwidth [20, 19, 27, 60]. In a Rayleigh block-fading channel [39], a memoryless wireless link employing multi-

antenna has a theoretical capacity that increases linearly with the number of transmit and receive antennas, providing that the complex-valued channel coefficients between all pairs of transmit and receive antennas are statistically independent and known to the receiver (not the transmitter). This independence of the coefficients provides spatial diversity, and can be achieved by physically separating antennas at the transmitter and receiver by a few wavelengths.

Main results of limits of bandwidth efficient delivery of information are obtained in [20]. For a multiple-input multiple-output (MIMO) channel represented by the $M \times N$ matrix $\mathbf{H}$ where N and M are the number of transmit and receive antennas, the capacity of a multiantenna wireless system over fading channel is given by

$$C = W \log_2 \det \left(\mathbf{I} + \frac{E_s}{N N_0} \mathbf{H}\mathbf{H}^\dagger \right) \quad \text{bits/s.} \tag{2.5}$$

Where $\mathbf{I}$ is the identity matrix with dimension M, W is the channel bandwidth. Overall transmitted power is fixed and independent of transmit antenna number N, so that as N increases, the constant total power P will be distributed more thinly among the antenna elements. This allows us to distinguish the impact of varying transmit antenna number N from the total transmitted power P. In [19], computing the outage capacity of MIMO fading channel involves finding the joint SISO subchannels limits that maximizes the mutual information between the N transmit and M receive antennas. E_s/N_0 is the average signal-to-noise ratio measured at each receiver branch, and the superscript † denotes matrix transpose and conjugate. Since the channel coefficients of $\mathbf{H}$ are random variables, the capacity C is modeled likewise. The outage capacity is defined as the capacity value C_{out} such that $C \geq C_{out}$ with a specified probability threshold.

Shannon's capacity over the AWGN channel indicates that in the high sign-to-noise ratio (SNR), a 3 dB increase in SNR is worth about one more bit/s/Hz of capacity. In the block-fading channel with two transmit and multiple receive antennas, Fig. 2.4 illustrates 99% outage capacity C of (2.5) versus SNR= E_s/N_0.

For large M receive antennas, for example $M = 10$, every 6 dB increase in SNR achieves $min(N, M) = 2$ more bits/s/Hz [61]. The outage capacity demonstrates significantly higher spectral efficiencies (bits/s/Hz) than are possible when multipath channel is traditionally viewed as an impairment for data transmission [20].

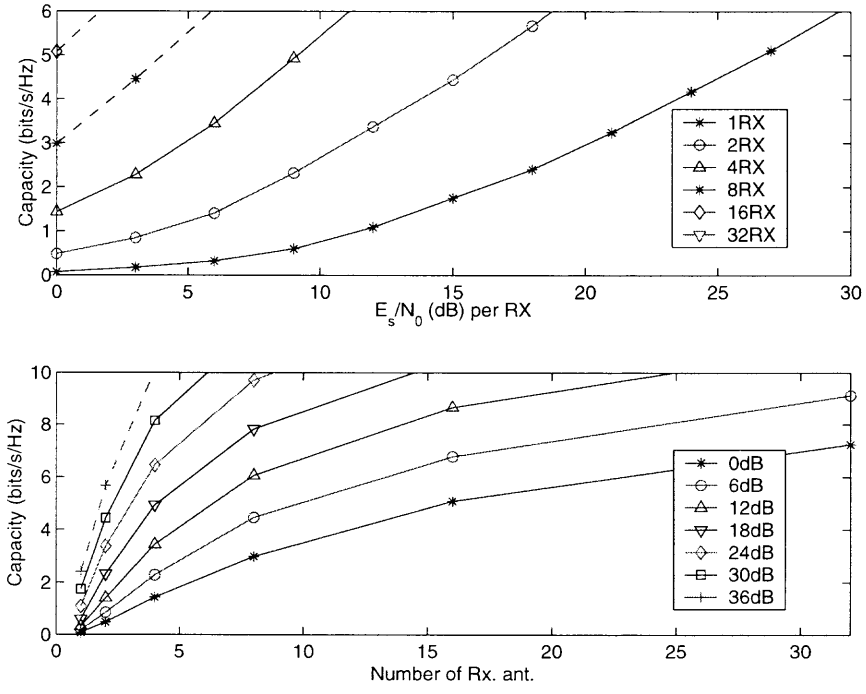

Figure 2.4 Capacity of two transmit and multiple receive antenna system.

2.3 Frame Error Limit of Multiantenna System

A block-fading channel [39] is assumed to be random from frame to frame but constant during the transmission of each frame. The channel is further assumed to be known at the receiver and unknown at the transmitter. The transmitter can send training signals that allow the receiver to estimate the channel propagation coefficients accurately, and the result of (2.5) is applicable.

The outage capacity of (2.5) can be viewed as the probability that the spectral efficiency (bits/s/Hz) is not supported by the block-fading channels $\mathbf{H}$. Outage capacity is treated as a random variable. For example, the outage probability

$P_{outage} = 1\%$ corresponds to frame error rate (FER) is 10^{-2}. The outage capacity for this case is the point of the 99 percentage on the complementary cumulative distribution function of outage capacity.

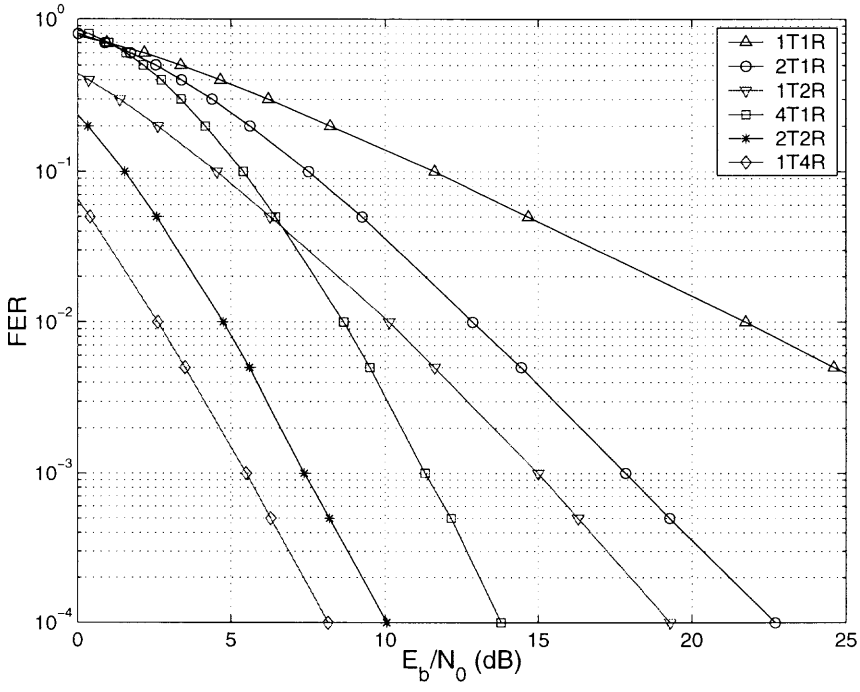

Figure 2.5 FER plot for multiantenna system.

Fig. 2.5 shows us the relation of frame error rate and minimum required signal-to-noise ratio per information bit E_b/N_0 for a 2 bits/s/Hz multiantenna system over the fading channel. It also illustrates that space-time coding provides full spatial diversity. For example, the asymptotic slope (at high SNR per symbol) of the FER curve is 4 dB/dB for two antennas at each end (2T2R) [31, 41]. The asymptotic diversity of the other curves is also as expected: 1 dB/dB for the single antenna configuration (1T1R), 2 dB/dB for the two transmit-one receive antenna configuration (2T1R) and one transmit-two receive antennas configuration (1T2R) whose advantage over 2T1R is exactly 3 dB due to the normalized transmitted power, and 4 dB/dB for four transmit-one receive antenna configuration (4T1R) and one transmit-four receive antennas configuration (1T4R). Those results will be applied in the next

chapter to demonstrate that the spatial diversity of turbo-STCM is the same as the spatial diversity of conventional space-time codes.

From the recent results of information theory [62, 63], the space-time block codes are one kind of STC with extremely low encoder/decoder complexity and provision of full diversity [33, 34]. However, their simple implementation comes at a cost in capacity loss. The loss is significant at SNR's of interest for very small numbers of receive antennas. In this thesis, the recursive systematic space-time codes are considered for turbo component encoders.

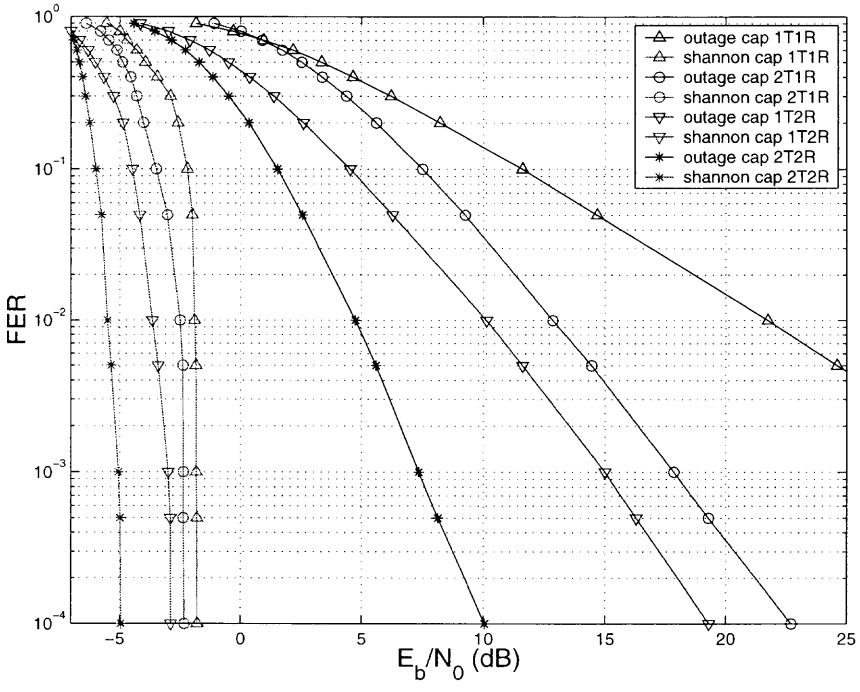

Figure 2.6 Comparison of outage and Shannon capacity.

Fig. 2.6 shows us the comparison of outage and Shannon capacity for a 2 bits/s/Hz multiantenna system over the fading channel. As we know, the multipath fading capacity is treated here as a random variable. Shannon capacity is the mean value of those multipath fading capacity set for each E_b/N_0. From the figure, Shannon capacity shows much lower minimum required E_b/N_0 than outage capacity. It is because its mean value can be viewed roughly as outage probability $P_{outage} = 50\%$,

which means half of the channel realizations can not promise spectral efficiency of 2 bits/s/Hz. Shannon lower bound is a kind of real lower limit while outage capacity shows us a more practical way to analyze the multipath fading channel.

2.4 Fano Lower Bound of Multiantenna System

Applying Fano's Inequality for a digital communication, a lower bound of bit error probability can be expressed as in [3, pp. 139],

$$P_b(e) \geq H_b^{-1}(1 - \frac{C}{r_c}) \tag{2.6}$$

where $H_b(e)$ is the entropy of a binary alphabet with bit error probabilities $P_b(e)$ and $1-P_b(e)$, i.e., $H_b(e) \triangleq -P_b(e)\log P_b(e) - [1-P_b(e)]\log[1-P_b(e)]$. C is system capacity defined as the maximum mutual information. The encoding rate r_c is defined as the ratio of input bits μ and output bits n.

This lower bound shows that there exists a lower bound to the bit error probability, different to zero, when the encoding rate r_c is greater than the channel capacity C. This is the "negative" result known as the converse to the channel coding theorem, which dictates the system behavior when the coding rate r_c is smaller than capacity C [1]. The inequality directs us to improve the performance of a digital communication system by increasing n but keep the coding rate r_c fixed. This approach does not require additional SNR and bandwidth. It simply increases the length of the codewords, at the expense of greater complexity of the encoder-decoder and of a longer signal processing delay. Turbo codes act in this way to improve performance.

In this section, the Fano inequality is further applied for the multiple input multiple output (MIMO) system over the block-fading channel. Suppose that the channel has bandwidth W. The noise is white Gaussian random variables, with two-sided power spectral density $N_0/2$. Thus the noise $\mathbf{z}$ has power $N_0/2 \cdot 2W = N_0 W$.

Since there are 2W samples each second, the outage capacity (2.5) of the MIMO channel is given by,

$$C = \frac{1}{2}\log_2 \det\left(\mathbf{I} + \frac{P}{N_0 W N}\mathbf{H}\mathbf{H}^\dagger\right) \text{ bits/s/Hz.} \tag{2.7}$$

where N is the transmit antenna number.

Define the information source rate r_s in bit/second and *energy per information bit* $E_b \triangleq P/r_s$ of a transmitter with total power P.

Substituting E_b into (2.7),

$$C = \frac{1}{2}\log_2 \det\left(\mathbf{I} + \frac{E_b r_s}{N_0 W N}\mathbf{H}\mathbf{H}^\dagger\right) \text{ bit/sample.} \tag{2.8}$$

Putting channel bandwidth $W = r_s/2r_c$ in (2.8),

$$C = \frac{1}{2}\log_2 \det\left(\mathbf{I} + \frac{2r_c E_b}{N_0 N}\mathbf{H}\mathbf{H}^\dagger\right) \text{ bits/s/Hz.} \tag{2.9}$$

Finally, by means of (2.6) and (2.9),

$$H_b(e) \geq 1 - \frac{1}{2r_c}\log_2 \det\left(\mathbf{I} + \frac{2r_c}{N} \cdot \frac{E_b}{N_0}\mathbf{H}\mathbf{H}^\dagger\right) \tag{2.10}$$

where E_b/N_0 (dB) is signal to noise ratio per information bit for a given coding rate r_c. With equality substituted for the inequality, (2.10) yields the relationship between the bit error probability and the signal-to-noise ratio per information bit. (2.10) is a non-linear function of bit error probability $P_b(e)$ versus E_b/N_0 without close-form mathematic solution. However, we can run the Monte Carlo analysis to find the $(P_b(e), E_b/N_0)$ for different conditions, such as multiple transmit and receive antennas (N, M).

In Fig. 2.7, there are the curves of $(P_b(e), E_b/N_0)$ for a 2 bits/s/Hz multiantenna system of different antenna configurations $N = 1, 2, 3, 4, M = 1, 2$. It points the Fano lower bound for space-time codes over the block-fading channel. For a given coding rate, the region above the respective curves is possible, that is, any space-time coding system can approach this lower bound with large complexity. It can

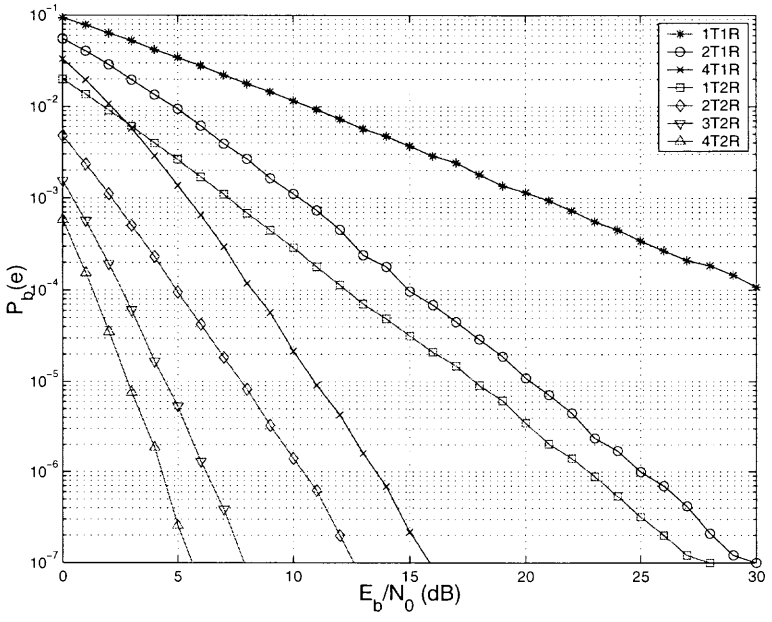

Figure 2.7 Fano lower bound of block-fading channel with multiple transmit and receive antennas.

be observed that multiple antennas at transmitter can improve system performance in spite of transmit power penalty per antenna. Fig. 2.7 also proves the spatial diversity advantage of space-time coding, in the exponential decrease of decoding bit error rate versus signal-to-noise ratio. For example, four transmit-one receive antenna configuration (4T1R) has the same spatial diversity as two transmit-two receive antenna configuration (2T2R), while their difference of E_b/N_0 is equal to 3 dB because of fixed transmit power. The Fano bound actually directs us to the reasonable region in which we can design the space-time processing technique.

2.5 Chapter Summary

In this chapter, the information theoretic limits of MIMO systems are considered over the AWGN and block-fading channel and also derive the Fano lower bound over the MIMO channel with multiantenna system. To achieve the projected capacity of the MIMO multipath channel, it is necessary to combine coding and spatial processing.

In the next Chapter, we will propose turbo-STCM merging turbo coding and space-time code, and also compare the simulation results of our proposed turbo-STCM schemes with the frame error rate limits as in Fig. 2.5 and bit error rate of Fano lower bound Fig. 2.7.

CHAPTER 3

TURBO SPACE-TIME CODED MODULATION

In this chapter, our turbo-STCM system is introduced, which combines the coding gain of turbo codes and spatial diversity advantage of space-time codes together. It is a promising way to obtain high bandwidth efficiency in wireless communications. We first present in detail of turbo-STCM encoder and decoder as well as the block diagram of the system transmission. A suboptimal iterative decoding algorithm is developed for turbo-STCM decoder. Several other important aspects of turbo-STCM are also discussed such as recursive systematic component encoders, interleaver design. Then the Monte Carlo simulations are illustrated for the performance of 4-PSK and 8-PSK turbo-STCM.

3.1 Turbo-STCM System Description

Turbo-STCM is presented as an improvement of conventional STC. In this subsection, we will explain why the constituent codes of turbo-STCM are the recursive systematic space-time codes. Then the turbo-STCM encoder and decoder are presented as well as the signal model of turbo-STCM transmission system. Also one important aspect of turbo code: interleaver design is discussed.

3.1.1 Recursive Systematic Space-Time Constituent Codes

Recursive systematic component codes are often encountered in turbo code applications. The component space-time codes are defined by the diagrams and trellis codes shown in the following figures. Turbo-STCM uses recursive systematic space-time codes as constituent codes. The recursive systematic 4 state 4-PSK STC in Fig. 3.1 and 8 state 4-PSK STC in Fig. 3.2 are provided for two transmit antennas with code implementation and trellis transitions. In this chapter, a recursive systematic 16 state 8-PSK STC is also considered as shown in Fig. 3.3.

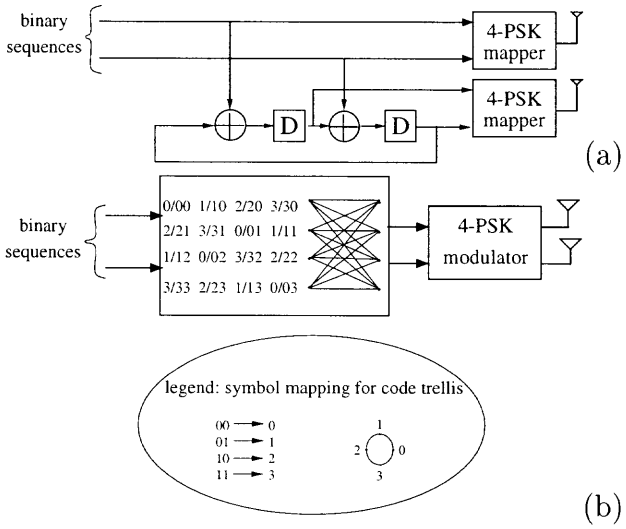

Figure 3.1 Recursive systematic space-time encoder for 4 state 4-PSK, two transmit antennas, 2 bits/s/Hz: (a) code implementation, (b) code trellis.

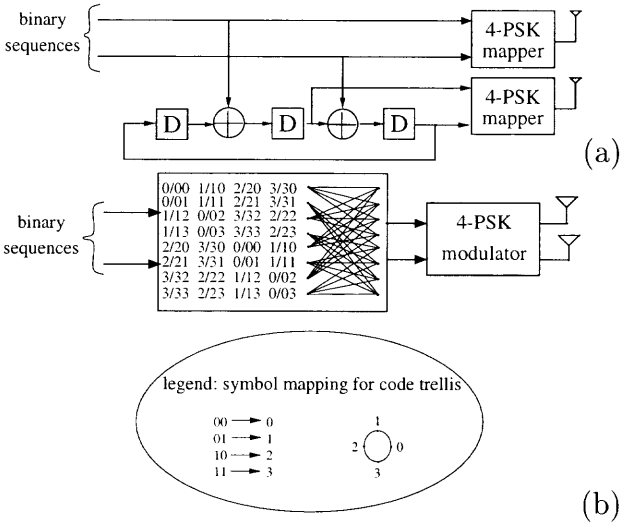

Figure 3.2 Recursive systematic space-time encoder for 8 state 4-PSK, two transmit antennas, 2 bits/s/Hz: (a) code implementation, (b) code trellis.

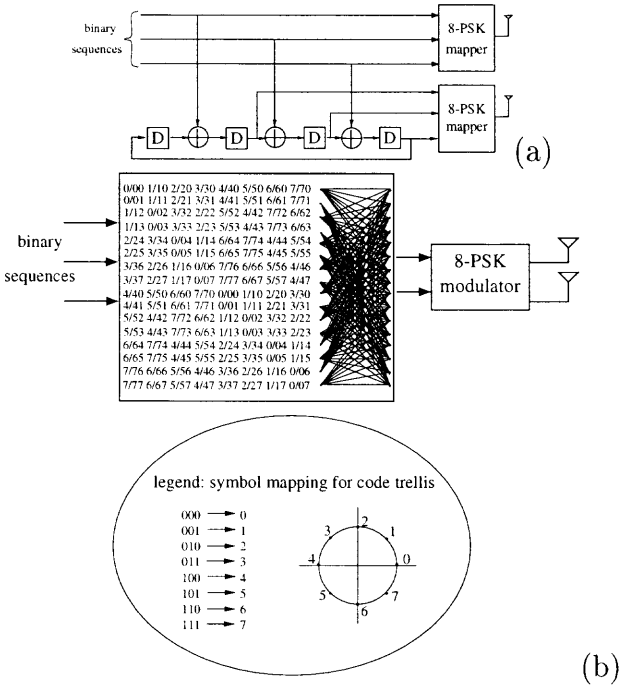

Figure 3.3 Recursive systematic space-time encoder for 16 state 8-PSK, two transmit antennas, 3 bits/s/Hz: (a) code implementation, (b) code trellis.

Why we use recursive systematic constituent code

Just as convolutional code can be made systematic without reducing the minimum free distance [59] and systematic codes are always non-catastrophic, so can STC also be made systematic. The systematic form for the component codes is dictated by the required separation and transmission through different antennas of the systematic and parity data. The systematic structure is further motivated by the need to puncture the parity data of the turbo code such that the data rate of the overall code is the same as that of the constituent codes. Note that STC encoders are considered to have full coding rate if the number of overall output bits $N\mu$ equals N times the number of input bits μ at time slot, where N is the number of transmit antennas. The requirements of recursive and systematic constituent codes cannot be satisfied by the feed-forward space-time codes, i.e., non-recursive systematic 4 state 4-PSK space-time code (Fig. 3.4), non-recursive non-systematic 8 state 4-PSK

space-time code (Fig. 1.5) that appear in literature [31, pp. 752] and [40], hence we had to design our own codes. A recursive systematic space-time codes is shown in Fig. 3.1. Since recursive component encoders should be considered for turbo codes, some numerical examples of turbo-STCM also prove this issue later as published in [64, 52].

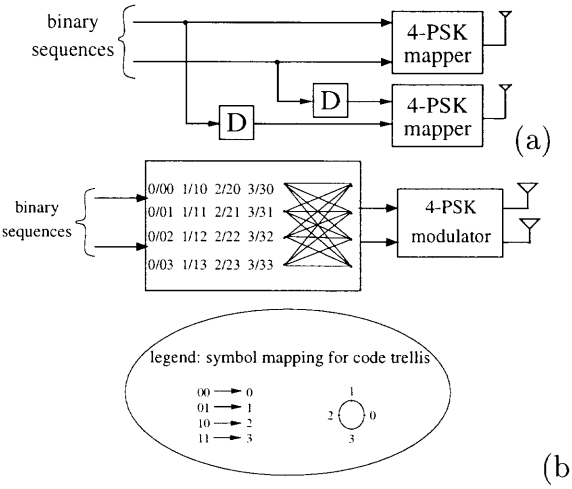

Figure 3.4 Non-recursive systematic space-time encoder for 4 state 4-PSK, two transmit antennas, 2 bits/s/Hz: (a) code implementation, (b) code trellis.

3.1.2 Turbo-STCM Encoder

Turbo-STCM consists of two (or more) space-time codes in recursive systematic form concatenated in parallel. An 8 state 4-PSK recursive systematic space-time encoder is shown in Fig. 3.2. The systematic and recursive nature of the constituent code is clearly seen in part (a) of Fig. 3.2. The input/output state transition labels and the symbol mapping used in the diagram are shown in part (b) of the figure. For example, the label '3/30' appears twice. It is to be interpreted as follows: case #1, state 1 transitions to state 4 when the input is '3' (i.e., '11' - see mapping in the figure), with the output consisting of symbols '3' to antenna 1 (systematic part) and symbol '0' to antenna 2 (parity part); case #2, same as #1, but the transition is from state 5 to state 2. The constituent code is recursive following Benedetto and

Montorosi [56], who have shown that turbo codes require recursive constituent codes to work properly. The systematic form of the constituent codes is motivated by the architecture of our turbo-STCM, where one antenna transmits symbols mapped by the systematic bits, and the other antenna transmits symbols mapped by the parity bits. This architecture provides a simple mechanism for puncturing of the parity data in order to maintain full rate. As shown in the simulations later in this chapter, our designed constituent codes feature full diversity, but lower gain than the non-systematic STC in the references [31, 40]. However, it will be shown that after several turbo iterations, the performance exceeds that of other space-time codes. The turbo-STCM architecture is shown in Fig. 3.5. A pseudorandom symbol-wise bit interleaver between the space-time encoding modules operates on groups of bits associated with symbols to ensure that the transmitted data stream possesses random-like properties. The interleaver size is K symbols. For 4-PSK modulation this corresponds to $2K$ bits and $3K$ bits for 8-PSK.

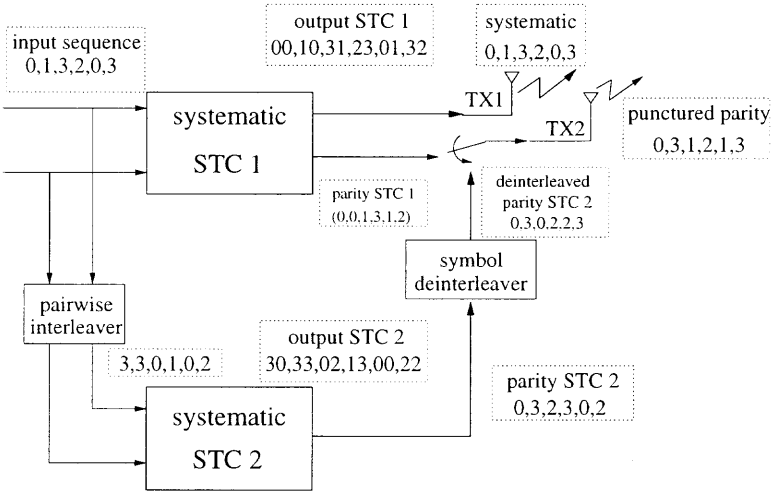

Figure 3.5 Turbo-STCM encoder for two transmit antennas, 2 bits/s/Hz.

The integration of space-time encoders into turbo-STCM is similar to the integration of coded modulation into the turbo-TCM structure of [15]. There are some important differences between the binary turbo codes in [2] and turbo-STCM:

(1) the constituent space-time codes need to be systematic at the symbol level rather than the bit level, (2) the interleaver operates symbol-wise (for example, with 4-PSK modulation the interleaver operates on pairs of bits). In addition, turbo-STCM is different from turbo-TCM in [15] in that the output consists of multiple streams of symbols that are being transmitted through multiple antennas. Multiple antennas may also be employed at the receiver.

Consider a wireless data system that employs turbo-STCM to transmit data through N transmit antennas. For clarity, it is based on a specific example of the 8 state 4-PSK space-time code shown in Fig. 3.2. The input to each constituent code consists of pairs of bits and the output is formed by $N = 2$ streams of 4-PSK symbols. For a specific example, assume a short sequence of six pairs of bits. In practice, sequences will be much longer such that the output of the interleaver is pseudo-random with respect to its input symbol sequence. Assume that the data block to be transmitted consists of the following pairs of bits: $(00, 01, 11, 10, 00, 11)$. For brevity of notation, the signal mapping is used in Fig. 3.2(b) to list the input sequence in terms of four level symbols $(0, 1, 3, 2, 0, 3)$. Let STC1 and STC2 denote the constituent codes. Then the output of STC1 consists of the sequence of pairs of 4-PSK symbols $(00, 10, 31, 23, 01, 32)$. Prior to being fed to STC2, the input sequence is interleaved by a pairwise bit interleaver. Let the interleaver output be $(3, 3, 0, 1, 0, 2)$. When this sequence is fed to STC2, the output is given by $(30, 33, 02, 13, 00, 22)$. The output of STC2 is then de-interleaved to ensure matching of the systematic parts at the output of each STC (i.e., the first of each pair of symbols). With that in mind, transmission of the systematic part can be accomplished by STC1 only. Both STC1 and STC2 transmit parity symbols. The deinterleaver can be applied only to the parity symbol at STC2's output. Following the deinterleaver, the parity symbol sequence becomes: $(0, 3, 0, 2, 2, 3)$. Antenna 1, which transmits the systematic part of the codeword, is connected only to STC1. A selector alternately selects the

output of STC1 or the deinterleaved output of STC2. Thus, the symbol sequences transmitted by the two antennas are $(0, 1, 3, 2, 0, 3)$ and $(0, 3, 1, 2, 1, 3)$, respectively. This arrangement ensures that the 4-PSK symbols are transmitted systematically and that the parity symbols are alternately chosen from STC1 and STC2.

3.1.3 System Model

In this subsection, the schematic diagram of the turbo-STCM transmission system is presented as shown in Fig. 3.6.

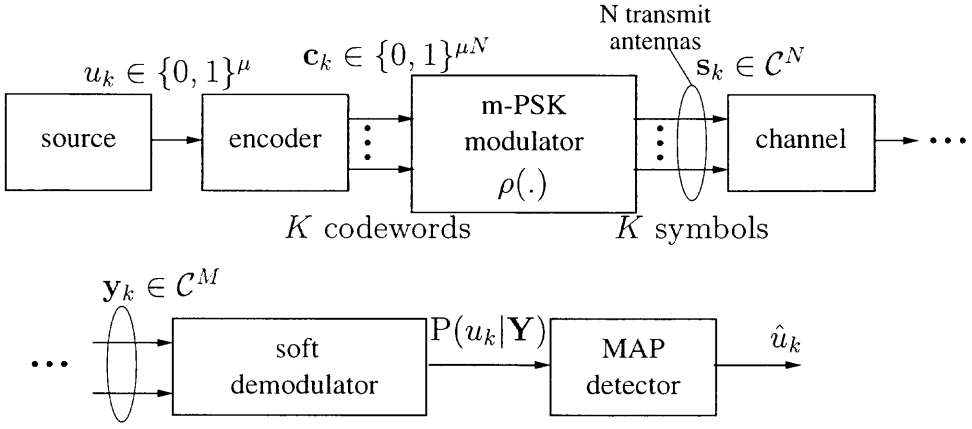

Figure 3.6 Schematic diagram of turbo-STCM transmission system.

Let a source generate an information sequence composed of symbols u drawn from an alphabet $\left\{u^{(1)}, \ldots, u^{(m)}\right\}$. Using k to denote the time index, each symbol u_k consists of $\mu = \log_2 m$ bits, i.e., $u_k \in \{0,1\}^{\mu}$. With Ungerboeck codes [12, 13], the μ input bits generate $\mu + 1$ coded bits that are then mapped to a symbol. With STC codes, the μ input bits are encoded into N groups of μ bits, where N is the number of transmit antennas. Similarly, turbo-STCM encodes the information symbols u_k to N symbols represented by the binary column vectors $\mathbf{c}_k^{(n)} \in \{0,1\}^{\mu}$, $n = 1, \ldots, N$. Those are fed into a memoryless mapper $\rho(\cdot)$ that emits the symbols $s_k^{(n)} = \rho\left(\mathbf{c}_k^{(n)}\right)$. In this Ph.D. thesis, $s_k^{(n)}$ are m-PSK symbols. Define the symbol vector $\mathbf{s}_k \in \mathcal{C}^N$, $\mathbf{s}_k = \left[s_k^{(1)} \ldots s_k^{(N)}\right]^T$, where $\mathcal{C}$ is a complex set of signal constellation points and the

superscript denotes transposition. Define the column vector with binary elements $\mathbf{c}_k \in \{0,1\}^{\mu N}$, $\mathbf{c}_k = \left[\mathbf{c}_k^{(1)} \ldots \mathbf{c}_k^{(N)}\right]^T$; then $\mathbf{s}_k = \rho(\mathbf{c}_k)$. The vector $\mathbf{c}_k$ is the binary label of $\mathbf{s}_k$. For an interleaver of size K (applied to input symbols), turbo-STCM transmits codewords of NK symbols (K symbols per antenna). The vector of binary labels $\mathbf{c}_k$ represents N output symbols and consists of μN bits. Hence, K input symbols correspond to NK output symbols and to μNK binary labels. The number of possible transmitted sequences is $2^{\mu NK}$.

For a turbo-STCM receiver utilizing an array of M antennas, the MIMO channel output symbols are represented by $M \times 1$ vectors $\mathbf{y}_k \in \mathcal{C}^M$ that can be expressed

$$\mathbf{y}_k = \sqrt{E_s}\mathbf{H}\mathbf{s}_k + \mathbf{z}_k, \tag{3.1}$$

where E_s is the energy per symbol, related to the energy per bit by $E_s = \mu E_b$. The $M \times N$ matrix $\mathbf{H}$ consists of the channel coefficients. The m, n element of $\mathbf{H}$, h_{mn}, represents the path gain from transmit antenna n to receive antenna m. The channel is assumed flat, Rayleigh and block-fading. This means that the matrix $\mathbf{H}$ consists of complex-valued scalars h_{mn} modeled as zero-mean, mutually independent, identically distributed Gaussian random variables with unity variance such that $E\left[h_{mn}h_{pq}^*\right] = \delta_{mp}\delta_{nq}$, where δ is the Kronecker symbol. Additive white Gaussian noise is modeled by the vector $\mathbf{z}_k$. The noise is assumed complex-valued, Gaussian distributed with zero-mean and variance $N_0/2$ for each dimension. The components of the noise vector are assumed independent and identically distributed.

Two different frame lengths play roles in our analysis. A frame length of F symbols is defined consistent with practical wireless systems. Later computer simulations for frame error rate (FER) analysis were run with a frame length of $F = 130$ symbols. The frame length F is also used in defining the block-fading channel: the channel is assumed fixed during a frame and independent frame to frame. The other frame length used in the thesis is related to the interleaver size.

Interleavers used in this thesis are of size $K = 130, 1300$ and 5200 symbols, respectively. The turbo decoder operates on sequences of received data of the same size as the interleaver. Since a turbo-code can be viewed as a block code with block length equal to the interleaver size, blocks of K symbols are used in the bit error analysis of next Chapter.

3.1.4 Full Diversity of Turbo-STCM Component Codes

In this subsection, there are the proof of the diversity order of the 4-PSK recursive systematic space-time codes. One is 4 state in Fig. 3.1 and another is 8 state in Fig. 3.2. Those codes are used as components of turbo-STCM with two transmit-one receive antenna. Define the code matrix $C(\underline{\mathbf{s}}_F)$ corresponding to a sequence of F arbitrary transmitted symbols

$$C(\underline{\mathbf{s}}_F) = \begin{bmatrix} s_1^{(1)}, & s_2^{(1)}, & \dots & s_F^{(1)} \\ s_1^{(2)}, & s_2^{(2)}, & \dots & s_F^{(2)} \end{bmatrix}, \tag{3.2}$$

where The symbol $s_k^{(1)}$ emitted by antenna 1 at time k, represents systematic information, while symbol $s_k^{(2)}$ transmitted by antenna 2 is the parity data. Consider the difference matrix $B(\underline{\mathbf{s}}_F, \underline{\mathbf{t}}_F) = C(\underline{\mathbf{s}}_F) - C(\underline{\mathbf{t}}_F)$ corresponding to a pair of distinct sequences $\underline{\mathbf{s}}_F$ and $\underline{\mathbf{t}}_F$. For full diversity, it is required that for any pair of distinct sequences the matrix $B(\underline{\mathbf{s}}_F, \underline{\mathbf{t}}_F)$ must have rank 2 [31]. Equivalently, it is necessary to prove that the rows of $B(\underline{\mathbf{s}}_F, \underline{\mathbf{t}}_F)$ are linearly independent for any distinct pair of sequences. The rows of $B(\underline{\mathbf{s}}_F, \underline{\mathbf{t}}_F)$ are linearly independent if and only if the determinant of the Gram matrix $B(\underline{\mathbf{s}}_F, \underline{\mathbf{t}}_F) B^H(\underline{\mathbf{s}}_F, \underline{\mathbf{t}}_F)$,

$$B(\underline{\mathbf{s}}_F, \underline{\mathbf{t}}_F) B^H(\underline{\mathbf{s}}_F, \underline{\mathbf{t}}_F) = \begin{bmatrix} \sum_{k=1}^{F} \left| s_k^{(1)} - t_k^{(1)} \right|^2 & \sum_{k=1}^{F} \left(s_k^{(1)} - t_k^{(1)} \right)^* \left(s_k^{(2)} - t_k^{(2)} \right) \\ \sum_{k=1}^{F} \left(s_k^{(1)} - t_k^{(1)} \right) \left(s_k^{(2)} - t_k^{(2)} \right)^* & \sum_{k=1}^{F} \left| s_k^{(2)} - t_k^{(2)} \right|^2 \end{bmatrix} \tag{3.3}$$

is non-zero [65, pp. 26].

4 state 4-PSK space-time code

As shown in Fig. 3.1, if the paths corresponding to sequences $\underline{\mathbf{s}}_F$ and $\underline{\mathbf{t}}_F$ diverge at time k_1, then by inspection, $s_{k_1}^{(1)} - t_{k_1}^{(1)} \neq 0$ and $s_{k_1}^{(2)} - t_{k_1}^{(2)} = 0$. Now consider the

differences at time k_1+1, $s_{k_1+1}^{(1)} - t_{k_1+1}^{(1)} \neq 0$ and $s_{k_1+1}^{(2)} - t_{k_1+1}^{(2)} \neq 0$. So that the determinant of Gram matrix can be zero if and only if $\left|s_{k_1+1}^{(2)} - t_{k_1+1}^{(2)}\right|^2 = 0$, which contradicts the assumption of divergence at time k_1.

This shows the rank of the Gram matrix $B\left(\underline{\mathbf{s}}_F, \underline{\mathbf{t}}_F\right) B^H\left(\underline{\mathbf{s}}_F, \underline{\mathbf{t}}_F\right)$ is two and hence that the recursive systematic 4 state 4-PSK space-time codes used as components in turbo-STCM feature full diversity.

8 state 4-PSK space-time code

As shown in Fig. 3.2, if the paths corresponding to sequences $\underline{\mathbf{s}}_F$ and $\underline{\mathbf{t}}_F$ diverge at time k_1, then by inspection, $s_{k_1}^{(1)} - t_{k_1}^{(1)} \neq 0$ and $s_{k_1}^{(2)} - t_{k_1}^{(2)} = 0$. Now consider the differences at time k_1+1. From Figure 1, note that if the divergence occurred at any of the states 1, 3, 5, or 7, then at time k_1+1 each diverging sequence will reach one of the states 1-4 (not the same state for both sequences). Similarly, if the divergence occurred at one of the states 2, 4, 6, or 8, then at time k_1+1 the diverging sequences will reach one of the states 5-8. We observe that for paths leaving two distinct states in any of the groups of states 1-4 or 5-8, $s_{k_1+1}^{(2)} - t_{k_1+1}^{(2)} \neq 0$. The preceding argument guarantees that $\sum_{k=1}^{F} \left|s_k^{(1)} - t_k^{(1)}\right|^2 > 0$, $\sum_{k=1}^{F} \left|s_k^{(2)} - t_k^{(2)}\right|^2 > 0$. With respect to $s_{k_1+1}^{(1)} - t_{k_1+1}^{(1)}$, there are two distinguished cases:

1. $s_{k_1+1}^{(1)} - t_{k_1+1}^{(1)} = 0$, then $\sum_{k=k_1}^{k_1+1} \left(s_k^{(1)} - t_k^{(1)}\right)^* \left(s_k^{(2)} - t_k^{(2)}\right) = 0$, and the determinant of the Gram matrix cannot be zero for any $F \geq 2$.

2. $s_{k_1+1}^{(1)} - t_{k_1+1}^{(1)} \neq 0$, then the determinant can be zero if and only if $\left|s_{k_1}^{(1)} - t_{k_1}^{(1)}\right|^2 = 0$, which contradicts the assumption of divergence at time k_1.

This completes the proof that the rank of the Gram matrix $B\left(\underline{\mathbf{s}}_F, \underline{\mathbf{t}}_F\right) B^H\left(\underline{\mathbf{s}}_F, \underline{\mathbf{t}}_F\right)$ is two and hence that the recursive systematic 8 state 4-PSK space-time codes used as components in turbo-STCM feature full diversity.

Following the similar steps, 16 state 8-PSK recursive systematic STC in Fig. 3.3 can also be proved to feature full diversity.

In the turbo-STCM scheme, when the component space-time encoders has full spatial diversity, the randomness of the interleaver between two component codes results in a full spatial diversity turbo code with relatively high probability.

3.1.5 Interleaver Design

Since interleavers operate symbol-wise, interleaver sizes are specified in terms of the number of symbols. Various interleaver sizes K were used later as noted in the Figures' captions. Two types of interleavers were used in the simulations. With the first type, each sequence of size K symbols was run with a different random interleaver chosen from a uniform distribution. Performance shown for random interleavers is the average over all interleavers. In the figures of simulation results shown later, curves representing performance averaged over uniform random interleavers are labeled 'UIL'. These simulations are based on Monte Carlo runs with interleaver realizations for each E_b/N_0. The second type of interleaver used in the simulations was an 'S-random' interleaver, as suggested in [11]. Following guidelines in the reference and choosing $S = 25$, an interleaver was obtained by generating random permutations (interleaves) without replacement, subject to the restriction that adjacent symbols are not interleaved within a distance of S symbols of each other. This interleaver was used in all simulations with fixed interleaver and the curves were labeled 'FIL'. For brevity of notation and for easier correlation with the figures, we use the 'UIL' and 'FIL' designations in the description. Performance of turbo-STCM is presented based on both random and fixed interleavers.

3.2 Iterative Maximum A Posteriori Decoder

The turbo-STCM decoder is an iterative receiver structure as shown in Fig. 3.7. The decoder employs two *a posteriori probability* (APP) computing modules concatenated in parallel: one module for each constituent code. The turbo-STCM decoding

algorithm is derived in two steps: (1) derivation of the generic APP algorithm for a multilevel trellis code given the observed data over the MIMO channel, (2) derivation of the iterative algorithm utilizing the soft outputs (the APP's) of the decoders associated with each constituent code. These decoders are denoted in Fig. 3.7, APP1 and APP2, respectively. Data is shared between the two decoders, and an iterative process is applied to refine the soft decisions.

The generic APP algorithm for nonbinary trellis and MIMO channel is based on the BCJR algorithm [8] and on [15]. Various forms of APP algorithms can be found in these and other references. Due to some differences with other algorithms (multiple transmit/receive antennas, for example), turbo-STCM decoding is based on the *maximum a posteriori* (MAP) criterion. The symbol-by-symbol MAP algorithm was formally introduced in [8] as an alternative to the Viterbi algorithm for decoding convolutional codes.

The MAP algorithm computes the APP of each trellis state transition, message bit, and/or code symbol produced by Markov process, given the noisy and fading observation $\mathbf{y}$. Once the APPs are calculated for all possible values of the desired quantity, a hard decision is made by selecting the quantity with highest occurrence probability. When used for turbo decoding, the MAP algorithm calculates the APPs of all possible message bits or symbols. The MAP algorithm used for turbo decoding does not make hard-decisions on the message bits until after the last decoder iteration.

3.2.1 APP Algorithm

This subsection consists of the development of the generic APP algorithm for space-time code and its iterative receiver structure as shown in Fig. 3.7. The algorithm is evolved from the BCJR algorithm [8] and from [15].

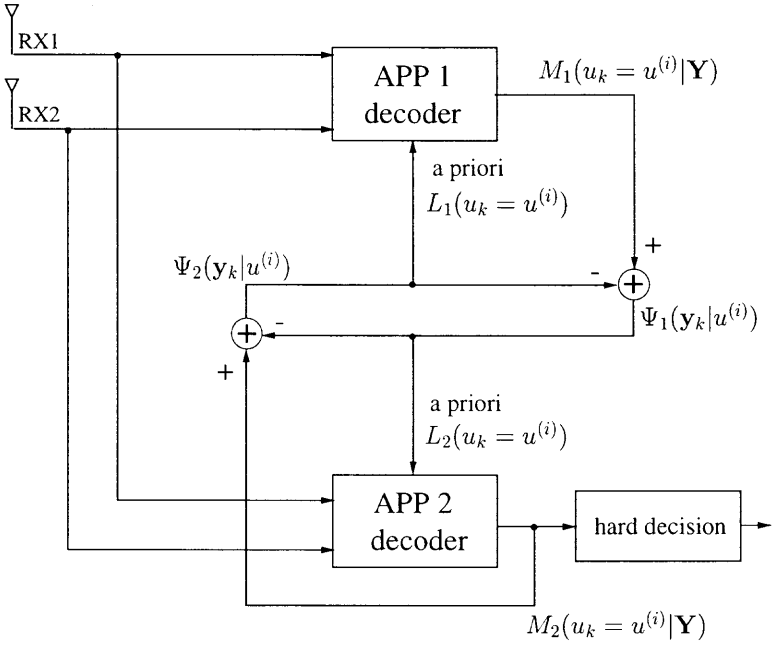

Figure 3.7 Turbo-STCM decoder, the interleavers/deinterleavers are not shown.

The APP's at time k can be expressed

$$P(u_k = u^{(i)}|\mathbf{Y}) = \sum_{\sigma_k} \sum_{\sigma_{k+1}} P(u_k = u^{(i)}, \sigma_k, \sigma_{k+1}|\mathbf{Y}), \tag{3.4}$$

where $P(u_k = u^{(i)}, \sigma_k, \sigma_{k+1}|\mathbf{Y})$ is the joint probability that, given the data $\mathbf{Y}$, the transition from state σ_k to state σ_{k+1} is with information symbol $u_k = u^{(i)}$. The notations are illustrated in Fig. 3.8. In this section, probability density functions are denoted by p, and probability mass distributions as well as mixed expressions are denoted by P. Assuming no parallel transitions between states, any two elements of the trio $(\sigma_k, \sigma_{k+1}, u_k)$ uniquely define a transition. Define $\mathbf{Y}_k^-$ as the sequence received before time k, and $\mathbf{Y}_k^+$ the sequence received after time k. From this definition, we have $\mathbf{Y} = \left(\mathbf{Y}_k^-, \mathbf{y}_k, \mathbf{Y}_k^+\right)$. Utilizing a procedure similar to BCJR [8] and [15], it is possible to express the joint probability $P(u_k = u^{(i)}, \sigma_k, \sigma_{k+1}|\mathbf{Y})$ in a recursive form. Bayes rule can be applied to (3.4) to obtain:

$$P(u_k = u^{(i)}, \sigma_k, \sigma_{k+1}|\mathbf{Y}) = hP(u_k = u^{(i)}, \sigma_k, \sigma_{k+1}, \mathbf{Y}), \tag{3.5}$$

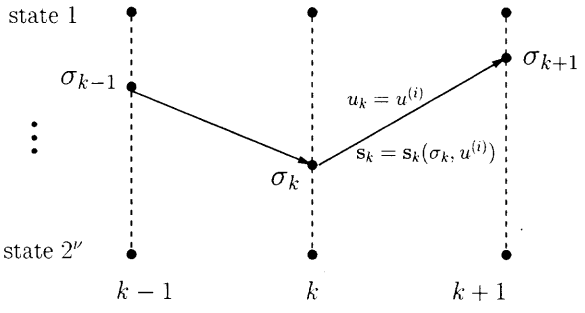

Figure 3.8 Notations for trellis transitions.

where h is chosen such that

$$h \sum_i \sum_{\sigma_k} \sum_{\sigma_{k+1}} P(u_k = u^{(i)}, \sigma_k, \sigma_{k+1}, \mathbf{Y}) = 1 \tag{3.6}$$

Next, compute the joint probability $P(u_k = u^{(i)}, \sigma_k, \sigma_{k+1}, \mathbf{Y})$. First, rewrite $P(u_k = u^{(i)}, \sigma_k, \sigma_{k+1}, \mathbf{Y})$:

$$P(u_k = u^{(i)}, \sigma_k, \sigma_{k+1}, \mathbf{Y}) = P(u_k = u^{(i)}, \sigma_k, \sigma_{k+1}, \mathbf{Y}_k^-, \mathbf{y}_k, \mathbf{Y}_k^+). \tag{3.7}$$

Then, apply the chain rule for conditional probabilities to obtain:

$$\begin{aligned} P(u_k &= u^{(i)}, \sigma_k, \sigma_{k+1}, \mathbf{Y}_k^-, \mathbf{y}_k, \mathbf{Y}_k^+) \\ &= p\left(\mathbf{Y}_k^+ | u_k = u^{(i)}, \sigma_k, \sigma_{k+1}, \mathbf{Y}_k^-, \mathbf{y}_k\right) P(u_k = u^{(i)}, \sigma_{k+1}, \mathbf{y}_k | \sigma_k, \mathbf{Y}_k^-) P\left(\sigma_k, \mathbf{Y}_k^-\right). \end{aligned} \tag{3.8}$$

From the properties of Markov chains if the state σ_{k+1} is known, $\mathbf{Y}_k^+$ does not depend on any of the other parameters,

$$p\left(\mathbf{Y}_k^+ | u_k = u^{(i)}, \sigma_k, \sigma_{k+1}, \mathbf{Y}_k^-, \mathbf{y}_k\right) = p\left(\mathbf{Y}_k^+ | \sigma_{k+1}\right) \tag{3.9}$$

Similarly, if σ_k is known, quantities at times k and on do not depend on $\mathbf{Y}_k^-$:

$$P(u_k = u^{(i)}, \sigma_{k+1}, \mathbf{y}_k | \sigma_k, \mathbf{Y}_k^-) = P(u_k = u^{(i)}, \sigma_{k+1}, \mathbf{y}_k | \sigma_k) \tag{3.10}$$

Define the following quantities:

$$\begin{aligned} \gamma_k^{(i)}(\sigma_k, \sigma_{k+1}, \mathbf{y}_k) &= P(u_k = u^{(i)}, \sigma_{k+1}, \mathbf{y}_k | \sigma_k) \\ \alpha_k(\sigma_k) &= P\left(\sigma_k, \mathbf{Y}_k^-\right) \\ \beta_{k+1}(\sigma_{k+1}) &= p\left(\mathbf{Y}_k^+ | \sigma_{k+1}\right) \end{aligned} \tag{3.11}$$

Then, the APP in (3.5) can be expressed

$$P(u_k = u^{(i)}, \sigma_k, \sigma_{k+1}|\mathbf{Y}) = h\alpha_k(\sigma_k)\gamma_k^{(i)}(\sigma_k, \sigma_{k+1}, \mathbf{y}_k)\beta_{k+1}(\sigma_{k+1}). \tag{3.12}$$

Next we show how to calculate $\gamma_k^{(i)}(\sigma_k, \sigma_{k+1}, \mathbf{y}_k)$ from the observations $\mathbf{Y}$ and how to calculate $\alpha_k(\sigma_k)$ and $\beta_{k+1}(\sigma_{k+1})$ recursively.

- $\gamma_k^{(i)}(\sigma_k, \sigma_{k+1}, \mathbf{y}_k)$ is the joint probability of the transition from state σ_k to state σ_{k+1} with input $u^{(i)}$, and of the observation $\mathbf{y}_k$. It can be expressed

$$\gamma_k^{(i)}(\sigma_k, \sigma_{k+1}, \mathbf{y}_k) = p\left(\mathbf{y}_k|\sigma_k, \sigma_{k+1}, u_k = u^{(i)}\right) P\left(u_k = u^{(i)}|\sigma_k, \sigma_{k+1}\right) P\left(\sigma_{k+1}|\sigma_k\right), \tag{3.13}$$

  where the conditional density $p\left(\mathbf{y}_k|\sigma_k, \sigma_{k+1}, u_k = u^{(i)}\right) = p(\mathbf{y}_k|\sigma_k, u^{(i)})$ can be computed from

$$p(\mathbf{y}_k|\sigma_k, u^{(i)}) = (\pi N_0)^{-M} \exp\left(-\frac{1}{N_0}\left\|\mathbf{y}_k - \sqrt{E_s}\mathbf{H}\mathbf{s}_k\right\|^2\right), \tag{3.14}$$

  $\mathbf{s}_k$ is the vector of symbols associated with the pair $\left(\sigma_k, u_k = u^{(i)}\right)$. We reiterate that any transition is uniquely defined by the initial state and the input. Hence, each codeword vector $\mathbf{s}_k$ is uniquely determined by $\left(\sigma_k, u_k = u^{(i)}\right)$. The term $P\left(u_k = u^{(i)}|\sigma_k, \sigma_{k+1}\right) = 1$ if there exists a transition $\sigma_k \to \sigma_{k+1}$ due to the input $u^{(i)}$, and it is zero otherwise. When $\sigma_k \to \sigma_{k+1}$ is due to $u^{(i)}$, it can be written as $P\left(\sigma_{k+1}|\sigma_k\right) = P\left(u_k = u^{(i)}\right)$, where the last term is the a priori probability of the information symbol $u^{(i)}$. Subsequently, (3.13) can be rewritten

$$\gamma_k^{(i)}(\sigma_k, \sigma_{k+1}, \mathbf{y}_k) = p(\mathbf{y}_k|\sigma_k, u^{(i)}) P\left(u_k = u^{(i)}\right) \tag{3.15}$$

  for existing transitions $\sigma_k \to \sigma_{k+1}$ due to input $u^{(i)}$.

- $\alpha_k(\sigma_k) = P\left(\sigma_k, \mathbf{Y}_k^-\right)$ are the joint probabilities of the states of the trellis at time k and the data observed until time $k-1$, $\mathbf{Y}_k^-$. These probabilities are

obtained from the forward recursion

$$\begin{aligned}
\alpha_{k+1}(\sigma_{k+1}) &= P\left(\sigma_{k+1}, \mathbf{Y}_{k+1}^{-}\right) \\
&= \sum_{\sigma_k} P\left(\sigma_k, \sigma_{k+1}, \mathbf{Y}_k^{-}, \mathbf{y}_k\right) \\
&= \sum_{\sigma_k} P\left(\sigma_{k+1}, \mathbf{y}_k | \sigma_k, \mathbf{Y}_k^{-}\right) P\left(\sigma_k, \mathbf{Y}_k^{-}\right) \\
&= \sum_{\sigma_k} P\left(\sigma_{k+1}, \mathbf{y}_k | \sigma_k\right) P\left(\sigma_k, \mathbf{Y}_k^{-}\right) \\
&= \sum_{\sigma_k} \alpha_k(\sigma_k)\, \gamma\left(\sigma_k, \sigma_{k+1}, \mathbf{y}_k\right), \qquad (3.16)
\end{aligned}$$

where $P\left(\sigma_{k+1}, \mathbf{y}_k | \sigma_k, \mathbf{Y}_k^{-}\right) = P\left(\sigma_{k+1}, \mathbf{y}_k | \sigma_k\right)$ (events after $k-1$ are not influenced by $\mathbf{Y}_k^{-}$ if σ_k is known), and the definition .

$$\gamma\left(\sigma_k, \sigma_{k+1}, \mathbf{y}_k\right) = P\left(\sigma_{k+1}, \mathbf{y}_k | \sigma_k\right). \qquad (3.17)$$

Comparing (3.11) with (3.17), we see that

$$\gamma\left(\sigma_k, \sigma_{k+1}, \mathbf{y}_k\right) = \sum_i \gamma_k^{(i)}\left(\sigma_k, \sigma_{k+1}, \mathbf{y}_k\right) \qquad (3.18)$$

- $\beta_{k+1}(\sigma_{k+1}) = p\left(\mathbf{Y}_k^{+} | \sigma_{k+1}\right)$ are the densities of the future observations (after time k) conditioned on the states at time k. A recursive expression for $\beta_{k+1}(\sigma_{k+1})$ can be developed as follows:

$$\begin{aligned}
\beta_k(\sigma_k) &= p\left(\mathbf{Y}_{k-1}^{+} | \sigma_k\right) \\
&= \sum_{\sigma_{k+1}} P\left(\sigma_{k+1}, \mathbf{Y}_{k-1}^{+} | \sigma_k\right) \\
&= \sum_{\sigma_{k+1}} P\left(\sigma_{k+1}, \mathbf{y}_k, \mathbf{Y}_k^{+} | \sigma_k\right) \\
&= \sum_{\sigma_{k+1}} p\left(\mathbf{Y}_k^{+} | \sigma_k, \sigma_{k+1}, \mathbf{y}_k\right) P(\sigma_{k+1}, \mathbf{y}_k | \sigma_k) \\
&= \sum_{\sigma_{k+1}} p\left(\mathbf{Y}_k^{+} | \sigma_{k+1}\right) P\left(\sigma_{k+1}, \mathbf{y}_k | \sigma_k\right) \\
&= \sum_{\sigma_{k+1}} \beta_{k+1}(\sigma_{k+1})\, \gamma\left(\sigma_k, \sigma_{k+1}, \mathbf{y}_k\right) \qquad (3.19)
\end{aligned}$$

where we used the Markov property $p\left(\mathbf{Y}_k^{+} | \sigma_k, \sigma_{k+1}, \mathbf{y}_k\right) = p\left(\mathbf{Y}_k^{+} | \sigma_{k+1}\right)$ and definition (3.17).

By combining (3.16), (3.19) and (3.15), and substituting in (3.12) and then back in (3.4), the APP can be expressed

$$P(u_k = u^{(i)}|\mathbf{Y}) = h \sum_{\sigma_k} \sum_{\sigma_{k+1}} \alpha_k(\sigma_k)\gamma_k^{(i)}(\sigma_k, \sigma_{k+1}, \mathbf{y}_k)\beta_{k+1}(\sigma_{k+1}) \tag{3.20}$$

The last expression can be simplified if we note that a given state σ_k and input $u_k = u^{(i)}$, determine the state σ_{k+1}. Denote $\tilde{\sigma}_{k+1}$ the specific state reached by applying $u_k = u^{(i)}$ to state σ_k. Thus rather than sum over σ_{k+1}, it is sufficient to set $\sigma_{k+1} = \tilde{\sigma}_{k+1}$. We can rewrite (3.20),

$$P(u_k = u^{(i)}|\mathbf{Y}) = h \sum_{\sigma_k} \alpha_k(\sigma_k)\gamma_k^{(i)}(\sigma_k, \tilde{\sigma}_{k+1}, \mathbf{y}_k)\beta_{k+1}(\tilde{\sigma}_{k+1}) \tag{3.21}$$

3.2.2 Log-APP Algorithm

For computational convenience and numerical precision it is desired to convert the multiplicative form of (3.21) into an additive form. This is done by passing to the log domain.

To handle additions in the log domain, we make use of the following expression for a sum of exponentials in the log domain [66, 67]:

$$\log\left(e^x + e^y\right) = \max\left(x, y\right) + \log\left(1 + \exp\left(-\left|y - x\right|\right)\right) \tag{3.22}$$

This expression suggests that addition in the log domain becomes a sum of a maximization with a correction function. When x and y are dissimilar, the correction function is close to zero, hence $\log\left(e^x + e^y\right) \approx \max\left(x, y\right)$. This property is applied to develop the log-APP algorithm.

Quantities in the log domain are denoted with an overbar. For computation of the log-APP there has (refer to (3.21)):

- $\overline{\gamma}_k^{(i)}\left(\sigma_k, \sigma_{k+1}, \mathbf{y}_k\right) = \log \gamma_k^{(i)}\left(\sigma_k, \sigma_{k+1}, \mathbf{y}_k\right)$. From (3.15):

$$\begin{aligned} \overline{\gamma}_k^{(i)}\left(\sigma_k, \sigma_{k+1}, \mathbf{y}_k\right) &= \log p(\mathbf{y}_k|\sigma_k, u^{(i)}) + \log P\left(u_k = u^{(i)}\right) \\ &= -M \log\left(\pi N_0\right) - \frac{1}{N_0}\left\|\mathbf{y}_k - \sqrt{E_s}\mathbf{H}\mathbf{s}_k\right\|^2 + \log P\left(u_k = u^{(i)}\right) \end{aligned} \tag{3.23}$$

- $\overline{\gamma}_k(\sigma_k, \sigma_{k+1}, \mathbf{y}_k) = \log \gamma_k(\sigma_k, \sigma_{k+1}, \mathbf{y}_k)$. From (3.18):

$$\begin{aligned} \overline{\gamma}_k(\sigma_k, \sigma_{k+1}, \mathbf{y}_k) &= \log\left(\sum_i \exp\left[\overline{\gamma}_k^{(i)}(\sigma_k, \sigma_{k+1}, \mathbf{y}_k)\right]\right) \\ &\simeq \max_i \left[\overline{\gamma}_k^{(i)}(\sigma_k, \sigma_{k+1}, \mathbf{y}_k)\right] \end{aligned} \tag{3.24}$$

- $\overline{\alpha}_k(\sigma_k) = \log \alpha_k(\sigma_k)$. From (3.16):

$$\begin{aligned} \overline{\alpha}_{k+1}(\sigma_{k+1}) &= \log\left(\sum_{\sigma_k} \exp\left[\overline{\alpha}_k(\sigma_k) + \overline{\gamma}_k(\sigma_k, \sigma_{k+1}, \mathbf{y}_k)\right]\right) \\ &\simeq \max_{\sigma_k}[\overline{\alpha}_k(\sigma_k) + \overline{\gamma}_k(\sigma_k, \sigma_{k+1}, \mathbf{y}_k)] \end{aligned} \tag{3.25}$$

  where we assume the trellis transmits from zero state, so the initial condition of forward recursion $\overline{\alpha}_0(\sigma_0 = 0) = 0$, $\overline{\alpha}_0(\sigma_0 \neq 0) = -\infty$.

- $\overline{\beta}_k(\sigma_k) = \log \beta_k(\sigma_k)$. From (3.19):

$$\begin{aligned} \overline{\beta}_k(\sigma_k) &= \log\left(\sum_{\sigma_{k+1}} \exp\left[\overline{\beta}_{k+1}(\sigma_{k+1}) + \overline{\gamma}_k(\sigma_k, \sigma_{k+1}, \mathbf{y}_k)\right]\right) \\ &\simeq \max_{\sigma_{k+1}}\left[\overline{\beta}_{k+1}(\sigma_{k+1}) + \overline{\gamma}_k(\sigma_k, \sigma_{k+1}, \mathbf{y}_k)\right] \end{aligned} \tag{3.26}$$

  where we can not assume the trellis is terminated at state $\sigma_K = 0$ due to the recursive and systematic component encoders even though adding the zero tail bits to data. Hence the initial condition of backward recursion $\overline{\beta}_K(\sigma_K) = -\nu \log 2$, ν is the component encoder shift register length.

Let $M(u_k = u^{(i)}|\mathbf{Y}) = \log P(u_k = u^{(i)}|\mathbf{Y})$, then from (3.21),

$$\begin{aligned} M(u_k &= u^{(i)}|\mathbf{Y}) = \log\left(h \sum_{\sigma_k} \exp\left[\overline{\alpha}_k(\sigma_k) + \overline{\gamma}_k^{(i)}(\sigma_k, \tilde{\sigma}_{k+1}, \mathbf{y}_k) + \overline{\beta}_{k+1}(\tilde{\sigma}_{k+1})\right]\right) \\ &\simeq \overline{h} + \max_{\sigma_k}\left[\overline{\alpha}_k(\sigma_k) + \overline{\gamma}_k^{(i)}(\sigma_k, \tilde{\sigma}_{k+1}, \mathbf{y}_k) + \overline{\beta}_{k+1}(\tilde{\sigma}_{k+1})\right], \end{aligned} \tag{3.27}$$

where $\overline{h} = \log h$, can be determined from the relation

$$\overline{h} = -\log\left(\sum_i \exp\left[M(u_k = u^{(i)}|\mathbf{Y})\right]\right) \tag{3.28}$$

It is completed by defining the a priori information

$$L(u_k = u^{(i)}) = \log P(u_k = u^{(i)})$$

and the systematic and extrinsic information

$$\Psi(\mathbf{y}_k|u^{(i)}) = M(u_k = u^{(i)}|\mathbf{Y}) - L(u_k = u^{(i)}) \tag{3.29}$$

The following expression is the log domain version of (3.21)

$$M(u_k = u^{(i)}|\mathbf{Y}) = \Psi(\mathbf{y}_k|u^{(i)}) + L(u_k = u^{(i)}) \tag{3.30}$$

The final result of log-APP is expression (3.30) at time k of an input information symbol $u_k = u^{(i)}$ and given the sequence of observations $\mathbf{Y}$:

$$M(u_k = u^{(i)}|\mathbf{Y}) = \Psi(\mathbf{y}_k|u^{(i)}) + L(u_k = u^{(i)}), \tag{3.31}$$

where $M(u_k = u^{(i)}|\mathbf{Y}) = \log P(u_k = u^{(i)}|\mathbf{Y})$ is the log-APP, $\Psi(\mathbf{y}_k|u^{(i)})$ incorporates the systematic and extrinsic information, and $L(u_k = u^{(i)}) = \log P(u_k = u^{(i)})$ is the a priori information.

The operation of the turbo-STCM decoder is explained assuming that the first iteration of APP1 is already available. We then describe how the turbo-STCM handles the punctured data. Finally, the first iteration of APP1 is addressed. The turbo-STCM decoder is based on [15], with the necessary modifications to account for the multiple transmit/receive antennas and other differences between TCM and STC codes.

Turbo Decoder Iterations

From (3.31), it follows that the APP decoder output is in logarithmic form and can be split into two additive parts: $L(u_k = u^{(i)})$ - the a priori data input to the decoder, and $\Psi(\mathbf{y}_k|u^{(i)})$, which depends on the systematic part (information symbols) and extrinsic part (other data supplied to the decoder). The key to the

iterative process of the turbo-STCM decoder is that the a priori input to each APP decoder can be derived from the output of the *other* decoder. We will use subscripts 1,2 to denote quantities associated with the respective APP decoder. To explain the iterative process, assume that the output of APP1 for $u_k = u^{(i)}$ at time k is $M_1(u_k = u^{(i)}|\mathbf{Y})$. This quantity is to be used to derive the a priori input into APP2, $L_2(u_k = u^{(i)})$. However, we want to feed to APP2 only new information generated by APP1. This is achieved by removing the a priori information that went into generating the output of APP1. Thus the a priori information into APP2 for $u_k = u^{(i)}$ at time k is given by

$$\begin{aligned} L_2(u_k = u^{(i)}) &= M_1(u_k = u^{(i)}|\mathbf{Y}) - L_1(u_k = u^{(i)}) \\ &= \Psi_1(\mathbf{y}_k|u^{(i)}). \end{aligned} \tag{3.32}$$

Then, the output of APP2 $M_2(u_k = u^{(i)}|\mathbf{Y})$, is computed from (3.31). The iterations continue with $L_1(u_k = u^{(i)}) = M_2(u_k = u^{(i)}|\mathbf{Y}) - L_2(u_k = u^{(i)})$ used as a priori input back into APP1. Note that these iterations take place for each input symbol $u^{(i)} \in \left\{u^{(1)}, \ldots, u^{(m)}\right\}$ and for all times $1 \leq k \leq K$.

Use of Punctured Observations

Each APP module has two inputs: the a priori information $L(u_k = u^{(i)})$ and the observation sequence $\mathbf{Y}$. Each APP module at the decoder is matched to a constituent space-time code at the turbo-STCM encoder. Consider the observations at the input of APP1. Ideally, this input would consists of the noisy and faded signal transmitted by STC1 (see Fig. 3.5). However, due to the encoder architecture, the input to APP1 consists of: (1) correct systematic data, (2) parity data that is alternately provided by STC1 or STC2, (3) noise. Thus, the input to APP1 consists of a sequence that contains correct STC1 symbols punctured by STC2 symbols. To overcome this difficulty, at times corresponding to punctured symbols STC1, the data

input to APP1 is set to zero, and the only input to APP1 is the *a priori* information. Observations at the input of APP1 are then handled as follows:

- For all non-punctured symbols ($k = 1, 3, 5 \ldots$), compute $\log p(\mathbf{y}_k|\sigma_k, u^{(i)}) = -M \log(\pi N_0) - \left\|\mathbf{y}_k - \sqrt{E_s}\mathbf{H}\mathbf{s}_k\right\|^2 / N_0$ (Euclidean norm) and use it as appropriate for the computation of $\gamma_k^{(i)}(\sigma_k, \sigma_{k+1}, \mathbf{y}_k)$, $\alpha_k(\sigma_k)$, $\beta_k(\sigma_k)$, and h in the APP1 algorithm.

- For all punctured symbols ($k = 2, 4, 6 \ldots$), let $0 \rightarrow \log p(\mathbf{y}_k|\sigma_k, u^{(i)})$, and use that in the APP1 algorithm.

From (3.23), for punctured symbols, $\log \gamma_k^{(i)}(\sigma_k, \sigma_{k+1}, \mathbf{y}_k) = \log P\left(u_k = u^{(i)}\right)$. A similar procedure is used for APP2, where the non-punctured symbols are ($k = 2, 4, 6 \ldots$).

First Iteration

At each iteration, the set of log APP's $M_{1,2}(u_k = u^{(i)}|\mathbf{Y})$, $k = 1, \ldots, K$ is generated for all information symbols $u^{(i)} \in \left\{u^{(1)}, \ldots, u^{(m)}\right\}$. In particular, the first turbo iteration also needs to generate $M_{1,2}(u_k = u^{(i)}|\mathbf{Y})$, $k = 1, \ldots, K$ for $u^{(i)} \in \left\{u^{(1)}, \ldots, u^{(m)}\right\}$. According to (3.31), computation of the APP requires a priori information. At each iteration, the a priori information $\log P\left(u_k = u^{(i)}\right)$ is provided by the other APP decoder. However, such input is not available for APP1 at the time of the first iteration. The a priori information for APP1 at the first iteration is generated as follows:

- For all symbols in the sequence ($k = 1, 2, 3 \ldots$), as $P\left(u_k = u^{(i)}\right)$ is unknown, assume that the input information symbol u_k could be with equal probability any of the m symbols $u^{(i)}$, $i = 1, \ldots, m$, i.e., $P\left(u_k = u^{(i)}\right) = 1/m$.

- The procedure delineated above, does not address another problem that arises at the first iteration of APP1. If we follow the procedure presented

in the subsection 'Use of Punctured Observations', for punctured symbols ($k = 2, 4, 6 \ldots$), we would apply $0 \rightarrow \log p(\mathbf{y}_k|\sigma_k, u^{(i)})$. However, this means that the systematic part of $\mathbf{y}_k$ is also lost. Since the APP algorithm needs to get the systematic information from somewhere, we find a way to utilize the punctured data $\mathbf{y}_k$. To that end, note that a transmitted symbol vector $\mathbf{s}_k$ consists of a systematic symbol $s_k^{(1)}$, which has the same binary label as the information symbol u_k and is transmitted through antenna 1, and a parity symbol $s_k^{(2)}$ transmitted through antenna 2. Punctured symbols with respect to APP1 have the parity data generated by space-time code 2, which is unknown to decoder APP1. However, the systematic data is embedded in the observation $\mathbf{y}_k$. The best that decoder APP1 can do is to average over the unknown parity symbols. Let $b^{(j)}$ denote the m-PSK parity symbol. Note that $b^{(j)} \in \left\{b^{(1)}, \ldots, b^{(m)}\right\}$. Then, at the first iteration of APP1, rather than applying $0 \rightarrow \log p(\mathbf{y}_k|\sigma_k, u^{(i)})$ for punctured data, we use $\log c \sum_{j=1}^{m} p(\mathbf{y}_k|u^{(i)}, b^{(j)}) \rightarrow \log p(\mathbf{y}_k|\sigma_k, u^{(i)})$ as extrinsic information. The constant c can be found from the condition $\sum_{i=1}^{m} P\left(u_k = u^{(i)}|\mathbf{y}_k\right) = 1$, which leads to the relation $\frac{c}{m} \sum_{i=1}^{m} \sum_{j=1}^{m} p(\mathbf{y}_k|u^{(i)}, b^{(j)}) = 1$.

3.3 Numerical Results

In this section, simulation results are presented on the performance of our turbo-STCM scheme for 2 and 3 bits/s/Hz (4-PSK and 8-PSK respectively). The channel model was Rayleigh block-fading, meaning that the channel was assumed constant during a frame of $F = 130$ symbols, but independent frame-to-frame. The block-fading channels are considered with known channel state information (CSI) at receiver. Interleaver sizes K are specified in terms of the number of symbols. In the simulations, performances are based on both random and fixed interleavers. Performance of non-turbo space-time codes is provided for comparison. Figure

captions specify the number of transmit-receive antenna, e.g., 2T1R = two transmit-one receive antenna. Individual codes are labeled according to the modulation and number of states ("4p4s" refers to 4-PSK modulation, 4 state code).

Recursive or non-recursive space-time constituent code?

As we have seen before, recursive component space-time codes are according to Fig. 3.1, while the non-recursive form is shown in Fig. 3.4. Fig. 3.9 and 3.10 show performance for 4 state 4-PSK turbo-STCM after eight iterations of the decoder. The figures display the frame error rate (FER) curves versus the bit signal-to-noise ratio E_b/N_0 in dB per receive antenna.

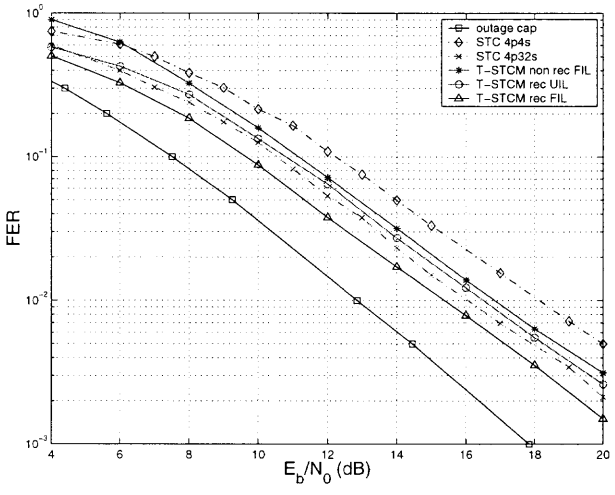

Figure 3.9 FER of 4 state 4-PSK turbo-STCM (2T1R) over the fading channel, with fixed interleaver (FIL) and averaged over interleavers (UIL).

Fig. 3.9 shows the FER for two transmit-one receive antenna turbo-STCM utilizing the recursive and non-recursive four state 4-PSK component space-time codes shown in Fig. 3.1 and 3.4, respectively. Curves are also provided for two transmit-one receive antenna, 4 and 32 state 4-PSK Tarokh *et. al.* codes [31]. The 32 state Tarokh code (labeled in the figure '4p32s') is shown since it has roughly the same decoding complexity as turbo-STCM with 4 state constituent codes, two APP decoders, and 8 iterations per APP decoder. Complexity of the decoder is

evaluated as proportional to $\nu \cdot 2^{\nu}$ per decoder and per iteration, where ν is the code memory [4]. It is well known that Tarokh's codes feature full diversity. Due to the puncturing operation, the turbo-STCM architecture of Fig. 3.5 cannot guarantee full diversity, yet as observed from the figure, both recursive and non-recursive forms of turbo-STCM have full diversity, a fact borne out by the asymptotic slopes (at high E_b/N_0) of the FER curves being parallel with the slopes of Tarokh's codes. Codes are differentiated only by their coding gain. Turbo-STCM with recursive component codes has an advantage of 2.7 dB over Tarokh's 4 state code (labeled '4p4s') at FER $= 10^{-2}$, while turbo-STCM with non-recursive component codes has a performance 1.3 dB below that of the recursive form. At FER $= 10^{-2}$, turbo-STCM with recursive codes has a 0.6 dB advantage over the 32 state conventional space-time code. Based on the $\nu \cdot 2^{\nu}$ formula for complexity, turbo-STCM has a relative complexity of 128 (for eight iterations), while the 32 state space-time code has a relative complexity of 160. Comparison with a 16 state code from [31] (complexity 64) shows an advantage for the turbo code of about 1 dB. The curve labeled "outage cap" is the outage channel capacity defined as the probability that the spectral efficiency (in this case 2 bits/s/Hz) is not supported with a probability given by the ordinate [20]. It is observed that turbo-STCM with recursive codes performs within 2.3 dB of the outage capacity at FER $= 10^{-2}$. Also note that the fixed interleaver has an advantage of approximately 1 dB over the uniform interleaver and that performance with recursive constituent codes is better by about 0.4 dB than performance of the fixed interleaver with non-recursive constituent codes .

Fig. 3.10 is similar to Fig. 3.9, except that two antennas are used at the receiver. In this case, the advantage of turbo-STCM with fixed interleaver (at FER $= 10^{-2}$) is 3.8 dB and 0.7 dB over the conventional Tarokh code with respectively, 4 and 32 states.

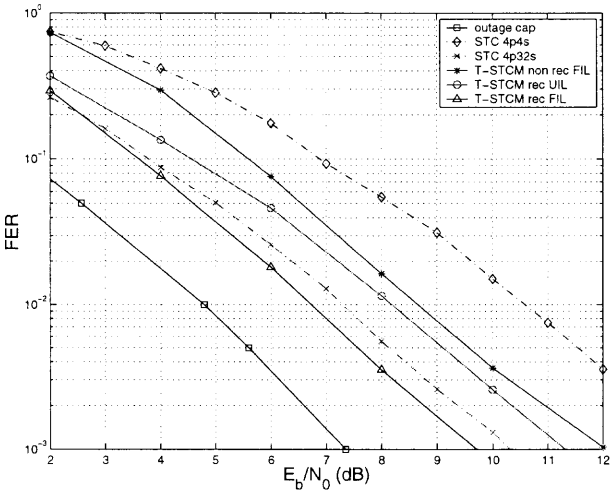

Figure 3.10 FER of 4 state 4-PSK turbo-STCM (2T2R) over the fading channel, with fixed interleaver (FIL) and averaged over interleavers (UIL).

Fig. 3.11 (a), (b), and (c) show the bit error rate (BER) versus the ratio E_b/N_0 dB per receive antenna for various interleaver sizes. Performance shown is averaged over random interleavers. For comparison, performance is also provided for two transmit-two receive antenna 16 state 4-PSK Tarokh *et. al.* code. The interleaver sizes used for turbo-STCM were respectively, 130, 1300, and 5200 symbols. Constituent space-time codes were recursive and systematic 8 state 4-PSK with two transmit-two receive antennas as per Fig. 3.2. The figure demonstrates the effect of turbo iterations and the interleaver size. For example, it can be observed in part (b) that at BER = 10^{-4}, the incremental gain achieved by 2, 4 and 8 iterations is respectively, 2 dB, 1.2 dB, and 0.3 dB. At BER = 10^{-5}, and for 8 iterations, the difference between the shortest and the longest interleaver is approximately 2.8 dB. For an interleaver longer than the data frame, there is additional temporal diversity due to independent realization of the channel. As we observed in Fig. 3.11 (c), the slope of BER curve after 8 iteration is steeper than that of Tarokh "STC" and "Fano LB" curves, whose slopes show the expected spatial diversity order 4. At BER = 10^{-4} and after 8 iterations, the advantage over the 16 state Tarokh code is between

1 dB (130 symbols interleaver) and 2.8 dB (5200 symbols interleaver). Figure 3.12 shows the BER plotted versus the number of iterations for various E_b/N_0 values. Also shown in the figure is the curve of Fano lower bound (Fano LB) as defined in (2.10) and shown in Fig. 2.7 of Chapter 2. At BER $= 10^{-4}$, turbo-STCM approach the Fano lower bound within approximately 4 dB, 3 dB and 2.2 dB from the shortest to the longest interleaver after 8 iterations. From Figure 3.12 it can be seen that about five iterations are sufficient for convergence.

Fig. 3.13 shows FER for two transmit-one receive antenna turbo-STCM, $K =$ 1300 symbols interleaver and with recursive systematic 8 state 4-PSK constituent codes as shown in Figure 3.2. Performance is shown for random interleavers (UIL) after 8 iterations and for the fixed interleaver (FIL) after 1, 4, and 8 iterations. Curves are also provided for two transmit-one receive antenna 4-PSK 8 state and 64 state Tarokh et al. codes. Finally, the performance of our designed recursive and systematic space-time constituent code is also shown. Decoding of Tarokh's codes and of the recursive systematic code is done using the Viterbi algorithm. It is observed that at high E_b/N_0, all codes provide full diversity as demonstrated by the parallel asymptotic slopes. In particular, our systematic recursive code has the same diversity as Tarokh's code (same slope) but lower coding gain (approximately 3 dB at FER $= 10^{-2}$ compared to Tarokh's 8 state code). The simulations for our recursive systematic codes demonstrate the full diversity proved in the previous section. After 4 iterations, turbo-STCM with fixed interleaver has an advantage of 3.5 dB over Tarokh's 8 state code. This advantage becomes 4 dB after 8 iterations. The turbo-STCM after one iteration is inferior to the performance of one of its constituent codes, since it uses a sub-optimal log MAP decoding algorithm rather than the optimal maximum likelihood Viterbi algorithm. The 64 state Tarokh code is shown since it has roughly the same decoding complexity as turbo-STCM with 8 state constituent codes, 8 iterations and two APP decoders per iteration. Complexity

of the decoder is evaluated: for the 64 state space-time code, the code memory is $\nu = 6$, and the complexity is proportional to $\nu \cdot 2^{\nu} = 6 \times 2^6 = 384$. Similarly, for the turbo code, we have 8 states or $\nu = 3$. Then the complexity is proportional to $3 \times 2^3 \times$ (2 APP decoders) $\times$ (8 iterations) $= 384$. At FER $= 10^{-2}$ and after 8 iterations, turbo-STCM with fixed interleaver (FIL) has a 3 dB advantage over a stand-alone space-time code of comparable complexity. Also note the approximately 1.5 dB advantage of the fixed interleaver (FIL) over the uniform random interleaver (UIL).

Fig. 3.14 shows the FER performance comparison of turbo-STCM with the other following methods: 1T1R (one transmit-one receive antenna) uncoded 4-PSK (4p), 1T1R 8 state 8-PSK TCM (TCM 8p8s) [59], 2T1R 8 state 4-PSK conventional space-time code (STC 4p8s) [31], 1T1R 8 state 8-PSK turbo-TCM (T-TCM 8p8s) [15], 2T1R 8 state 4-PSK turbo-STCM (T-STCM 4p8s). All methods compared have the spectral efficiency of 2 bits/s/Hz. Performance is shown for turbo-TCM and turbo-STCM after 8 iterations. Also shown in the figure is the curve of outage channel capacity (outage cap). Methods using a single antenna at the transmitter, have a lower diversity, a fact indicated by the smaller slopes of the top three curves. At FER $= 10^{-2}$, turbo-STCM provides a gain of 10 dB over turbo-TCM without transmit diversity and a gain of approximately 4 dB over the conventional space-time code. The performance of turbo-STCM is within 0.7 dB of the outage capacity as well as STC within 5 dB of capacity.

Fig. 3.15 is similar to Fig. 3.13, except that two antennas are used at the receiver. The approximately parallel slopes of all curves indicate that all methods shown provide full diversity. In this case, the advantage of turbo-STCM with fixed interleaver over Tarokh code with 64 states is only about 1 dB (at FER $= 10^{-2}$). The performance of turbo-STCM is within 2.7 dB of the outage capacity.

Fig. 3.16 and 3.17 demonstrate the performance of 16 state 8-PSK turbo-STCM codes utilizing the space-time constituent code as shown in Fig. 3.3. The fixed symbol interleaver $K = 1300$ was the same as the one used in Figures 3.13,3.15. In both Figures 3.16 and 3.17, full diversity is displayed by all codes. In Fig. 3.16, performance of our designed recursive systematic code is about 1.5 dB inferior to 16 state 8-PSK Tarokh code (at FER $= 10^{-1}$), but has the same slope. After 8 turbo iterations, turbo-STCM with fixed interleaver has a 2 dB advantage over Tarokh 64 state 8-PSK code. The advantage over Tarokh 16 state 8-PSK is about 3 dB. Fig. 3.17 displays similar trends for the two transmit-two receive antenna case. In this case, after 8 iterations, the advantage of turbo-STCM with fixed interleaver over conventional 64 state 8-PSK space-time code is about 0.8 dB (at FER $= 10^{-2}$). The performance of turbo-STCM is within 3 dB of the outage capacity.

3.4 Chapter Summary

While information theory suggests that multiple antennas are an effective and practical way to increase capacity in a wireless system, it is still necessary to devise new techniques such as turbo-STCM that operate close to the capacity limits.

In this Chapter, the new turbo codes are introduced as turbo-STCM, featuring space-time constituent codes. The constituent codes are recursive and systematic. Turbo-STCM scheme utilizes two transmit antennas: one for systematic data and the other for parity data. The random-like property of the turbo code is provided by a symbol-wise interleaver used between the inputs to the two constituent space-time codes. A suboptimal MAP iterative decoder utilizing log APP modules is presented. The codes feature full diversity and full rate. Performance over a flat block-fading Rayleigh channel is demonstrated by simulations for 2 bits/s/Hz 4-PSK and 3 bits/s/Hz 8-PSK turbo-STCM codes. It is shown that 4-8 iterations are sufficient for convergence of the decoded sequence. As with other turbo codes,

performance is affected by the interleaver design and size. Comparison at FER $= 10^{-2}$ of the 8 state 4-PSK two transmit-one receive antenna scheme with a fixed interleaver of size 1300 symbols, to Tarokh's 8 state code shows an advantage of 3.5 dB after 4 decoding iterations and 4 dB after 8 iterations. Complexity is comparable with Tarokh's 64 state code, but turbo-STCM has an advantage over that code of 3 dB after 8 iterations.

Such turbo-STCM codes can be extended to higher efficiency modulation and more complex STC for additional coding and diversity gain. Our future work include the generalization of turbo-STCM for higher multilevel modulation. These codes have the potential to facilitate high-rate data transmission over fading channels in future wireless networks.

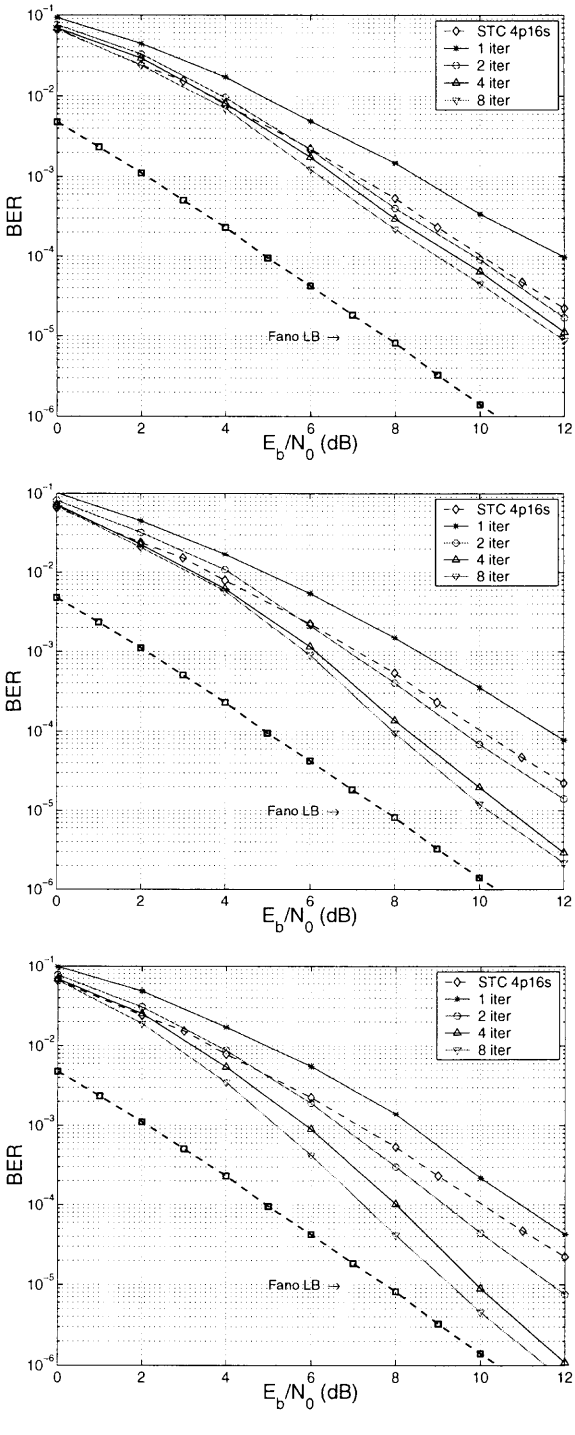

Figure 3.11 BER of 8 state 4-PSK turbo-STCM (2T2R) over the fading channel, averaged over interleavers (UIL) of size (symbols): (a) $K = 130$, (b) $K = 1300$, (c) $K = 5200$.

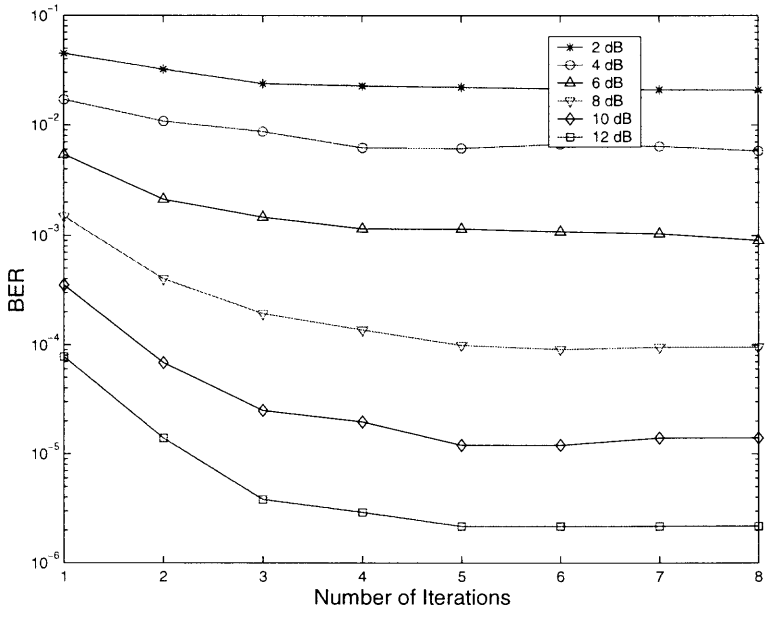

Figure 3.12 Iterations of 8 state 4-PSK turbo-STCM (2T2R) decoder, average over interleavers (UIL) of size $K = 1300$ symbols.

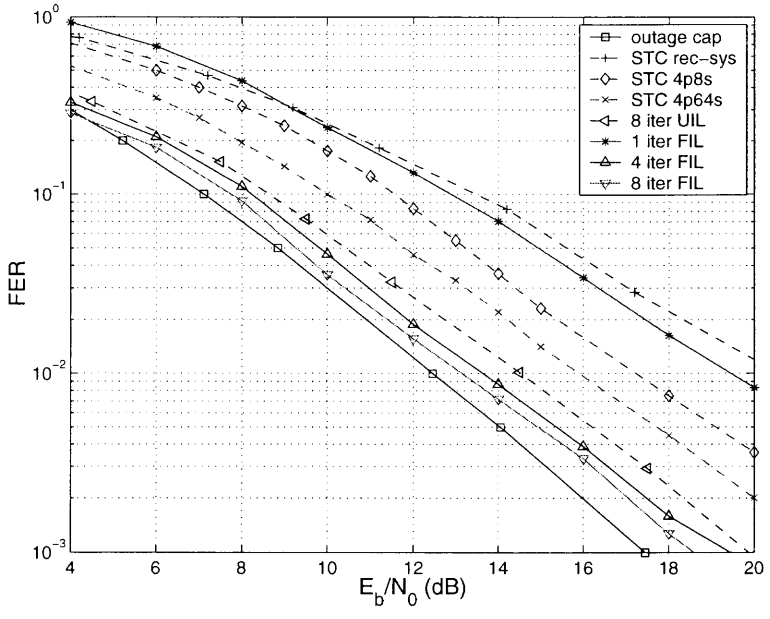

Figure 3.13 FER of 8 state 4-PSK turbo-STCM (2T1R) over the fading channel, with fixed interleaver (FIL) and averaged over interleavers (UIL) of size $K = 1300$ symbols.

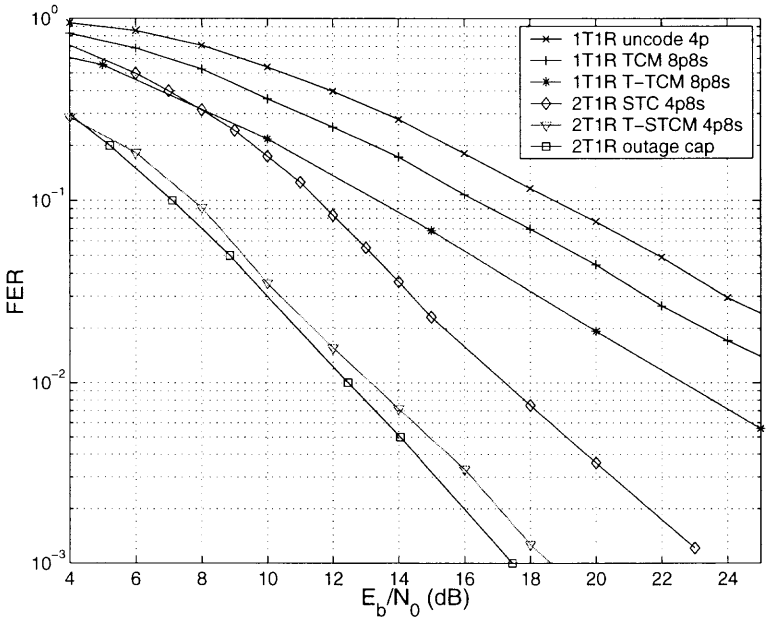

Figure 3.14 FER comparison of turbo-STCM with other methods.

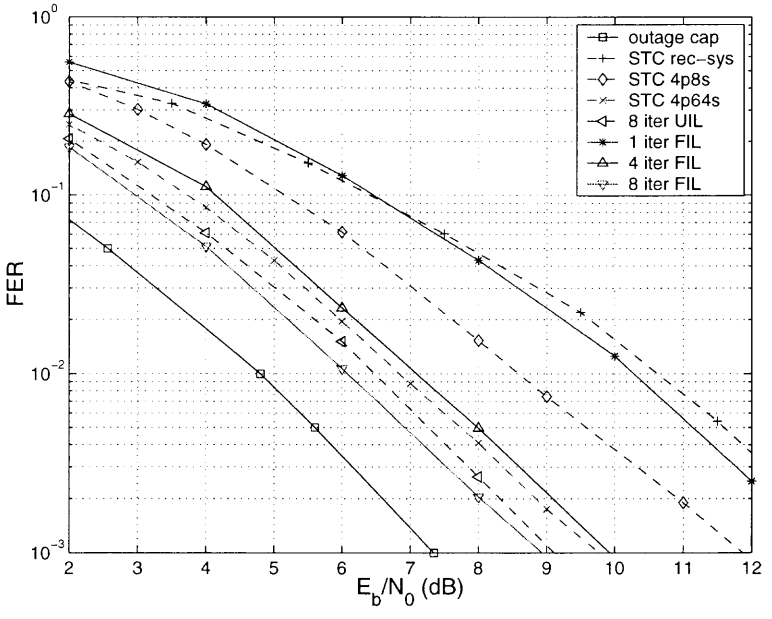

Figure 3.15 FER of 8 state 4-PSK turbo-STCM (2T2R) over the fading channel, with fixed interleaver (FIL) and averaged over interleavers (UIL) of size $K = 1300$ symbols.

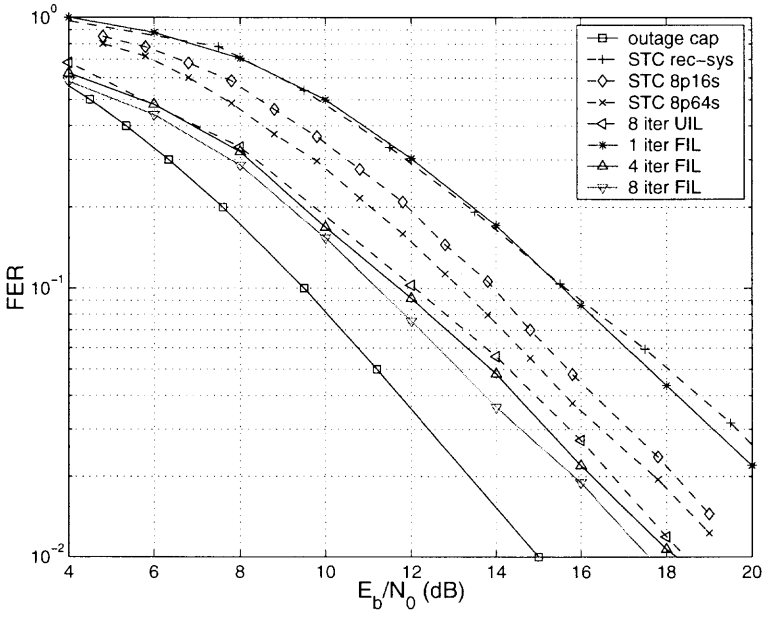

Figure 3.16 FER of 16 state 8-PSK turbo-STCM (2T1R) over the fading channel, with fixed interleaver (FIL) and averaged over interleavers (UIL) of size $K = 1300$ symbols.

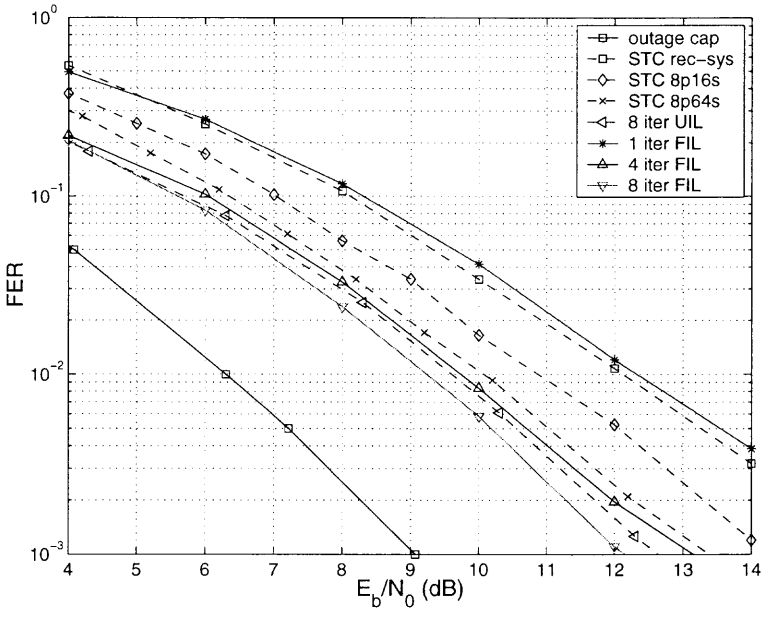

Figure 3.17 FER of 16 state 8-PSK turbo-STCM (2T2R) over the fading channel, with fixed interleaver (FIL) and averaged over interleavers (UIL) of size $K = 1300$ symbols.

CHAPTER 4

ERROR PERFORMANCE ANALYSIS OF TURBO-STCM

The analytical union bound on the bit error rate (BER) is developed for turbo-STCM with multiple transmit/receive antennas. This analytical approach is complementary to simulations. Performance analysis of the turbo code for a specific interleaver is not mathematically tractable. The approach suggested to overcome this problem is to make the bound independent of the particular interleaver used by introducing a uniformly average interleaver, which maps an input word into all its permutations [56]. The analysis technique resembles that of random coding, with the distinction that the constituent codes are fixed and the interleaver is random. The ensemble of codes is generated by varying interleaving permutations for a given size interleaver. This approach enables to express the union bound of the turbo code in terms of the input-output weight enumerators of the constituent codes and the interleaver size. As an interim step, the bound is found first conditioned on the channel. This is essentially the additive white Gaussian noise case [50]. Subsequently, the bounds are averaged over the Rayleigh fading channel [51, 54, 52]. These bounds are demonstrated by comparison to computer simulations utilizing iterative log-APP decoding.

The chapter is organized as follows. In the first section, we present a brief introduction of turbo-STCM system assumption. After that, the union bounds are derived for turbo-STCM over the AWGN channels with the uniform random interleaver. Then we extend the bounds, that applied for turbo-STCM over the AWGN channels, for the block-fading channels. Finally, the use of the new bounds are illustrated for turbo-STCM scheme with multiple antennas via some numerical examples.

4.1 Definitions and Notations

Turbo codes are essentially very long block codes. This makes their analysis a challenging problem. The analysis of turbo codes for a specific interleaver is intractable. A framework for the theoretical analysis of binary turbo codes for the additive white Gaussian noise (AWGN) channel is suggested in [56, 57]. In these publications, the upper bound of the maximum likelihood (ML) soft decoder is evaluated as an ensemble average over all possible interleaver permutations. This enables to express the upper bound independent of the interleaver and in terms of the individual constituent codes. In [68], analytical bounding of parallel concatenated turbo codes over the AWGN channel was extended from binary codes to multi-level turbo coded modulation systems with single transmit/receive antenna. In [69], this analysis was carried out for the fading channel. In this thesis, we further extend those results to the multiple transmit/receive antennas turbo-STCM.

Consider an example of turbo-STCM with two transmit antennas as shown in Fig. 4.1. The signal and channel models are defined in (3.1). The specific constituent space-time codes used to demonstrate the analysis are 8 state 4-PSK as per Fig. 3.2. The turbo-STCM scheme employs symbol uniformly random interleaver of specified size K. For 4-PSK modulation, the interleaver size in bits is $2K$, while for 8-PSK modulation, the interleaver size in bits is given by $3K$.

The turbo-STCM scheme accepts $\mu = 2$ binary symbols at a time and transforms them into $N = 2$ (number of transmit antenna) blocks of 2 binary symbols that are fed to a memoryless mapper $\rho(\cdot)$. In the notation defined in Chapter 3, the transmitted symbol vector $\mathbf{s}_k = \left[s_k^{(1)}\ s_k^{(2)}\right]^T$ is obtained from the mapping $\rho(\mathbf{c}_k) = \mathbf{s}_k$, where $\rho : \{0,1\}^4 \rightarrow \mathcal{C}^2$ and $\mathbf{c}_k \in \{0,1\}^4$ is the binary label "4" associated with the symbol vector $\mathbf{s}_k$. The symbol $s_k^{(1)}$ emitted by antenna 1 at time k, represents systematic information, while symbol $s_k^{(2)}$ transmitted by antenna 2 is the parity data. In the analysis of turbo-STCM, the receiver employs a single

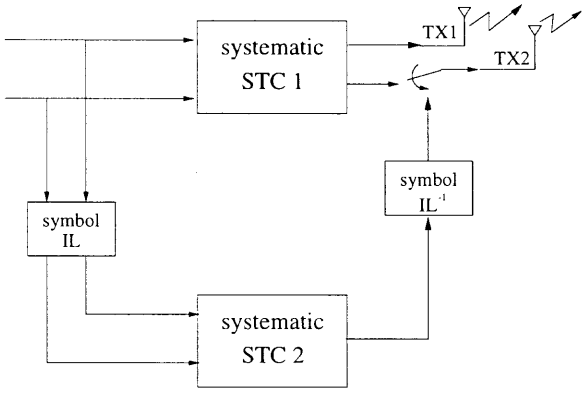

Figure 4.1 Turbo-STCM encoder for two transmit antennas.

antenna $M = 1$. The received signal is constituted by the sum of systematic and parity symbols. The noiseless received signal conditioned on the channel can then be expressed,

$$x_k = h_1 s_k^{(1)} + h_2 s_k^{(2)} = \mathbf{h}^T \rho(\mathbf{c}_k), \tag{4.1}$$

where the channel vector is defined $\mathbf{h} = [h_1 \; h_2]^T$, and h_1, h_2 are respectively, the channel gains between antenna 1,2 at the transmitter and the receiver. In the notation of (3.1), $\mathbf{h} = \mathbf{H}$. In this interim step over AWGN channel, $h_1 = h_2 = 1$.

The symbol squared Euclidean distance (SED) for two transmitted symbols is

$$d^2(\mathbf{c}_k, \mathbf{e}_k) \triangleq \left| \mathbf{h}^T \left(\rho(\mathbf{c}_k) - \rho(\mathbf{c}_k \oplus \mathbf{e}_k) \right) \right|^2, \tag{4.2}$$

where $\mathbf{c}_k \oplus \mathbf{e}_k$ is a binary label associated with a symbol, and $a \oplus b = (a + b) \bmod 2$. Note that similar to $\mathbf{c}_k$, $\mathbf{e}_k \in \{0, 1\}^4$. To separate constellation and channel effects on the symbol SED, let $\delta(\mathbf{c}_k, \mathbf{e}_k) = \rho(\mathbf{c}_k) - \rho(\mathbf{c}_k \oplus \mathbf{e}_k)$ and rewrite (4.2),

$$d^2(\mathbf{c}_k, \mathbf{e}_k) = \left| \mathbf{h}^T \delta(\mathbf{c}_k, \mathbf{e}_k) \right|^2. \tag{4.3}$$

Turbo-codes can be viewed as block codes with block length equal to the interleaver size. The analysis of turbo-STCM is based on the enumeration of error sequences according to the pattern of the underlying binary labels. For an input

block of length K symbols (corresponding to an interleaver of size K symbols), the output consists of K symbols for each of the two transmit antennas. Equivalently, the output consists of a sequence of K vectors $\mathbf{s}_k$, $\underline{\mathbf{s}}_K = (\mathbf{s}_1, \ldots, \mathbf{s}_K)$. Each output vector $\mathbf{s}_k$ has a binary label $\mathbf{c}_k$ as defined in (4.1). Denote the sequence of binary labels associated with the transmitted block $\underline{\mathbf{c}}_K = (\mathbf{c}_1, \ldots, \mathbf{c}_K)$. An error event occurs when the demodulation chooses the transmitted sequence of symbols corresponding to binary labels $\underline{\mathbf{c}}_K \oplus \underline{\mathbf{e}}_K$, where $\underline{\mathbf{e}}_K = (\mathbf{e}_1, \ldots, \mathbf{e}_K)$ and $\underline{\mathbf{e}}_K$ is not an all zero sequence. Note that for 4-PSK modulation and two transmit antennas, $\underline{\mathbf{c}}_K$, $\underline{\mathbf{e}}_K$ are binary sequences with $4K$ elements. Error events are characterized by their cumulative SED defined as the sum of symbol SED's:

$$\begin{aligned} d^2\left(\underline{\mathbf{c}}_K, \underline{\mathbf{e}}_K\right) &= \sum_{k=1}^{K} d^2\left(\mathbf{c}_k, \mathbf{e}_k\right) \\ &= \sum_{k=1}^{K} \left|\mathbf{h}^T \delta\left(\mathbf{c}_k, \mathbf{e}_k\right)\right|^2 . \end{aligned} \tag{4.4}$$

4.2 Input-Output Weight Enumerator

The main tool for analysis of the bit error probability of turbo-STCM is the enumeration of error sequences. This enumeration is carried out according to the binary labels of the underlying binary code. We proceed to define parameters of error sequences necessary for our analysis and to determine ways for the evaluation of these parameters. An error sequence is a start-to-end path through a trellis *error-state diagram*. The error-state diagram is a copy of the state diagram describing the code, but with the distinction that the binary labels of the trellis branches represent error patterns rather than encoder outputs. As explained in the previous section, for 4-PSK turbo-STCM with K symbol interleaver, we need to consider error sequences of length $4K$ bits. Given a systematic block code of length $4K$ bits, the set of transmitted codewords, and the set of received codewords, the input-output weight enumerator (IOWE) $a\left(4K, w, z\right)$ denotes the number of error sequences of length

$4K$ bits that have Hamming weight w for the information bits and z for the parity bits. Such error sequences are referred as (w, z) sequences. The overall Hamming weight of these sequences is $w+z$. The enumeration of error sequences with specified number of information and parity bits will play an important role in our analysis. We describe below how to evaluate the IOWE's for both stand-alone space-time codes and for turbo-STCM.

Computation of the IOWE $a\,(4K, w, z)$ of a space-time code is possible from the *error-state diagram* of the code. We follow the approach in [57] to find the enumerators for the 8 state 4-PSK space-time code in Fig. 3.2 and 16 state 8-PSK space-time code in Fig. 3.3. Labeling state transitions with monomials JW^wZ^z, where w is the number of systematic bit errors and z is the number of parity bit errors, the following one-step transition matrix are obtained.

2 bits/s/Hz spectral efficiency

From Fig. 3.2, the transition from state 1 to state 4 occurs with an input symbol '3' (binary '11'). The output is labeled '30', meaning binary '11' for antenna 1 (systematic part) and binary '00' for antenna 2 (parity part). Consequently the weight of systematic bits in the error sequence is 2 and the weight of parity bits is 0. This matches the powers 2 and 0 of W and of Z, respectively, of the (1,4) term (JW^2) in the matrix Υ_1. The variable J indicates that there exists a transition between states 1 and 4.

$$\Upsilon_1(J,W,Z) = \begin{bmatrix} J & JW & JW & JW^2 & 0 & 0 & 0 & 0 \\ 0 & 0 & 0 & 0 & JZ & JWZ & JWZ & JW^2Z \\ JWZ & JZ & JW^2Z & JWZ & 0 & 0 & 0 & 0 \\ 0 & 0 & 0 & 0 & JWZ^2 & JZ^2 & JW^2Z^2 & JWZ^2 \\ JW & JW^2 & J & JW & 0 & 0 & 0 & 0 \\ 0 & 0 & 0 & 0 & JWZ & JW^2Z & JZ & JWZ \\ JW^2Z & JWZ & JWZ & JZ & 0 & 0 & 0 & 0 \\ 0 & 0 & 0 & 0 & JW^2Z^2 & JWZ^2 & JWZ^2 & JZ^2 \end{bmatrix} \tag{4.5}$$

3 bits/s/Hz spectral efficiency

From Fig. 3.3,

$\boldsymbol{\Upsilon}_1(J,W,Z)=$

$$\begin{bmatrix}
J & JW & JW & JW^2 & JW & JW^2 & JW^2 & JW^3 & 0 & 0 & 0 & 0 & 0 & 0 & 0 & 0 \\
0 & 0 & 0 & 0 & 0 & 0 & 0 & 0 & JZ & JWZ & JWZ & JW^2Z & JWZ & JW^2Z & JW^2Z & JW^3Z \\
JWZ^2 & JZ & JW^2Z & JWZ & JW^2Z & JWZ & JW^3Z & JW^2Z & 0 & 0 & 0 & 0 & 0 & 0 & 0 & 0 \\
0 & 0 & 0 & 0 & 0 & 0 & 0 & 0 & JWZ^2 & JZ^2 & JW^2Z^2 & JWZ^2 & JW^2Z^2 & JWZ^2 & JW^3Z^2 & JW^2Z^2 \\
JWZ & JW^2Z & JZ & JWZ & JW^2Z & JW^3Z & JWZ & JW^2Z & 0 & 0 & 0 & 0 & 0 & 0 & 0 & 0 \\
0 & 0 & 0 & 0 & 0 & 0 & 0 & 0 & JWZ^2 & JW^2Z^2 & JZ^2 & JWZ^2 & JW^2Z^2 & JW^3Z^2 & JWZ^2 & JW^2Z^2 \\
JW^2Z^2 & JWZ^2 & JWZ^2 & JZ^2 & JW^3Z^2 & JW^2Z^2 & JW^2Z^2 & JWZ^2 & 0 & 0 & 0 & 0 & 0 & 0 & 0 & 0 \\
0 & 0 & 0 & 0 & 0 & 0 & 0 & 0 & JW^2Z^3 & JWZ^3 & JWZ^3 & JZ^3 & JW^3Z^3 & JW^2Z^3 & JW^2Z^3 & JWZ^3 \\
JW & JW^2 & JW^2 & JW^3 & J & JW & JW & JW^2 & 0 & 0 & 0 & 0 & 0 & 0 & 0 & 0 \\
0 & 0 & 0 & 0 & 0 & 0 & 0 & 0 & JWZ & JW^2Z & JW^2Z & JW^3Z & JZ & JWZ & JWZ & JW^2Z \\
JW^2Z & JWZ & JW^3Z & JW^2ZJWZ & & JZ & JW^2Z & JWZ & 0 & 0 & 0 & 0 & 0 & 0 & 0 & 0 \\
0 & 0 & 0 & 0 & 0 & 0 & 0 & 0 & JW^2Z^2 & JWZ^2 & JW^3Z^2 & JW^2Z^2 & JWZ^2 & JZ^2 & JW^2Z^2 & JWZ^2 \\
JW^2Z & JW^3Z & JWZ & JW^2ZJWZ & & JW^2Z & JZ & JWZ & 0 & 0 & 0 & 0 & 0 & 0 & 0 & 0 \\
0 & 0 & 0 & 0 & 0 & 0 & 0 & 0 & JW^2Z^2 & JW^3Z^2 & JWZ^2 & JW^2Z^2 & JWZ^2 & JW^2Z^2 & JZ^2 & JWZ^2 \\
JW^3Z^2 & JW^2Z^2 & JW^2Z^2 & JWZ^2 & JW^2Z^2 & JWZ^2 & JW^2Z^2 & JWZ^2 & JWZ^2 & JZ^2 & 0 & 0 & 0 & 0 & 0 & 0 \\
0 & 0 & 0 & 0 & 0 & 0 & 0 & 0 & JW^3Z^3 & JW^2Z^3 & JW^2Z^3 & JWZ^3 & JW^2Z^3 & JWZ^3 & JWZ^3 & JZ^3
\end{bmatrix} \tag{4.6}$$

In the following, the computation of turbo-STCM is concentrated in 4-PSK case (4.5) while 8-PSK (4.6) follows the same steps. The output of turbo-STCM code (see scheme in Fig. 4.1) consists of the sum of the systematic part of a constituent space-time code and the punctured parity part. The systematic part is common to both constituent codes. The parity part is chosen alternately from the two space-time codes, hence it is 1/2 punctured with respect to both codes. To represent the constituent space-time codes, we need the transfer matrix of the codes with 1/2 puncturing of the parity part. An approach for incorporating puncturing in a transfer matrix is suggested in [68, 70]. Following the procedure in the reference, it can be shown that the transfer matrix of the punctured space-time code consists of the matrix in (4.5) with all Z^b, $b \in \{0,1,2\}$ terms replaced by the 2×2 matrix $\begin{pmatrix} 0 & Z^b \\ 1 & 0 \end{pmatrix}$, resulting in a 16×16 one-step transition matrix denoted $\boldsymbol{\Upsilon}(J,W,Z)$ for punctured 8-state 4-PSK space-time constituent code.

The one-step transition matrix represents the number of systematic/parity bit errors for transitions between two states specified by the matrix. The number of states for the punctured code is 16. A complete characterization of the error-state diagram is required to express the input-output relation for *any* number k of steps through the trellis, $0 \leq k \leq K$ (each trellis transition yields an output represented by a four bit binary label). Let the initial input state vector be the 16×1 vector $\sigma_0 = [1, 0, \ldots, 0]^T$, indicating that the code starts operating from state 1. Then the input-output transmittance is determined by accounting for all possible number of steps (from 0 to K) that it takes to produce the system output from the input. The output state can then be expressed

$$\sigma = \sum_{k=0}^{K} \boldsymbol{\Upsilon}^k(J, W, Z)\sigma_0. \tag{4.7}$$

By definition, the transfer function $T(J, W, Z)$ of the space-time code is the transmittance from the output state to the input state. If no assumption is made on the termination of the space-time code trellis, the transfer function from *either* of the output states to the input zero state is given by the sum of the first row of $\sum_{k=0}^{K} \boldsymbol{\Upsilon}^k(J, W, Z)$ as in [68, 70],

$$T(J, W, Z) = \sum_i \left[\sum_{k=0}^{K} \boldsymbol{\Upsilon}^k(J, W, Z) \right]_{1,i}, \tag{4.8}$$

where $[\mathbf{A}]_{1,i}$ are the first row elements of the matrix $\mathbf{A}$.

In [57, 71], it is shown that the code transfer function can also be expanded in the power series

$$T(J, W, Z) = \sum_{j \geq 0} \sum_{w \geq 0} \sum_{z \geq 0} a\,(j, w, z)\, J^j W^w Z^z. \tag{4.9}$$

We are interested in error sequences of length $4K$ bits, and the summation is restricted to sequences such that $w \leq 2K$ and $z \leq 2K$. The previous expression provides the relation between the code transfer function $T(J, W, Z)$ and the IOWE's $a\,(j, w, z)$. Once $T(J, W, Z)$ is found using the techniques presented in this section,

$a(j, w, z)$ are just the coefficients of the power series expansion. This completes the procedure for the computation of the IOWE of the stand-alone space-time code.

Next, we enumerate the error sequences of the turbo-STCM code. Interleaving does not change the input Hamming weight, hence both components of the parallel concatenated structure of turbo-STCM share the same input Hamming weight w. Let the IOWE's for error sequences of the constituent codes with information weight w, parity weight z, and length $4K$ bits, be denoted $a_1(4K, w, z)$ and $a_2(4K, w, z)$, respectively. A uniformly random interleaver is introduced, which maps a given input word of weight w into all its $\binom{2K}{w}$ distinct permutations with equal probability $1/\binom{2K}{w}$. Using this approach, it is shown in [56] that for a parallel concatenated turbo code utilizing a random uniform interleaver, the average number of (w, z) error sequences of length $4K$ bits is given by the enumerator

$$\tilde{a}(4K, w, z) = \sum_{z_1+z_2=z} \frac{a_1(4K, w, z_1)a_2(4K, w, z_2)}{\binom{2K}{w}}, \tag{4.10}$$

where $0 \leq w \leq 2K$ and $0 \leq z \leq 2K$. This expression is used to evaluate the IOWE's of turbo-STCM given the IOWE's of the constituent codes.

The denominator in the expression (4.10) is suitable for a bit interleaver and is not easily extended to the symbol interleaver employed by turbo-STCM. However, the application of (4.10) to turbo-STCM is justified based on the following argument. A symbol interleaver is just a restricted form of bit interleaver, where bits are interleaved in groups. In particular, the symbol interleaver ensures that the pairs of binary labels '01', '10', and '11' are interleaved as pairs. This will result in fewer permutations than for a bit interleaver. Since the number of permutations appears in the denominator of (4.10), a symbol interleaver will tend to increase the values of the IOWE. This effect is however minimal, since the IOWE will be used later in this Chapter to express the union bound to the bit error probability, and the bound is

dominated by terms with small weight w. For hundreds/thousands bit long sequences (values of $2K$) with low weight (single digit values of w), the number of pairs '01', '10', and '11' is negligible compared to the number of '00' pairs. We conclude that use of the bit interleaver in the denominator of (4.10) introduces only a negligible error in the computation of the IOWE.

4.3 Derivation of the Union Bound

In this section, the union bound is developed for turbo-STCM system described in the previous Chapter.

In [56], the union bound idea was initially introduced for finding average performance bound of binary turbo codes (averaged over all possible interleavers). After that, this method was applied to turbo-coded modulation systems [68, 70]. The average bounds was provided for maximum-likelihood decoding of turbo scheme with one transmit-one receive antenna configuration. In this chapter, the average bound idea is further extended to turbo-STCM with multiple antennas configuration. The basic difference is that we need to find the IOWE of the punctured space-time component encoders, rather than the underlying binary encoders [56, 68].

In order to derive the bound, we analyze the error event probability at first, and identify different types of error sequences. Then, the ensemble distance spectrum of all possible error sequences are found to average over all uniform random interleaver. Instead of all-zero codeword, each of the possible codewords is considered as the transmitted one with equal probability. This is also why we make the sum of the error probabilities over all possible transmitted and received codewords rather than over all the possible codewords for a given transmitted codeword. Finally, according to average SED of all error type sequences, the union bound is computed by summing the contributions of all error sequences.

The analytical union bound is derived by conditioning on the channel. This is essentially the non-fading AWGN case.

1. Error event probability

The pairwise error probability $P(\underline{\mathbf{c}}_K \rightarrow \underline{\mathbf{c}}_K \oplus \underline{\mathbf{e}}_K)$ of transmitting a sequence $\underline{\mathbf{s}}_K$ of K vector symbols corresponding to a sequence of binary labels $\underline{\mathbf{c}}_K$ and choosing a sequence corresponding to binary labels $\underline{\mathbf{c}}_K \oplus \underline{\mathbf{e}}_K$, is given by the well known relation

$$P(\underline{\mathbf{c}}_K \rightarrow \underline{\mathbf{c}}_K \oplus \underline{\mathbf{e}}_K) = Q\left(\sqrt{\frac{r_c E_b d^2(\underline{\mathbf{c}}_K, \underline{\mathbf{e}}_K)}{2N_0}}\right), \tag{4.11}$$

where $r_c = 2/4$ is the turbo-STCM code rate and $d^2(\underline{\mathbf{c}}_K, \underline{\mathbf{e}}_K)$ is the cumulative SED of the two sequences as defined in (4.4). The pairwise error probability is upper bound by the Bhattacharyya bound

$$P(\underline{\mathbf{c}}_K \rightarrow \underline{\mathbf{c}}_K \oplus \underline{\mathbf{e}}_K) \leq \frac{1}{2} Z^{d^2(\underline{\mathbf{c}}_K, \underline{\mathbf{e}}_K)}, \tag{4.12}$$

where $Z = e^{-r_c E_b/4N_0}$. Let $P_K(e|\mathbf{h})$ denote the average probability of error of a sequence of length K symbols, conditioned on the channel vector $\mathbf{h}$. The union bound to $P_K(e|\mathbf{h})$ is obtained by summing over all possible error sequences $\underline{\mathbf{e}}_K$ and averaging with respect to all possible transmitted sequences $\underline{\mathbf{c}}_K$. Assuming transmitted codewords with equal probability,

$$\begin{aligned} P_K(e|\mathbf{h}) &\leq \sum_{\underline{\mathbf{c}}_K} P(\underline{\mathbf{c}}_K) \sum_{\underline{\mathbf{e}}_K \neq 0} P(\underline{\mathbf{c}}_K \rightarrow \underline{\mathbf{c}}_K \oplus \underline{\mathbf{e}}_K) \\ &\leq 2^{-4K} \sum_{\underline{\mathbf{c}}_K} \sum_{\underline{\mathbf{e}}_K \neq 0} \frac{1}{2} Z^{d^2(\underline{\mathbf{c}}_K, \underline{\mathbf{e}}_K)} = B_K(e|\mathbf{h}), \end{aligned} \tag{4.13}$$

where for 4-PSK turbo-STCM with two transmit antenna, $P(\underline{\mathbf{c}}_K) = 2^{-4K}$ is the probability of a single sequence of $4K$ bits. In the previous expression, the Bhattacharyya bound was applied to the union bound. We use the notation $B_K(e|\mathbf{h})$ to denote the Bhattacharyya union bound to the sequence error probability conditioned on the channel. It is not difficult to check that the symbol mapping for

space-time coding, as shown in Fig. 2.2 and defined in (4.13), is not an isometry, hence SED's associated with different transmitted sequences are not preserved. It follows that all possible transmitted and received codewords need to be taken into account in computing the union bound.

2. Ensemble distance spectrum

The computation of the union bound are concerned for 4-PSK turbo-STCM with $N = 2$ transmit antennas and an interleaver size of K symbols. Computation of the union bound proceeds by enumerating all SED's. The union bound for turbo-TCM with single antenna was developed in [68, 69]. We follow the methodology used in the reference with suitable modifications to account for the differences between STC and TCM. We start by noting that expression (4.13) is of a union bound that incorporates all error sequences and it is averaged over all transmitted sequences. The goal is to list all possible SED's and their multiplicity, i.e., to determine the ensemble SED spectrum for the code.

Consider the binary labels $\mathbf{c}_k$, $k = 1, \ldots, K$. Each consists of a systematic part and a parity part. In particular, for the 4-PSK two transmit antenna code, the systematic and parity parts consist of two bits each. At the binary label level, errors will be manifested as bit errors in the systematic and/or parity parts of $\mathbf{c}_k$. The information are collected as to how many symbols have errors in some specified values of i systematic bits and j parity bits.

For 2 bits/s/Hz, 4-PSK two transmit antenna

$$(i, j) \in \{(1,0), (2,0), (0,1), (0,2), (1,1), (1,2), (2,1), (2,2)\}. \tag{4.14}$$

For 3 bits/s/Hz, 8-PSK two transmit antenna

$$\begin{aligned}(i,j) \in \{&(0,1),(0,2),(0,3),(1,0),(1,1),(1,2),(1,3),(2,0),(2,1),(2,2),\\ &(2,3),(3,0),(3,1),(3,2),(3,3)\}.\end{aligned} \tag{4.15}$$

As in [69], we define n_{ij} to be the number of symbols that have i systematic bit errors and j parity bit errors. The *type* of an error sequence is the vector $\mathbf{n} = (n_{i,j})$, whose elements are the number of symbols associated with each error (i, j). The cumulative SED of sequences of type $\mathbf{n}$ depends on the transmitted sequence $\underline{\mathbf{c}}_K$ as well as on the actual disposition of the systematic and parity bit errors in the sequence. Indeed, an element of the vector $\mathbf{n}$, say $n_{1,0}$, corresponds to different SED's depending on whether the systematic bit error is in the first or second of the two systematic bits. For a given type $\mathbf{n}$, cumulative SED's can be modeled as a discrete random variable $D^2_{\mathbf{n}}$, with $D^2_{\mathbf{n}} \in \left\{d^2_{\mathbf{n},1}, \ldots, d^2_{\mathbf{n},Q_{\mathbf{n}}}\right\}$, where $Q_{\mathbf{n}}$ is the number of possible distances associated with the type $\mathbf{n}$. Statistical characterization of $D^2_{\mathbf{n}}$ is provided by its probability mass distribution $(p_1, \ldots, p_{Q_{\mathbf{n}}})$.

We proceed to assemble the bit error union bound by enumerating the cumulative SED's and their multiplicity for each type $\mathbf{n}$. The Bhattacharyya bound for an error sequence with SED $d^2_{\mathbf{n},\alpha}$ is given by $\frac{1}{2}Z^{d^2_{\mathbf{n},\alpha}}$. The contribution to the union bound of a type $\mathbf{n}$ sequence is found by averaging over all possible cumulative SED's associated with $\mathbf{n}$:

$$P(\mathbf{n}) = \frac{1}{2}E\left[Z^{D^2_{\mathbf{n}}}\right] = \frac{1}{2}\sum_{\alpha=1}^{Q_{\mathbf{n}}} p_\alpha Z^{d^2_{\mathbf{n},\alpha}}. \tag{4.16}$$

3. Union bound of the bit error probability

Previously, we have established the contribution to the union bound of a single sequence of specified type $\mathbf{n}$. Consider now the multiplicity of error sequences of type $\mathbf{n}$. Given an error sequence of type $\mathbf{n}$, it is possible to determine the total number of systematic bit errors w and parity bit errors z.

Indeed, for 2 bits/s/Hz, 4-PSK two transmit antenna

$$\begin{aligned} n_{1,0} + n_{1,1} + n_{1,2} + 2n_{2,0} + 2n_{2,1} + 2n_{2,2} &= w \\ n_{0,1} + 2n_{0,2} + n_{1,1} + 2n_{1,2} + n_{2,1} + 2n_{2,2} &= z. \end{aligned} \tag{4.17}$$

For 3 bits/s/Hz, 8-PSK two transmit antenna

$$n_{10} + n_{11} + n_{12} + n_{13} + 2n_{20} + 2n_{21} + 2n_{22} + 2n_{23} + 3n_{30} + 3n_{31} + 3n_{32} + 3n_{33}=w$$

$$n_{01} + 2n_{02} + 3n_{03} + n_{11} + 2n_{12} + 3n_{13} + n_{21} + 2n_{22} + 3n_{23} + n_{31} + 2n_{32} + 3n_{33}=z. \tag{4.18}$$

All type $\mathbf{n}$ error sequences are also (w, z) sequences (i.e., with weight w systematic bits and z parity bits). We refer to these as $(w, z, \mathbf{n})$ sequences. However, the set of (w, z) error sequences contains also sequences other than $\mathbf{n}$, as the system (4.17) and (4.18) has more than a single solution. The fraction of type $\mathbf{n}$ sequences among all (w, z) sequences represents the probability of such sequence and it is given by the ratio of the number of possible $(w, z, \mathbf{n})$ sequences, $T_{w,z,\mathbf{n}}$, to the total number of possible (w, z) sequences, $T_{w,z}$. The total number of possible sequences with $n_{1,0}$, $n_{2,0}$, etc., symbols in error out of K symbols is given by:

$$\binom{K}{n_{1,0}, n_{2,0}, \ldots, n_{2,2}} = \frac{K!}{\prod_{i,j} (n_{i,j})! \left(K - \sum_{i,j} n_{i,j}\right)!}, \tag{4.19}$$

where (i, j) pairs are given by (4.14). Consider $n_{1,0}$, the number of symbol errors caused by a single systematic bit error. Since there are two systematic bits and any could be in error, there are two symbol errors associated with each of the $n_{1,0}$ symbols. This multiplies the number of arrangements by 2 for each of the $n_{1,0}$ symbols. For $n_{1,1}$ symbols, the number of possible arrangements increases by 4 for each of the $n_{1,1}$ symbols, since both the systematic bit and the parity bit error can each be in two different positions. Conversely, only a single arrangement is associated with $n_{2,2}$. It can be concluded that the multiplicity of $(w, z, \mathbf{n})$ error sequences is:

$$T_{w,z,\mathbf{n}} = \binom{K}{n_{1,0}, n_{2,0}, \ldots, n_{2,2}} 2^{n_{1,0}} \cdots 4^{n_{1,1}} \cdots 2^{n_{2,1}}. \tag{4.20}$$

The number of possible (w, z) sequences is the product of the number of arrangements of w out $2K$ bits by the number of arrangements of z out of $2K$ bits:

$$T_{w,z} = \binom{2K}{w} \binom{2K}{z}, \tag{4.21}$$

where $2K$ is the number of bits corresponding to the sequence of K symbols transmitted by each antenna. It follows that the probability of a $(w, z, \mathbf{n})$ sequence is given by

$$\Phi(w, z, \mathbf{n}) = \frac{T_{w,z,\mathbf{n}}}{T_{w,z}}. \tag{4.22}$$

The transmitted sequence of K symbols through each antenna corresponds to a received sequence of $2K$ symbols. In terms of binary labels the received sequence has a length of $4K$ bits. The multiplicity of (w, z) error sequences of length $4K$ bits is precisely the quantity $\tilde{a}(4K, w, z)$, which was evaluated in (4.10). Subsequently, the multiplicity of $(w, z, \mathbf{n})$ sequences is given by $\tilde{a}(4K, w, z)\Phi(w, z, \mathbf{n})$. A reminder that since $\tilde{a}(4K, w, z)$ is averaged over interleavers, the contribution of $(w, z, \mathbf{n})$ sequences to the union bound is likewise averaged over interleavers,

$$\begin{aligned} P(w, z, \mathbf{n}) &= \tilde{a}(4K, w, z)\Phi(w, z, \mathbf{n})\, P(\mathbf{n}) \\ &= \frac{1}{2}\tilde{a}(4K, w, z)\Phi(w, z, \mathbf{n})\, E\left[Z^{D^2_{\mathbf{n}}}\right]. \end{aligned} \tag{4.23}$$

Next we proceed to account for all types $\mathbf{n}$ and all weights w and z. This completes the evaluation of the bound over all error sequences. With reference to (4.13),

$$\frac{1}{2}\sum_{\underline{\mathbf{e}}_K \neq 0} Z^{d^2(\underline{\mathbf{c}}_K, \underline{\mathbf{e}}_K)} = \sum_{w=1}^{2K}\sum_{z=0}^{2K}\sum_{\mathbf{n}_\beta(w,z)} P(w, z, \mathbf{n}_\beta), \tag{4.24}$$

where β indexes all possible types $\mathbf{n}_\beta(w, z)$ for sequences with specified w and z, i.e., all solutions to the system of equations (4.17). Note that averaging over the interleavers has the effect of making the bound, independent of the transmitted codeword $\underline{\mathbf{c}}_K$. Substituting (4.23) and (4.24) in (4.13), we obtain the bound on the probability of error of a sequence of length K symbols, conditioned on the channel vector $\mathbf{h}$

$$B_K(e|\mathbf{h}) = \frac{1}{2}\sum_{w=1}^{2K}\sum_{z=0}^{2K}\sum_{\mathbf{n}_\beta(w,z)} \tilde{a}(4K, w, z)\Phi(w, z, \mathbf{n}_\beta)\, E\left[Z^{D^2_{\mathbf{n}_\beta}}\right]. \tag{4.25}$$

The result in (4.25) is to find the union bound for the bit error probability. First, determine the union bound of the probability of error sequences with

systematic bits weight w:

$$P(w) \leq \frac{1}{2} \sum_{z=0}^{2K} \sum_{\mathbf{n}_\beta(w,z)} \tilde{a}(4K, w, z) \Phi(w, z, \mathbf{n}_\beta) E\left[Z^{D^2_{\mathbf{n}_\beta}}\right]. \tag{4.26}$$

Utilizing the approach in [6], averaging over all weights w, we compute the expected number of errors. When divided by $2K$, the number of information bits in the transmitted sequence, we obtain the bit error probability conditioned on the channel $\mathbf{h}$, $P(e|\mathbf{h})$:

$$\begin{aligned} P(e|\mathbf{h}) &= \frac{E[w]}{2K} \\ &\leq \sum_{w=1}^{2K} \sum_{z=0}^{2K} \sum_{\mathbf{n}_\beta(w,z)} \frac{w}{4K} \tilde{a}(4K, w, z) \Phi(w, z, \mathbf{n}_\beta) E\left[Z^{D^2_{\mathbf{n}_\beta}}\right] = B(e|\mathbf{h}), \end{aligned} \tag{4.27}$$

where the notation $B(e|\mathbf{h})$ is used for the union bound on the bit error probability conditioned on the channel.

4. Average SED spectrum

The expression (4.27) shows that for given w, z and $\mathbf{n}$, the bit error is a function of the average $E\left[Z^{D^2_{\mathbf{n}}}\right]$ over the cumulative SED spectrum. Note that the random variable representing the cumulative SED for a sequence of type $\mathbf{n}$, $D^2_{\mathbf{n}}$, and hence, $E\left[Z^{D^2_{\mathbf{n}}}\right]$, are conditioned on the channel $\mathbf{h}$. The cumulative SED is constituted by the sum of SED's associated with single symbol errors,

$$D^2_{\mathbf{n}} = n_{1,0} D^2(1,0) + \cdots + n_{2,2} D^2(2,2), \tag{4.28}$$

where $n_{i,j} D^2(i,j)$ is the contribution to the cumulative SED of the $n_{i,j}$ symbols with i information bit errors and j parity bit errors and $D^2(i,j)$ is a random variable modeling the SED for a single received symbol with (i,j) errors. Assuming that the SED's $D^2(i,j)$ in an error sequence are uncorrelated,

$$E\left[Z^{D^2_{\mathbf{n}}}\right] = E\left[\left(Z^{D^2(1,0)}\right)^{n_{1,0}}\right] \cdot \ldots \cdot E\left[\left(Z^{D^2(2,2)}\right)^{n_{2,2}}\right]. \tag{4.29}$$

Recalling the notation $\mathbf{c}_k$ for binary labels of transmitted symbols, and $\mathbf{e}_k$ for binary labels of errors, the average contribution to the bound by a symbol error with i information bits and j parity bits in error is given by

$$E\left[Z^{D^2(i,j)}\right] = \sum_{\mathbf{c}_k} P(\mathbf{c}_k) \sum_{\mathbf{e}_k:i,j} P(\mathbf{c}_k \to \mathbf{c}_k \oplus \mathbf{e}_k) Z^{d^2(\mathbf{c}_k,\mathbf{e}_k)}, \tag{4.30}$$

where $P(\mathbf{c}_k)$ is the probability of a symbol with binary label $\mathbf{c}_k$, $P(\mathbf{c}_k \to \mathbf{c}_k \oplus \mathbf{e}_k)$ is the pairwise error probability, and the sum is taken over all errors with i systematic and j parity bits.

An example is provided below to help clarify the preceding argument.

Example

The equivalent symbol mapping in the AWGN channel is shown in Fig. 2.2. The STC encoder is clearly not optimized for operation over the AWGN channel. No attempt is made to optimize the codes, as we focus on the analysis rather than on the performance.

For simplicity, it is assumed in this example that $\mathbf{h}^T = [1, 1]$. For the case of 4-PSK two transmit antenna, and assuming equally likely transmitted symbols, $P(\mathbf{c}_k) = 1/16$. Consider errors with one systematic bit $i = 1$ and one parity bit $j = 1$. Since either of the two errors can occur in either one of two bits, there are four possible $\mathbf{e}_k$'s. Assuming those errors to be equally likely, $P(\mathbf{c}_k \to \mathbf{c}_k \oplus \mathbf{e}_k) = 1/4$. Thus

$$E\left[Z^{D^2(1,1)}\right] = \frac{1}{64} \sum_{\mathbf{c}_k} \sum_{\mathbf{e}_k:1,1} Z^{d^2(\mathbf{c}_k,\mathbf{e}_k)}. \tag{4.31}$$

The computation proceeds by considering each of the individual errors for each of the transmitted symbols. For example, the contribution of error label $\mathbf{e}_k = (1010)$ is determined from the following table

c_k	0000	0001	0010	0011	0100	0101	0110	0111
$c_k \oplus (1010)$	1010	1011	1000	1001	1110	1111	1100	1101
$d^2(c_k \oplus (1010))$	16	8	0	8	8	16	8	0

c_k	1000	1001	1010	1011	1100	1101	1110	1111
$c_k \oplus (1010)$	0010	0011	0000	0001	0110	0111	0100	0101
$d^2(c_k \oplus (1010))$	0	8	16	8	8	0	8	16

It follows that $\mathbf{e}_k = (1010)$ contributes SED's with the following multiplicity:

$d^2(1,1)$	0	8	16
Multiplicity	4	8	4

The computation of $E\left[Z^{D^2(1,1)}\right]$ is completed by listing the contributions of the other $i = j = 1$ errors, namely (1001), (0110), and (0101). When all results are aggregated, the following spectrum of SED's is obtained for such errors:

$d^2(1,1)$	0	2	8	10	16
Multiplicity	12	16	16	16	4

It follows that

$$E\left[Z^{D^2(1,1)}\right] = \frac{1}{16}\left(3 + 4Z^2 + 4Z^8 + 4Z^{10} + Z^{16}\right).$$

Other terms $E\left[Z^{D^2(i,j)}\right]$ are evaluated in a similar manner.

4.4 Examples of Performance Analysis over the AWGN Channel

This part contains numerical examples of the computation of the union bound of turbo-STCM over the AWGN channel. The turbo-STCM system consists of two parallel concatenated 8 state 4-PSK space-time codes as shown in Fig. 3.2 with throughput 2 bits/s/Hz and two transmit-one receive antenna configuration.

Fig. 4.2 (a), (b) and (c), illustrate the performance analysis of interleaver sizes of 130, 1300, and 5200 symbols, respectively. An approximation (since not all terms are computed) to the union bound is found for 8 state 4-PSK turbo-STCM. Each figure has a vertical line passing through the capacity $E_b/N_0 = 2.1$ dB, which is referred to the expression (2.3) and come from Fig. 2.3 in Chapter 2. Fig. 4.2 also presents the simulation results after eight iterations. As we see, simulations results are consistent with the expectation of performance improving with the size of

interleaver. The bounds are computed from expression (4.27). Note that the union bound is obtained by summing over all error sequences with systematic and parity weights, w and z, respectively, from 1 to $2K$ bits. Computation of the full bound is prohibitive in its complexity; fortunately it is also unnecessary. One of the goals here is to investigate how many terms are required to obtain good approximations of the union bound. Main contributions to the bound are provided by error sequences with low weights w and z. Low weights will results in small SED's, which in turn will be the dominant terms in the union bound. To generate the union bound curves in the figures, we summed over error sequences with systematic part weight w as indicated and with parity weight $0 \leq z \leq 32$. Comparison of the simulation results with the curves of $w = 1$ show that when only error sequences with a single systematic bit are incorporated, the bound serves as a lower bound. For $K = 130$ in Fig. 4.2 (a), about $w = 5$ terms need to be summed to get the upper bound. For larger interleavers, Fig. 4.2 (b) and (c), $w = 2$ terms suffice. Note that as the signal-to-noise ratio increases, the curves for the different systematic weights coalesce, which indicates that the lower weights are indeed dominant.

4.5 Union Bound for the Fading Channel

To evaluate the average union bound on the bit error probability over the Rayleigh fading channel, it is necessary to average the right hand side of (4.27) over the channel $\mathbf{h}$. The average union bound is given by

$$\begin{aligned} B(e) &= E_{\mathbf{h}}\left[B(e|\mathbf{h})\right] \\ &= \sum_{w=1}^{2K}\sum_{z=0}^{2K}\sum_{n_\beta(w,z)} \frac{w}{4K}\tilde{a}(4K,w,z)\Phi(w,z,\mathbf{n}_\beta)\, E_D\left\{E_{\mathbf{h}}\left[Z^{D^2_{n_\beta}}\right]\right\}, \end{aligned} \tag{4.32}$$

where the order of the expectation operations is switched with respect to squared Euclidean distance (SED) D and $\mathbf{h}$. We now focus on evaluating the term $E_{\mathbf{h}}\left[Z^{D^2_{n_\beta}}\right]$.

(4.4) is used to express the cumulative SED associated with an error sequence:

$$\begin{aligned} d^2\left(\underline{\mathbf{c}}_K, \underline{\mathbf{e}}_K\right) &= \sum_{k=1}^{K} \left|\mathbf{h}^T \delta\left(\mathbf{c}_k, \mathbf{e}_k\right)\right|^2 \\ &= \mathbf{x}^H \mathbf{x}, \end{aligned} \tag{4.33}$$

where the definition of the $K \times 1$ vector $\mathbf{x}$ is obvious from the context, and the superscript denotes complex and transposed. Since $\mathbf{h}$ is a complex-valued Gaussian vector, the vector $\mathbf{x}$ is a complex-valued Gaussian multivariate with zero mean and covariance matrix $\mathbf{R}_{\mathbf{x}} = E\left[\mathbf{x}\mathbf{x}^H\right]$ with elements m_{kl}, $1 \leq k, l \leq K$. Recalling the assumption of independent SED's in an error sequence, it is easy to show that

$$m_{kl} = \begin{cases} \delta_k^2, & k = l \\ 0, & k \neq l \end{cases}, \quad 1 \leq k, l \leq K, \tag{4.34}$$

where $\delta_k^2 = \left\|\delta\left(\mathbf{c}_k, \mathbf{e}_k\right)\right\|^2$, $\delta\left(\mathbf{c}_k, \mathbf{e}_k\right)$ was defined in (4.3), and the norm is Euclidean, i.e., $\|\delta\|^2 = \delta^H \delta$. It follows from the definition of Z (right after (4.12)) and from (4.33), that

$$\begin{aligned} E_{\mathbf{h}}\left[Z^{D_{n_\beta}^2} \middle| D_{n_\beta}^2 = d^2\left(\underline{\mathbf{c}}_K, \underline{\mathbf{e}}_K\right)\right] &= E_{\mathbf{h}}\left[e^{-\gamma d^2\left(\underline{\mathbf{c}}_K, \underline{\mathbf{e}}_K\right)}\right] \\ &= E_{\mathbf{h}}\left[e^{-\gamma \mathbf{x}^H \mathbf{x}}\right], \end{aligned} \tag{4.35}$$

where $\gamma = r_c E_b / 4N_0$. Evaluation of the right hand side amounts to the computation of a Laplace transform with respect to the quadratic form of a complex Gaussian random variable. Using [72],

$$\begin{aligned} E_{\mathbf{h}}\left[e^{-\gamma \mathbf{x}^H \mathbf{x}}\right] &= \det\left(\mathbf{I}_K + \gamma \mathbf{R}_{\mathbf{x}}\right)^{-1} \\ &= \prod_{k=1}^{K} \left(1 + \gamma \delta_k^2\right)^{-1}, \end{aligned} \tag{4.36}$$

where $\mathbf{I}_K$ is the $K \times K$ identity matrix.

To continue with the evaluation of (4.32), it is necessary to compute $E_D\left\{E_{\mathbf{h}}\left[Z^{D_{\mathbf{n}_\beta}^2}\right]\right\}$. Identify $E_D\left\{E_{\mathbf{h}}\left[Z^{D_{\mathbf{n}_\beta}^2}\right]\right\} = E_D\left[e^{-\widetilde{D}_{\mathbf{n}_\beta}^2}\right]$, where $\widetilde{D}_{\mathbf{n}_\beta}^2$ is a function whose domain are random variables with realizations in the set of SED's possible

for an error sequence of type $\mathbf{n}_\beta$. The quantity $\widetilde{D}^2_{\mathbf{n}_\beta}$ is interpreted as an equivalent cumulative SED averaged over fading. Using (4.36) and grouping symbol SED's according to the number of systematic bit errors i and parity bit errors j, (similar to the steps leading to (4.29)), we can write

$$\begin{aligned} E_D\left[e^{-\widetilde{D}^2_{\mathbf{n}_\beta}}\right] &= E_D\left[\left(1+\gamma D^2(1,0)\right)^{-n_{1,0}} \cdot \ldots \cdot \left(1+\gamma D^2(2,2)\right)^{-n_{2,2}}\right] \\ &= E_D\left[\left(1+\gamma D^2(1,0)\right)^{-n_{1,0}}\right] \cdot \ldots \cdot E_D\left[\left(1+\gamma D^2(2,2)\right)^{-n_{2,2}}\right]. \end{aligned} \quad (4.37)$$

The last expression is analogous with (4.29) for the non-fading case. Retracing the steps after (4.29), we identify

$$e^{-\widetilde{D}^2(i,j)} = \left(1+\gamma D^2(i,j)\right)^{-1}, \quad (4.38)$$

where $\widetilde{D}^2(i,j)$ are the equivalent symbol SED's in the relation $\widetilde{D}^2_{\mathbf{n}} = n_{1,0}\widetilde{D}^2(1,0) + \cdots + n_{2,2}\widetilde{D}^2(2,2)$.

To evaluate (4.38) in analogy to (4.30)

$$E\left[e^{-\widetilde{D}^2(i,j)}\right] = \sum_{\mathbf{c}_k} P(\mathbf{c}_k) \sum_{\mathbf{e}_k : i,j} P(\mathbf{c}_k \to \mathbf{c}_k \oplus \mathbf{e}_k)\, e^{-\widetilde{d}^2(\mathbf{c}_k, \mathbf{e}_k)}. \quad (4.39)$$

In this expression, $\widetilde{d}^2(\mathbf{c}_k, \mathbf{e}_k)$ is the equivalent symbol SED averaged over fading. From (4.36), it can be expressed in terms of the symbol SED for the non-fading case,

$$\widetilde{d}^2(\mathbf{c}_k, \mathbf{e}_k) = \log\left(1+\gamma\delta_k^2\right), \quad (4.40)$$

where δ_k^2 was defined earlier in the expression (4.34). Computation of $E\left[e^{-\widetilde{D}^2(i,j)}\right]$ is continued with steps similar to those in the example following (4.30). The difference between the fading and non-fading case is that in (4.30), Z is substituted with e and $d^2(\mathbf{c}_k \oplus \mathbf{e}_k)$ is substituted with $\widetilde{d}^2(\mathbf{c}_k \oplus \mathbf{e}_k) = \log\left(1+\gamma\delta_k^2(\mathbf{c}_k \oplus \mathbf{e}_k)\right)$.

When the computation of $E\left[e^{-\widetilde{D}^2(i,j)}\right]$ for all allowed (i,j) (see (4.14)) is completed, the result can be used in (4.38) to obtain $E_D\left[e^{-\widetilde{D}^2_{\mathbf{n}_\beta}}\right]$ for an error sequence of type $\mathbf{n}_\beta(w,z)$. By substituting $E_D\left[e^{-\widetilde{D}^2_{\mathbf{n}_\beta}}\right]$ for $E_D\left\{E_{\mathbf{h}}\left[Z^{D^2_{n_\beta}}\right]\right\}$ in (4.32), the

union bound of bit error for turbo-STCM over the Rayleigh fading channel can be written

$$P_e \leq \sum_{w=1}^{2K} \sum_{z=0}^{2K} \sum_{n_\beta(w,z)} \frac{w}{4K} \tilde{a}(4K, w, z) \Phi\left(w, z, \mathbf{n}_\beta\right) E\left[e^{-\widetilde{D}^2_{\mathbf{n}_\beta}}\right]. \tag{4.41}$$

Extension to Multiple Receive Antennas

In this subsection, we outline the extension of the union bound from a single receive antenna to M receive antennas. The channel matrix $\mathbf{H}$ of (3.1) can be expressed $\mathbf{H} = [\mathbf{h}_1, \ldots, \mathbf{h}_M]^T$, where $\mathbf{h}_m$, $1 \leq m \leq M$ is a vector of channel coefficients between the transmit antennas and antenna index m at the receiver. The symbol SED in (4.2) can be rewritten for the case of M antennas at the receiver

$$d^2\left(\mathbf{c}_k, \mathbf{e}_k\right) = \sum_{m=1}^{M} \left|\mathbf{h}_m^T \delta\left(\mathbf{c}_k, \mathbf{e}_k\right)\right|^2. \tag{4.42}$$

It follows that the cumulative SED can be expressed

$$\begin{aligned} d^2\left(\underline{\mathbf{c}}_K, \underline{\mathbf{e}}_K\right) &= \sum_{k=1}^{K} d^2\left(\mathbf{c}_k, \mathbf{e}_k\right) \\ &= \sum_{k=1}^{K} \sum_{m=1}^{M} \left|\mathbf{h}_m^T \delta\left(\mathbf{c}_k, \mathbf{e}_k\right)\right|^2 \\ &= \underline{\mathbf{x}}^H \underline{\mathbf{x}}, \end{aligned} \tag{4.43}$$

where the $MK \times 1$ vector $\underline{\mathbf{x}}$ is a complex Gaussian multivariate with zero mean and covariance matrix related to that of $M = 1$ case (see (4.34)) as follows:

$$\mathbf{R}_{\underline{\mathbf{x}}} = \mathbf{I}_M \otimes \mathbf{R}_{\mathbf{x}}. \tag{4.44}$$

The symbol $\otimes$ is the Kronecker product and $\mathbf{I}_M$ is the $M \times M$ identity matrix. Similar to (4.36), it follows that

$$\begin{aligned} E_{\mathbf{h}}\left[e^{-\gamma \underline{\mathbf{x}}^H \underline{\mathbf{x}}}\right] &= \det\left(\mathbf{I}_{MK} + \gamma \mathbf{R}_{\underline{\mathbf{x}}}\right)^{-1} \\ &= \prod_{k=1}^{K} \left(1 + \gamma \delta_k^2\right)^{-M}. \end{aligned} \tag{4.45}$$

Retracing the steps after (4.36), it is easy to show that the equivalent symbol SED averaged over fading is related to the non-fading symbol SED through the relation

$$\widetilde{d}^2(\mathbf{c}_k, \mathbf{e}_k) = M \log\left(1 + \gamma \delta_k^2\right). \tag{4.46}$$

The last expression is a generalization of (4.40) to the M receive antenna case. The symbol SED's in this expression are then used to determine the distribution of the equivalent cumulative SED $\widetilde{D}^2_{\mathbf{n}_\beta}$. The expression for the union bound of the bit error probability is given by (4.41), where the random variable $\widetilde{D}^2_{\mathbf{n}_\beta}$ now incorporates the effect of M receive antennas.

4.6 Numerical Results for the Fading Channel

This section contains numerical examples that demonstrate the union bound of turbo-STCM over the block-fading channel. For comparison, simulation results are also provided. The simulation is based on Monte Carlo runs with 10,000 channel realizations for each E_b/N_0. As in the numerical examples of Chapter 3, the channel model was Rayleigh block-fading, meaning that the channel was assumed constant during a frame of $F = 130$ symbols, but independent frame-to-frame. Simulation results shown are averaged over random interleavers of size as specified in the figures. The turbo-STCM example considered here consists of two parallel concatenated space-time codes throughput 2 bits/s/Hz 4-PSK and 3 bits/s/Hz 8-PSK for two transmit and one/two receive antennas.

Fig. 4.3 and 4.4 provides the performance analysis of 8 state 4-PSK turbo-STCM, corresponding to the one and two receive antennas, respectively. Each figure is divided in three parts corresponding to interleaver sizes $K = 130, 1300$ and 5200 symbols. Computation of the union bound is based on (4.41). The expression specifies a bound obtained by summing over all error sequences with systematic weights $1 \leq w \leq 2K$, and parity weights $0 \leq z \leq 2K$. Computation of the full

bound is prohibitive in its complexity and it is also unnecessary. One of the analysis goals is to investigate how many terms are required to obtain a good approximation of the union bound. Each curve in each figure is labeled with the weights w of the error sequences. In all cases, the parity terms were $0 \leq z \leq 15$. For example, the union bound curve labeled $w = 2$, was generated using all error sequences with systematic weight $1 \leq w \leq 2$ and parity weight $0 \leq z \leq 15$. Note that for computing the double sum in (4.41), this is just a small subset of 32 different types of sequences (corresponding to different w and z) out of some 10^8 possible for $K = 5200$. The justification of using only a small subset of error sequences is that the small weights result in sequences with small SED's, which in turn, contribute the dominant terms to the union bound. From the figures it can be observed that error sequences corresponding to $w = 2$ are sufficient to provide a good approximation to the error bound. For example, it can be observed from Fig. 4.3 (b) that the curves for $w \geq 2$ coalesce for $E_b/N_0 \geq 20$ dB. Similarly, for the two receive antenna case, in Fig. 4.4 (b) the curves coalesce for $E_b/N_0 \geq 12$ dB. These results justify simplifying the bound evaluation by neglecting terms with large weights.

Fig. 4.5 and 4.6 show performance analysis for 16 state 8-PSK turbo-STCM with one and two receive antennas, respectively. In this case, the performance analysis follows the same steps of 4-PSK turbo-STCM except employing the IOWE of the individual 16 state 8-PSK constitute space-time codes, as shown in (4.6 and the average SED spectra. The expression (4.41) will specify a bound obtained by summing overall error sequences with systematic weights $1 \leq w \leq 3K$, and parity weights $0 \leq z \leq 3K$. In all cases, the parity terms included in the bound were $0 \leq z \leq 20$. From the figures it can be observed that error sequences corresponding to $w = 2$ are sufficient to provide a good approximation to the error bound. For example, it can be observed from Fig. 4.5 (b) of interleave size $K = 1300$ that the

curves for $w \geq 2$ coalesce for $E_b/N_0 \geq 20$ dB. Similarly, for the two receive antenna case, in Fig. 4.6 (b) the curves coalesce for $E_b/N_0 \geq 14$ dB.

4.7 Chapter Summary

In this chapter, the performance bounds are developed for turbo-STCM over AWGN and Rayleigh block-fading channels with multiple transmit and multiple receive antennas. The performance bounds are based on the union bound. The union bound is expressed in terms of IOWE of the individual constitute space-time codes and the average SED spectra. It is shown that a subset of dominant error paths provide a good approximation of the bound thereby alleviating the computational effort involved in computing the full union bound. The bound is expressed in terms of parameters of the individual space-time codes that make up the turbo-STCM code, interleaver length, number of transmit/receive antennas, the squared Euclidean distance spectra, and the statistical properties of the channel. It is shown that a small number of terms with low systematic bit weights is sufficient to yield an accurate upper bound on the bit error. The theoretical expressions are demonstrated by a close match with simulation results. This bound provides researchers with a useful analytical tool for the design and analysis of turbo space-time codes.

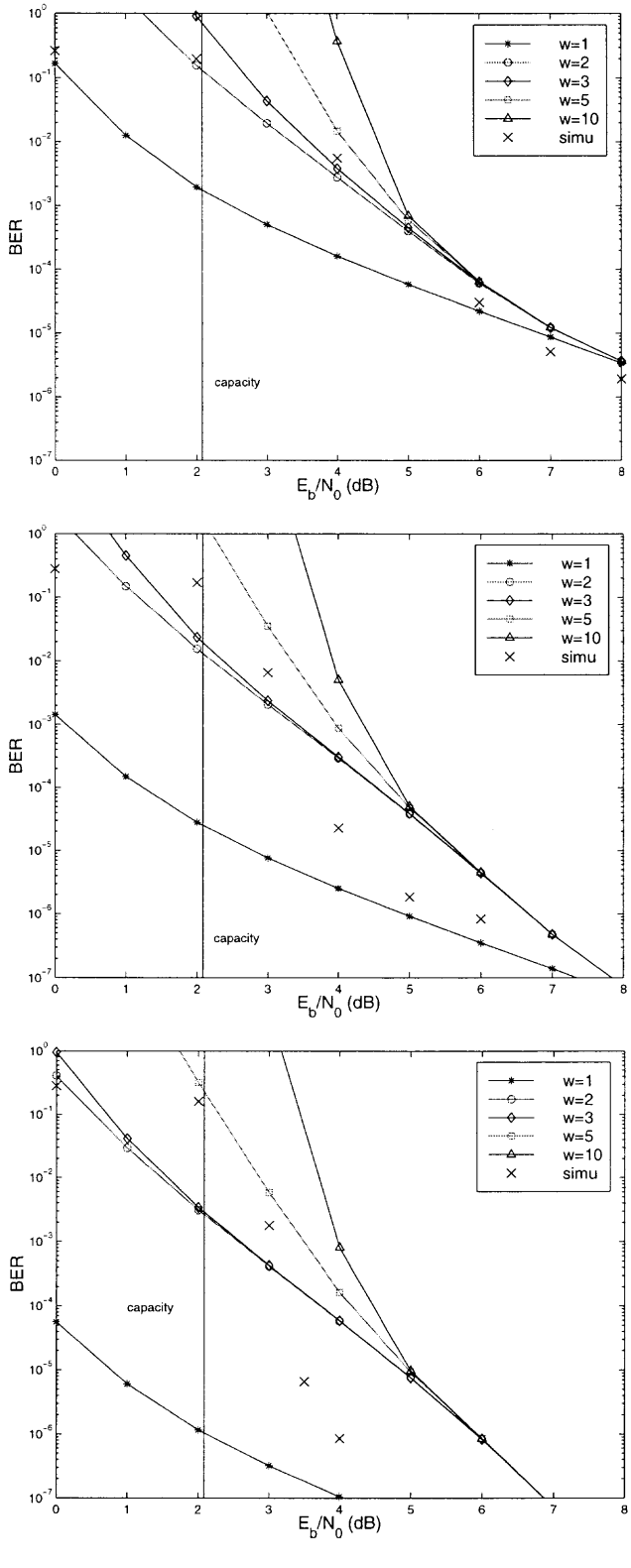

Figure 4.2 Union bound for 8 state 4-PSK turbo-STCM (2T1R) over the AWGN channel with interleavers of size (symbols): (a) $K = 130$, (b) $K = 1300$, (c) $K = 5200$.

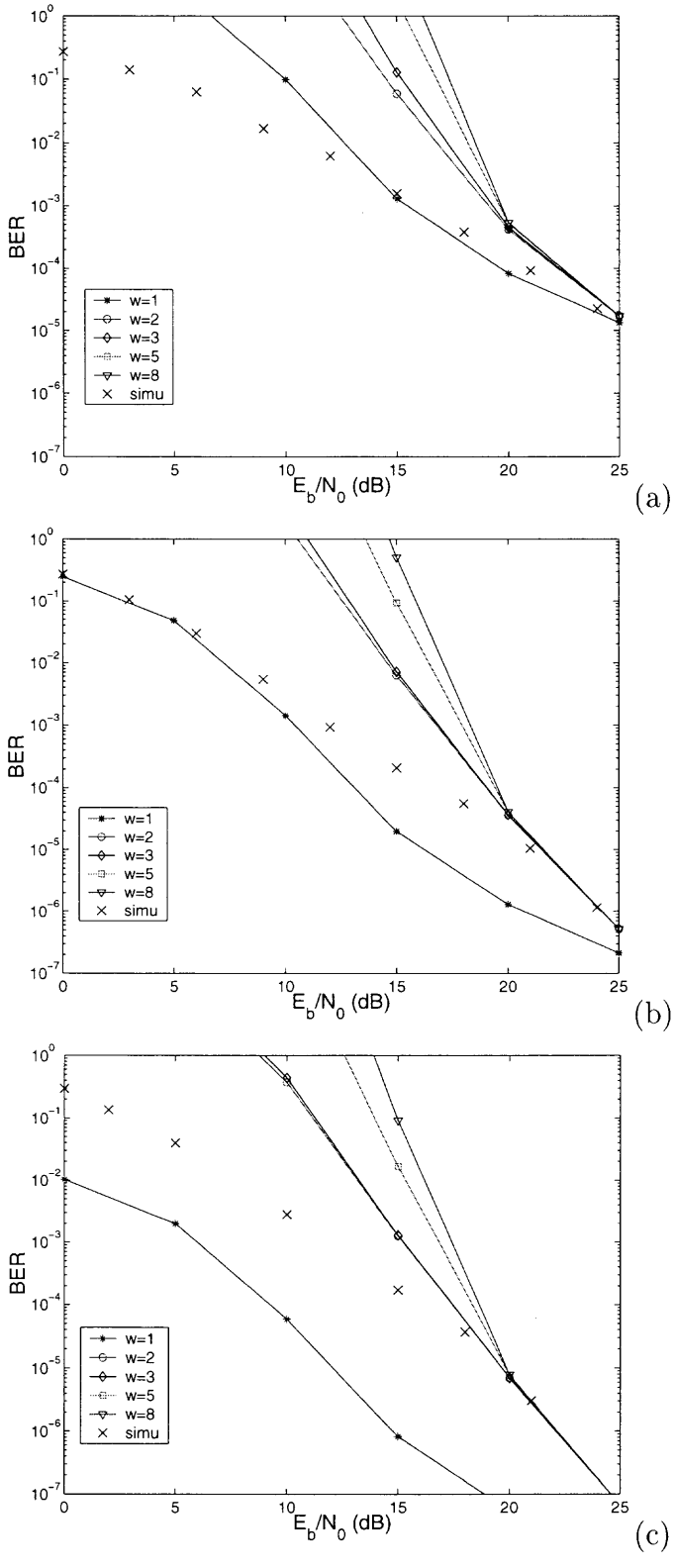

Figure 4.3 Union bound for 8 state 4-PSK turbo-STCM (2T1R) over the block-fading channel with interleaver of size (symbols): (a) $K = 130$, (b) $K = 1300$ and (c) $K = 5200$.

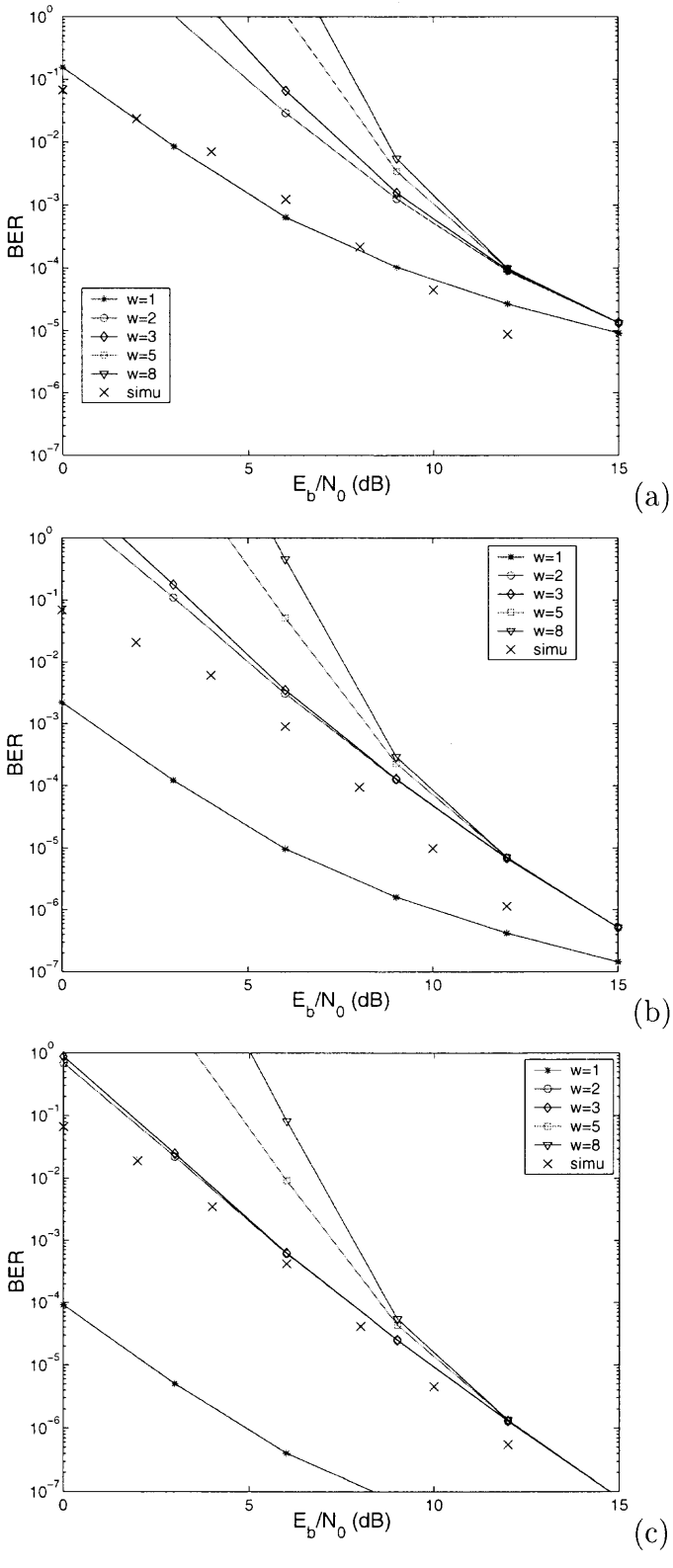

Figure 4.4 Union bound for 8 state 4-PSK turbo-STCM (2T2R) over the block-fading channel with interleaver of size (symbols): (a) $K = 130$, (b) $K = 1300$ and (c) $K = 5200$.

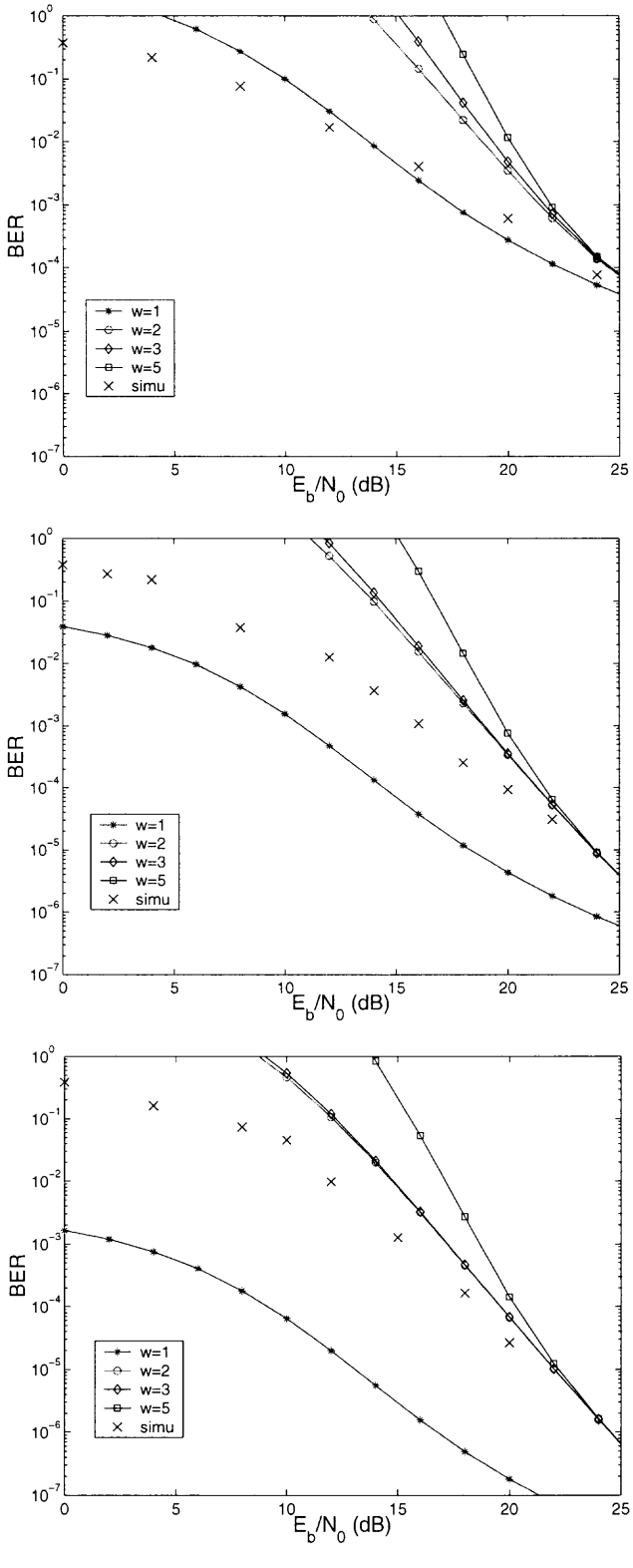

Figure 4.5 Union bound for 16 state 8-PSK turbo-STCM (2T1R) over the block-fading channel with interleaver of size (symbols): (a) $K = 130$, (b) $K = 1300$ and (c) $K = 5200$.

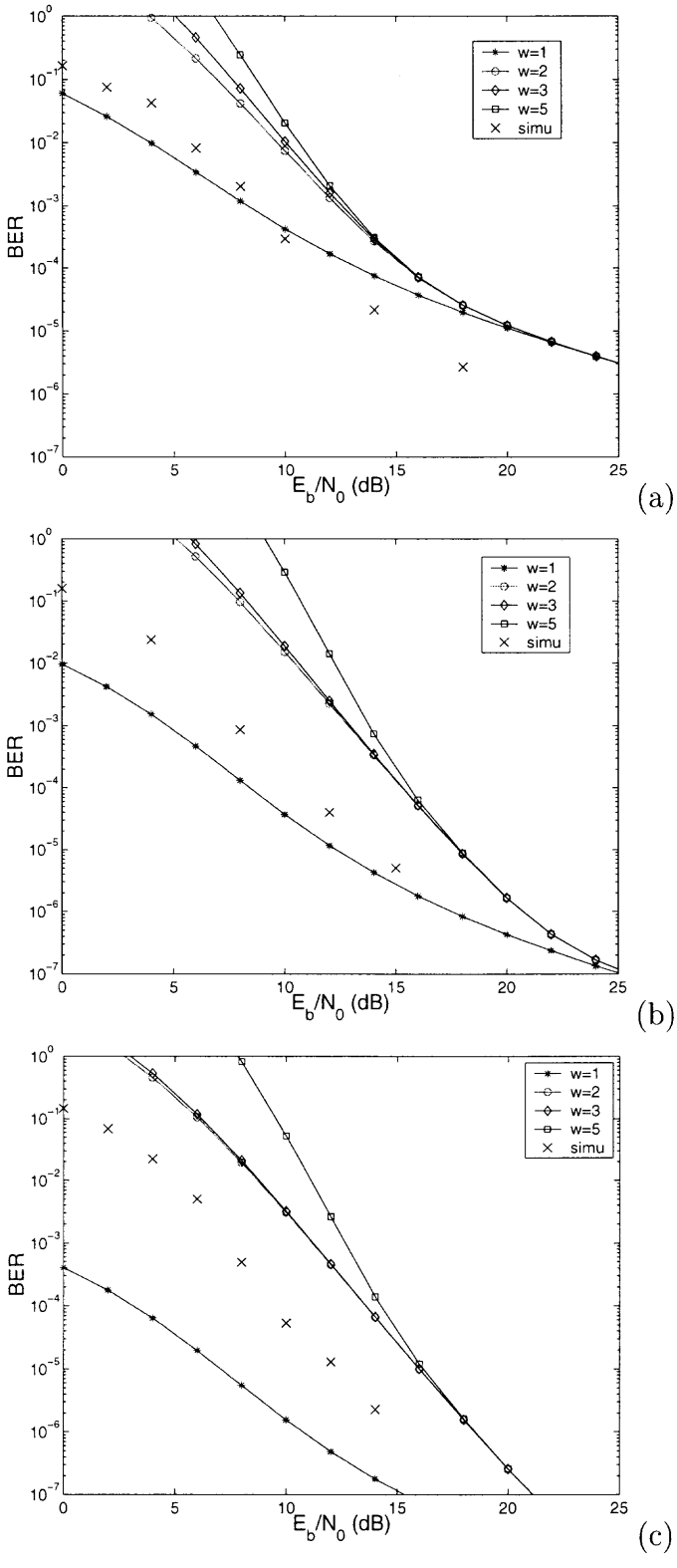

Figure 4.6 Union bound for 16 state 8-PSK turbo-STCM (2T2R) over the block-fading channel with interleaver of size (symbols): (a) $K = 130$, (b) $K = 1300$ and (c) $K = 5200$.

CHAPTER 5
CONCLUSIONS AND FURTHER WORK

Various channel coding, diversity combining and other techniques have been proposed, studied and applied to improve performance of wireless communications operating in severe signal environments. The turbo coding technique, which was introduced in 1993 [2], is a way of concatenating two simple convolutional codes in parallel to obtain an overall powerful code. However, Coding alone cannot exploit the richness of the multipath channel. Recent new results in capacity show that multiple antennas at both the transmitter and receiver sides can improve performance without expanding bandwidth. To approach the projected outage capacity of the multiple-input multiple-output (MIMO) multipath channel [20, 73, 19, 60], new techniques are required that combine turbo coding and both transmit and receive spatial diversity.

The first phase of this research investigated the interpretation of space-time processing from the point of view of information theory. We computed the capacity and cut-off rate of multiantenna system over the AWGN channel. Then the outage capacity is extended for frame error rate and signal-to-noise ratio, the ultimate limits of bandwidth efficiency [20] in the fading channel. We also derived the Fano lower bound for the MIMO channel to obtain a relation between bit error probability and signal-to-noise ratio for a fixed data transmission rate.

The second phase of this research proposed a new channel coding scheme of turbo space-time coded modulation with multiple transmit and receive antennas. Turbo-STCM combines the advantages of powerful turbo codes with the transmit/receive diversity of space-time codes. The scheme utilizes recursive and systematic constituent space-time codes and features full diversity and full rate. An iterative symbol-by-symbol *maximum a posteriori* algorithm operating in the log domain is developed for decoding turbo-STCM. Using simple space-time component encoders,

system performance is studied for 4-PSK and 8-PSK turbo-STCM codes with multiple transmit and receive antennas. It is shown that significant gain can be obtained in performance over the Rayleigh fading channel. The new scheme provides an advantage of 1-3 dB over conventional space-time codes of similar complexity.

In the third phase of this research, as a initial step, we derived the union bound of turbo-STCM system with multiple transmit antennas and one receiver antenna over the AWGN channel. This bound is independent of the particular interleaver used by introducing a uniform interleaver, which maps an input word into all its permutations [56]. The ensemble of codes is generated by varying interleaving permutations for a given size interleaver. This approach enables us to express the union bound of the turbo code in terms of the IOWE of the constituent codes and the interleaver size. It is shown that a small number of terms with low systematic bit weight is sufficient to yield an accurate upper bound on the bit error. After that, this idea was extended to other high level modulations and block fading channel. These bounds are demonstrated by comparison to computer simulations utilizing iterative log-MAP decoding. Turbo-STCM schemes have the potential to facilitate high-rate data transmission over fading channels in future wireless networks.

The original contributions of this research are:

- Fano lower bound concept of space-time processing in block fading channel. It shows us the direction of spatial diversity with multiantenna system [64] as shown in [31].

- Turbo-STCM: a new scheme of combining turbo coding with the spatial diversity advantage of space-time processing and the bandwidth efficiency of coded modulation under a *single* framework [49].

- Performance analysis of turbo-STCM scheme over AWGN channel [50].

- Error Performance analysis of turbo-STCM over the Fading channel [51, 52].

There are some possible future work that involves:

1. A more detailed study of space-time coding limits from point of view of information theory. As we know, Fano's inequality is a quite weak converse condition [74]. Fano lower bound of space-time coding on bit error probability is rather optimistic for practical code. Thus, to be able to answer questions such as "How close is the particular turbo decoding algorithm to maximum a posteriori solution?", "how does conventional Viterbi decoding of space-time codes approach to theoretical methods?", from a theoretical perspective, we need much more accurate analysis of space-time codes.

2. As conventional space-time codes [31], turbo-STCM in this Ph.D. thesis is only for a small number of transmit antennas (for example $N = 2$). But recently there are several papers that investigate the design of space-time code [33, 41, 47] for large number of transmit antennas. Serial concatenation of space-time block codes with simple recursive inner encoder is probably one solution for the extension of turbo-STCM to more general cases.

3. A method for computing the union bound of turbo-STCM is developed on the bit error probabilities over fading channel. This method is currently the only approach available for evaluating the performance of turbo space-time systems analytically. Although there is now an abundance of literature on turbo codes and some on turbo space-time system, there are numerous other wide open and very important problems. For example, different channel models, different concatenation methods (e.g. parallel versus serial concatenation), space-time constituent code design, interleaver optimal design, etc. All of those should be done by both Monte Carlo numerical simulations and the union bounding techniques developed in this dissertation. Such a study would serve as a very useful reference for further development on the subject.

REFERENCES

1. C.E. Shannon, "A mathematical theory of communications i, ii," *Bell System Technical Journal*, vol. 27, pp. 379–423; 623–656, 1948.

2. C. Berrou, A. Glavieux, and P. Thititmajshima, "Near Shannon limit error-correcting coding and decoding: Turbo-codes (1)," *IEEE International Conference on Communications (ICC '93)*, pp. 1064–1070, May 1993.

3. S. Benedetto and E. Biglieri, *Principles of Digital Transmission with Wireless Applications*, Kluwer Academic / Plenum Publishers, New York, NY, 1999.

4. C. Berrou and A. Glavieux, "Near optimum error correcting coding and decoding: Turbo-codes," *IEEE Transactions on Communications*, vol. 44, pp. 1261–1271, Oct 1996.

5. M.C. Valenti, *Iterative Detection and Decodign for Wireless Communication*, Ph.D. thesis, Electrical and Computer Engineering Department, Northeastern University, Boston, MA., May. 1998.

6. A.J. Viterbi and J.K. Omura, *Principles of Communications and Coding*, McGraw-Hill, New York, NY, 1979.

7. J. Hagenauer, E. Offer, and L. Papke, "Iterative decoding of binary block and convolutional codes," *IEEE Transactions on Information Theory*, vol. 42, pp. 429–445, Mar. 1996.

8. L.R. Bahl, J. Cocke, F. Jelinek, and J. Raviv, "Optimal decoding of linear codes for minimizing symbol error rate," *IEEE Transactions on Information Theory*, pp. 284–287, Mar. 1974.

9. G. Ungerboeck, "Channel coding with multilevel phase signals," *IEEE Transactions on Information Theory*, vol. 28, pp. 55–67, Jan. 1982.

10. S. Benedetto, D. Divsalar, G. Montorsi, and F. Pollara, "Serial concatenation of interleaved codes: Performance analysis, design and iterative decoding," *IEEE Transactions on Information Theory*, vol. 44, pp. 909–926, May. 1998.

11. D. Divsalar and F. Pollara, "Turbo codes for PCS applications," *IEEE International Conference on Communications (ICC '95)*, vol. 1, pp. 54–59, 1995.

12. G. Ungerboeck, "Trellis-coded modulation with redundant signal sets part I: Introduction," *IEEE Communications Magazine*, vol. 25, pp. 5–11, Feb. 1987.

13. G. Ungerboeck, "Trellis-coded modulation with redundant signal sets part II: State of the art," *IEEE Communications Magazine*, vol. 25, pp. 12–21, Feb. 1987.

14. S. LeGoff, A. Glavieux, and C. Berrou, "Turbo-codes and high-spectral efficiency modulation," *IEEE International Conference on Communications (ICC '94)*, pp. 645–649, 1994.

15. P. Robertson and T. Wörz, "Bandwidth-efficient turbo trellis-coded modulation using punctured component codes," *IEEE Journal on Selected Areas in Communications*, vol. 16, pp. 206–218, Feb. 1998.

16. S. Benedetto, D. Divsalar, G. Montorosi, and F. Pollara, "Parallel concatenated trellis coded modulation," *IEEE International Conference on Communications (ICC '96)*, pp. 974–978, 1996.

17. W.C. Jakes, *Microwave Mobile Communications*, IEEE Press, New York, NY, 1974.

18. P.V. Rooyen, M. Lötter, and D.V. Wyk, *Space-time processing for CDMA Mobile Communications*, Kluwer Academic Publishers, Boston, MA, 2000.

19. T.L. Marzetta and B.M. Hochwald, "Capacity of a mobile multiple-antenna communication link in Rayleigh flat fading," *IEEE Transactions on Information Theory*, vol. 45, pp. 139–157, Jan. 1999.

20. G.J. Foschini and M.J. Gans, "On limits of wireless communications in a fading environment when using multiple antennas," *Wireless Personal Communications*, pp. 6:311–335, 1998.

21. A. Shah, A.M. Haimovich, M.K. Simon, and M.S. Alouini, "Exact bit error probability for optimum combining with a rayleigh fading co-channel interferer," *IEEE Transactions on Communications*, vol. 48, pp. 908–912, Jun. 2000.

22. A. Shah and A.M. Haimovich, "A performance comparison of optimum combining and maximal ratio for digital cellular mobile radio communication systems with cochannel interference," *IEEE Transactions on Vehicular Technology*, vol. 49, pp. 1454–1463, Jul. 2000.

23. J.H. Winters, "The diversity gain of transmit diversity in wireless systems with rayleigh fading," *IEEE International Conference on Communications (ICC '94)*, pp. 1121–1125, 1994.

24. G.W. Wornell and M.D. Trott, "Signal processing techniques for efficient use of transmit diversity in wireless communications," *IEEE ICASSP '96*, pp. 1057–1064, 1996.

25. S.M. Alamouti, "A simple transmit diversity technique for wireless communications," *IEEE Journal on Selected Areas in Communications*, vol. 16, pp. 1451–1458, Oct. 1998.

26. G.G. Raleigh and J.M. Cioffi, "Spatio-temporal coding for wireless communications," *IEEE Globecom '96*, vol. 3, pp. 1809–1814, 1996.

27. A. Narula, M.D. Trott, and G.W. Wornell, "Performance limits of coded diversity methods for transmitter antenna arrays," *IEEE Transactions on Information Theory*, vol. 45, pp. 2418–2433, Nov. 1999.

28. G.J. Foschini, "Layered space-time architecture for wireless communications in a fading channel environment when using multi-element antennas," *AT&T, Bell-Labs Technical Journal*, pp. 41–59, Autumn 1996.

29. G. D. Golden, G. J. Foschini, R. A. Valenzuela, and P. W. Wolniansky, "Detection algorithm and initial laboratory results using the V-BLAST space-time communication architecture," *Electronics Letters*, vol. 35, pp. 14–15, Jan. 1999.

30. G. J. Foschini, G.D. Golden, R.A. Valenzuela, and P.W. Wolniansky, "Simplified processing for high spectral efficiency wireless communication employing multi-element arrays," *IEEE Journal on Selected Areas in Communications*, vol. 17, pp. 1841–1852, Nov. 1999.

31. V. Tarokh, N. Seshadri and A.R. Calderbank, "Space-time codes for high data rate wireless communications: Performance criterion and code construction," *IEEE Transactions on Information Theory*, vol. 44, pp. 744–765, Mar. 1998.

32. A.F. Naguib, V. Tarokh, N. Seshadri, and A.R. Calderbank, "A space-time coding modem for high-data-rate wireless communications," *IEEE Journal on Selected Areas in Communications*, vol. 16, pp. 1459–1478, Oct. 1998.

33. V. Tarokh, H. Jafarkhani, and A.R. Calderbank, "Space-time block coding for wireless communications: Performance results," *IEEE Journal on Selected Areas in Communications*, vol. 17, pp. 451–460, Mar. 1999.

34. V. Tarokh, H. Jafarkhani, and A.R. Calderbank, "Space-time block coding for wireless communications: Theory of generalized orthogonal designs," *IEEE Transactions on Information Theory*, vol. 45, pp. 1456–1467, July. 1999.

35. V. Tarokh, A. Naguib, N. Seshadri, and A.R. Calderbank, "Combined array processing and space-time coding," *IEEE Transactions on Information Theory*, vol. 45, pp. 1121–1128, May. 1999.

36. A.R. Calderbank, "The art of signals: Fifty years of coding theory," *IEEE Transactions on Information Theory*, vol. 44, pp. 2561–2595, Oct. 1998.

37. D. Bevan and R. Tanner, "Performance comparison of space-time coding techniques," *Electronics Letters*, vol. 35, pp. 1707–1708, Sept. 1999.

38. J.C. Guey, M.P. Fitz, M.R. Bell, and W.Y. Kuo, "Signal design for transmitter diversity wireless communications systems over Rayleigh fading channels," *IEEE Transactions on Communications*, vol. 47, pp. 527–537, Apr. 1999.

39. E. Malkamaki and H. Leib, "Coded diversity on block-fading channels," *IEEE Transactions on Information Theory*, vol. 45, pp. 771–781, Mar. 1999.

40. S. Baro, G. Bauch, and A. Hansmann, "Improved codes for space-time trellis-coded modulation," *IEEE Communications letters*, vol. 4, pp. 20–22, Jan. 2000.

41. A.R. Hammons and H. El Gamal, "On the theory of space-time codes for psk modulation," *IEEE Transactions on Information Theory*, vol. 46, pp. 524–542, Mar. 2000.

42. G. Bauch, "Concatenation of space-time block codes and turbo-TCM," *IEEE International Conference on Communications (ICC'99)*, pp. 1202–1206, June 1999.

43. K.R. Narayanan, "Turbo decoding of concatenated space-time codes," *37th Annual Allerton Conference on Communication, Control and Computing*, Sept. 1999.

44. H. Su and E. Geraniotis, "Spectrally efficient Turbo codes with full antenna diversity," *Multiaccess Mobility and Teletraffic for Wireless Communications (MMT '99)*, Oct. 1999.

45. X. Lin and R.S. Blum, "Improved space-time codes using serial concatenation," *IEEE Communications letters*, vol. 4, pp. 221 –223, Jul. 2000.

46. Y. Liu and M.P. Fitz, "Space-time turbo codes," *37th Annual Allerton Conference on Communication, Control and Computing*, Sept. 1999.

47. Y. Liu, M.P. Fitz, and O.Y. Takeshita, "QPSK space-time turbo codes," *IEEE International Conference on Communications (ICC '00)*, June 2000.

48. A. Stefanov and T.M. Duman, "Turbo coded modulation for systems with transmit and receive antenna diversity," *IEEE Globecom'99*, pp. 2336–2340, Dec. 1999.

49. D. Cui and A.M. Haimovich, "A new bandwidth efficient antenna diversity scheme using turbo codes," *34th Annual Conference on Information Sciences and Systems (CISS '00)*, vol. 1, pp. TA–6.24–29, Mar. 2000, Princeton, NJ.

50. D. Cui and A.M. Haimovich, "Design and performance analysis of turbo space-time coded modulation," *IEEE Global Telecommunications conference (Globecom '00)*, vol. 3, pp. 1627–1631, Nov. 27-Dec. 1 2000, San Francisco, CA.

51. D. Cui and A.M. Haimovich, "Error performance analysis of turbo space-time coded modulation over fading channels," *IEEE International Conference on Communications (ICC '01)*, Jun. 2001, Helsinki, Finland.

52. D. Cui and A.M. Haimovich, "Parallel concatenated turbo multiple antenna coded modulation: Principles and performance analysis," *submitted to IEEE Journal on Selected Areas in Communication*, Apr. 2001.

53. A. Stefanov and T.M. Duman, "Turbo coded modulation for wireless communications with antenna diversity," *IEEE VTC '99*, pp. 1565–1569, 1999.

54. D. Cui and A.M. Haimovich, "A multilevel turbo-code with antenna diversity," *The 13th Annal International Conference on Wireless Communications (Wireless 2001)*, Jul. 2001, Calgary, Alberta, Canada.

55. P. Robertson and T. Wörz, "Bandwidth-efficient Turbo trellis-coded modulation using punctured component codes," *IEEE Journal on Selected Areas in Communications*, pp. 206–218, Feb. 1998.

56. S. Benedetto and G. Montorsi, "Unveiling turbo codes: Some results on parallel concatenated coding schemes," *IEEE Transactions on Information Theory*, vol. 42, pp. 409–428, Mar. 1996.

57. D. Divsalar, S. Dolinar, and F. Pollara, "Transfer function bounds on the performance of Turbo codes," Tech. Rep., TDA Progress Report, JPL, Aug. 1995.

58. J.G. Proakis, *Digital Communications*, McGraw-Hill, New York, NY, 1995.

59. E. Biglieri, D. Divsalar, P.J. McLane, and M.K. Simon, *Introduction to Trellis Coded Modulation with Applications*, Macmillan, New York, NY, 1991.

60. E. Biglieri, G. Caire, and G. Taricco, "Limiting performance of block-fading channels with multiple antennas," *IEEE Transactions on Information Theory*, 2001, to be published.

61. Da-shan Shiu and M. Kahn, "Layered space-time codes for wireless communications using multiple transmit antennas," *IEEE International Conference on Communications (ICC '99)*, vol. 1, pp. 436–440, 1999.

62. D. Gesbert, H. Boleskei, D. Gore, and A. Paulraj, "Mimo wireless channels: capacity and performance prediction," *IEEE Global Telecommunications Conference (Globecom '00)*, vol. 2, pp. 1083 –1088, Nov. 27-Dec. 1 2000, San Francisco, CA.

63. S. Sandhu and A. Paulraj, "Space-time block codes: A capacity perspective," *IEEE Communications letters*, vol. 4, pp. 384–386, Dec. 2000.

64. D. Cui and A.M. Haimovich, "Performance of parallel concatenated space-time codes," *Accepted by IEEE Communications Letter*, Jan. 2001.

65. L.L. Scharf, *Statistical Signal Processing: Detection, Estimation, and Time Series Analysis*, Addison-Wesley Series in Electrical & Computer Engineering Series, New York, NY, 1991.

66. J. Erfanian, S. Pasupathy, and G. Gulak, "Reduced complexity symbol detectors with parallel structures for ISI channels," *IEEE Transactions on Communications*, vol. 42, pp. 1661–1671, Feb./Mar./Apr. 1994.

67. R. Lidi and H. Niederreiter, *Finite Fields*, Addison Wesley, 1983.

68. T.M. Duman and M. Salehi, "Performance bounds for Turbo-coded modulation systems," *IEEE Transactions on Communications*, vol. 47, pp. 511–521, Apr. 1999.

69. T.M. Duman and M. Salehi, "The union bound for Turbo-coded modulation systems over fading channels," *IEEE Transactions on Communications*, vol. 47, pp. 1495–1502, Oct. 1999.

70. T.M. Duman, *Turbo Codes and Turbo Coded Modulation Systems: Analysis and Performance Bounds*, Ph.D. thesis, Electrical and Computer Engineering Department, Virginia Polytechnic Institute and State University, Blacksburg, Virginia., July. 1999.

71. R.P. Stanley, *Enumerative Combinatorics*, Wadsworth & Brooks/Cole, Monterey, CA, 1986.

72. G.L. Turin, "The characteristic function of hermitian quadratic forms in complex normal variables," *Biometrika*, vol. 47, pp. 199–212, Jun. 1960.

73. P.F. Driessen and G.J. Foschini, "On the capacity formula for multiple input-multiple output wireless channels: A geometric interpretation," *IEEE Transactions on Information Theory*, vol. 47, pp. 173–176, Feb. 1999.

74. R. Knopp and P.A. Humblet, "On coding for block fading channels," *IEEE Transactions on Information Theory*, vol. 46, pp. 189–205, Jan. 2000.